Institut für Theoretische Physik
Fakultät Mathematik und Naturwissenschaften
Technische Universität Dresden

Spatiotemporal calcium-dynamics in presynaptic terminals

Dissertation
zur Erlangung des
Doktorgrades der Naturwissenschaften
(Doctor rerum naturalium)

vorgelegt von
Frido Erler
geboren am 25. November 1971 in Dresden

Dresden 2004

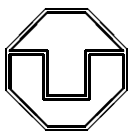

Eingereicht am 30. Juli 2004

1. Gutachter: Prof. Dr. Gerhard Soff
2. Gutachter: Prof. Dr. Jonathon Howard
3. Gutachter: Prof. Dr. Santiago Schnell

Verteidigt am: _____

Abstract

This thesis deals with a newly-developed model for the spatiotemporal calcium dynamics within presynaptic terminals. The model is based on single-protein kinetics and has been used to successfully describe different neuron types such as pyramidal neurons in the rat neocortex and the Calyx of Held of neurons from the rat brainstem. A limited number of parameters had to be adjusted to fluorescence measurements of the calcium concentration. These values can be interpreted as a prediction of the model, and in particular the protein densities can be compared to independent experiments. The contribution of single proteins to the total calcium dynamics has been analysed in detail for voltage-dependent calcium channel, plasma-membrane calcium ATPase, sodium-calcium exchanger, and endogenous as well as exogenous buffer proteins. The model can be used to reconstruct the unperturbed calcium dynamics from measurements using fluorescence indicators. The calcium response to different stimuli has been investigated in view of its relevance for synaptic plasticity. This work provides a first step towards a description of the complete synaptic transmission using single-protein data.

Contents

Chapter 1

Introduction

In the past decade, the focus of biological research has shifted towards quantitative methods and results. Especially the past years have witnessed a number of successful investigations mapping out the genomes of different species, genuinely an interdisciplinary effort bringing together biology, chemistry, physics, and informatics. Modern genetics centers around ongoing attempts to connect the genome to elementary properties of creatures, such as their capabilities of metabolism, homoeostasis, regulation, and differentiation. This quantitative approach has been established as some kind of "standard model" in biology and highlights the shift in the paradigm of biological research. In fact, there is a huge and rising amount of accumulated knowledge on quite particular and sometimes very specialised phenomena. The ever-increasing number of qualitative hypotheses explaining these seems to necessitate ever-intensifying attempts to validate them quantitatively. The overall intention is to merge their results into a more uniform picture of biological processes. To operate on such a quantitative level, some methods become of paramount importance, which have so far been located in the realm of other sciences such as physics. These methods include skills to construct mathematical abstractions of involved situations, to formulate detailed models of complex phenomena and to process them through analytical or numerical methods. In addition, it is often relied on precise simulations based on "first-principles". In particular, this familiarity with mathematical tools and with the quantitative concepts of exact sciences renders physics an ideal partner for biology in its road towards a quantitative understanding of nature.

Apart from methods alone, there are a number of other aspects common to both physics and biology. The most prominent of these aspects is to try to understand comparably simple processes within complex systems on a very elementary level: an approach with a long and successful tradition in physics, becoming a sine qua non in biology. This approach starts from microscopic findings, such as the laws of atomic interactions in physics or the rules of protein interplay in biology. It ends with the overall behaviour of a system, such as the structure of matter in its different states of aggregation or of the network of neurons inside a brain. Especially the latter, a network of neurons, exemplifies in a very sophisticated way self-organising complex systems,

which are in the focus of current physics research on a more abstract level. Their origin and development as well as their capabilities to adapt to new situations are of special interest for both disciplines.

From the considerations above it is obvious that the functional dependence of networks of neurons on their basic units, such as the synapses, and their respective interplay is a topic of ongoing research. In the comprehension of such networks the topological structure and the coupling of neurons with each other through synapses seems to be an elementary key. It is commonly accepted that the understanding of such systems is closely related to the question of how the brain processes information. The processing of information is nothing but a tautology to the processing of signals: In neurons these signals consist of short electrical pulses caused by ion currents, which are transmitted through synapses with messenger molecules. Synapses are subject to a continuous change, their efficiency in transmitting signals, called efficacy, depends on the respective input and their history[1].

In order to follow the successful approach outlined above, namely trying to understand macroscopic phenomena in terms of microscopic dynamics, the details governing the behaviour of this basic unit needs to be investigated. This includes the study of basic neuronal dynamics reflected in the propagation of corresponding electrical signals. Consequently, specific ion permeable channel proteins have to be investigated, which allow ion currents to pass into and out of the neuron. The microscopic behaviour of synapses in turn is defined by their response to such electrical pulses activating and transmitting messenger molecules caused by the activation of transmembrane and intracellular proteins. This response depends on the form and duration of electrical stimuli and on the history of the individual synapse with respect to such stimuli.

Potassium and sodium ion fluxes through appropriate channel proteins are responsible for the existence and the propagation of electrical pulses within the neurons. These ions follow gradients of the electrochemical potential through pores in the membrane emerging from potential-sensitive conformation changes of the channel proteins. However, the electrical pulses do not interact directly with the synapse. For their transmission at synapses calcium-ions play the dominant role. The appearance of an electrical pulse at the presynaptic terminal triggers the opening of channel proteins which are permeable to calcium-ions only. These ions flow into the terminal from the extracellular space and bind to messenger proteins, which in turn are activated. The activated messenger proteins are attached to vesicles, which release a neurotransmitter into the synaptic cleft. Once being in the synaptic cleft, the neurotransmitter molecules can bind to receptors of the partner neuron. As a consequence, these receptors open pores which trigger the flux of potassium and sodium ions again thus initiating a new small electrical pulse in the partner neuron.

From this sketch of neuronal signal transmission it is clear that the calcium-ions act as the prime trigger of synaptic activity. In this thesis the spatiotemporal dynamics of calcium-ions and their influence on signal transmission is analysed. Especially the

[1] Such a "learning rule" has already been postulated by Hebb in 1949 [1]: "When an axon of cell A is near enough to excite cell B or repeatedly or persistently takes part in firing it, some growth process or metabolic change takes place in one or both cells such that A's efficiency, as one of the cells firing B, is increased."

response of the calcium-concentrations to different patterns of stimulation is a good starting point to understand the complex interplay of ions and proteins on a fundamental level. Therefore, this thesis is organised as follows:

- In the next section, Ch. (2), a general overview of the nervous system with its connection to ion dynamics will be given. The focus will rest predominantly on the mechanisms responsible for the synaptic transmission of signals. The different phenomena related to calcium-ions as messengers will briefly be highlighted. The chapter will close with a short discussion of phenomena changing the synaptic efficacy.

- Then, in Ch. (3), the functionality of synapses in connection with the various proteins taking part in signal transmission will be reviewed. Besides introducing them individually, their interplay will be sketched. Special emphasis will be put on the presynaptic side of signal transmission, since this thesis mainly centers around calcium dynamics in presynaptic terminals. This natural choice of focus is due to the complexity of the full signal transmission process.

- Ch. (4) will be devoted to a presentation of the model underlying this thesis. This model can be understood as an extension of previous models, such as e.g. [2, 3, 4, 5]. It is based on a system of partial differential equations of the reaction-diffusion type, which is supplemented with a number of diffusion equations for individual proteins. The emerging multi-dimensional system of differential equations is integrated numerically with dynamic and static conditions taken directly from appropriate experimental data, where possible. The complete model is encoded in a simulation software application called SYNDICAD.

- Results obtained with this model will be presented and discussed in Ch. (5). SYNDICAD will be adjusted to different types of neurons by using optical measurements of the calcium-dynamics. Different stimulation patterns will be investigated and the differences in the appropriate calcium-dynamics will be discussed in detail. Also the relevance for different phenomena of changing synaptic efficacy will be highlighted. Finally, some special spatial problems of the calcium-dynamics will be studied.

- The thesis closes with concluding remarks and a brief outlook of possible future directions.

Chapter 2

Phenomenological overview

2.1 From the nervous system to ion-dynamics

In many complex life-forms, the collective interactions of multicellular systems are organised by a nervous system. Stimuli of various kinds are received, transformed, transmitted and processed and may lead to appropriate and sometimes pre-defined actions. In the following an overview will be given in order to bridge the gap between the nervous system and the underlying mechanisms of information processing. For a detailed comprehension of neurophysiology, confer the standard textbooks, such as [6, 7, 8].

The elementary processing units of the nervous system are the neurons, in humans their total number amounts to approximately 10^{12}. The neurons, however, are not the only constituents of the nervous system. In addition, it contains also a large number of supporter cells, named glia cells, that are required for energy supply, structural stabilisation, and the insulation of axons in form of myelin. Since glia cells are not directly involved in information processing, they will not be discussed any further in the framework of this thesis. The neurons come in various types and different sizes and shapes which is illustrated in Fig. (2.1). All of them share the same general functionality (apart from a few rare exceptions, which are also neglected here):

A typical neuron can be divided into three functionally distinct and topologically well-separated parts: dendrites, soma, and axon (see Fig. 2.2). The tree-like dendrites (diameter 0.2-8 μm, length 15-2000 μm) act as an input device that collects small electrical pulses (amplitude 1-20 mV, width 1-5 ms) from other neurons and transmits them to the soma. The soma (diameter 50-120 μm) is the trigger device and performs an important processing step by generating a new output signal in case a certain potential threshold is exceeded during integration of the incoming pulses. The output pulse is taken over by the output device, the axon (diameter 0.2-20 μm, length 0.1-2000 mm) which passes the pulse to other neurons. Most axons are surrounded by a myelin sheath which is formed by glia cells. This sheath acts as an insulator and facilitates signal propagation along the axon through interceptions along the membrane. The neuronal output pulses are called action potentials. They have an amplitude of about 100 mV and a typical width of 1-5 ms. Interestingly, the form of the pulse is not

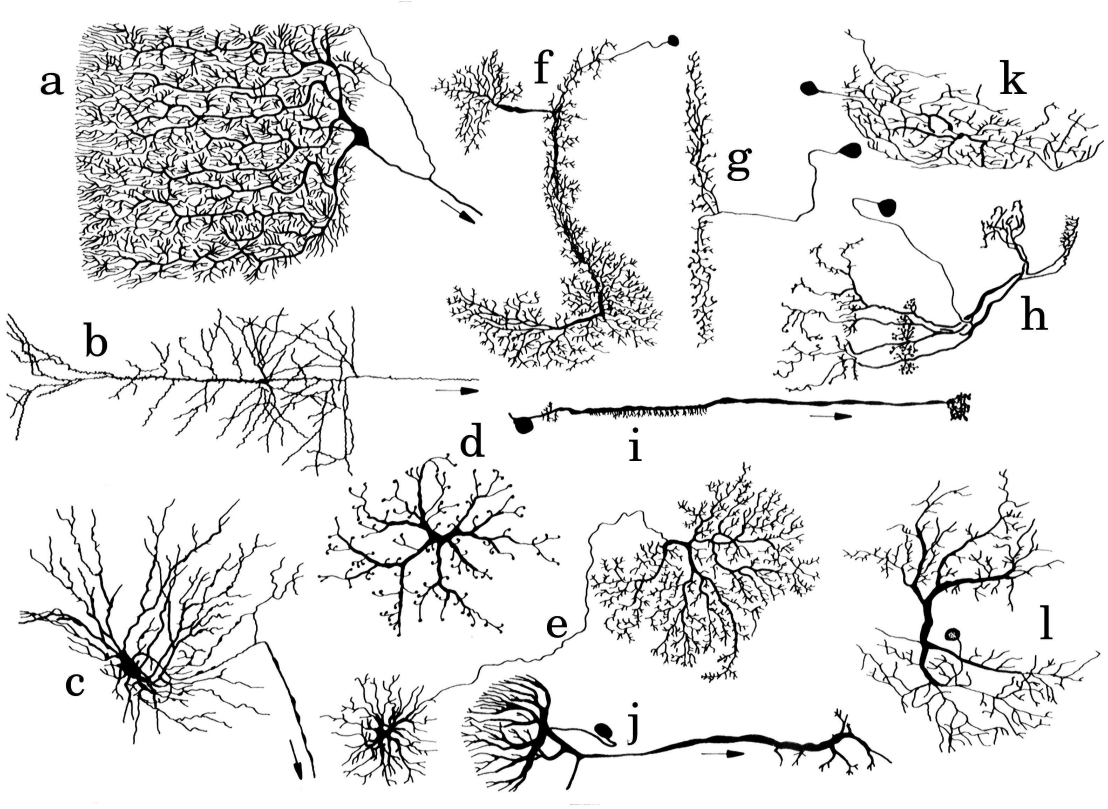

Figure 2.1: **Anatomical diversity of neuronal cells:** *a* Purkinje neuron from human *b* pyramidal neuron (rabbit) *c* motor neuron (cat) *d,e* horizontal neuron (cat) *f* pre-motor interneuron (locust) *g* visual amacrinal neuron (fly) *h* multipolar neuron (fly) *i* visual monopolar neuron (fly) *j* visual interneuron (locust) *k* pre-motor interneuron (crayfish) *l* mechanical sensory neuron (crayfish); The arrows indicate the signal output zone. (from Cajal, Fisher and Boycott, Burrows, Strausfeld, O'Shea, Rowell and Reichert). The illustration has been taken from: H. Reichert; *Neurobiologie*, page 23 [9].

altered as the action potential propagates along the axon. Generally, action potentials result from ion currents - mainly sodium and potassium - through specific channels[1] floating into and out of the neuron. These channels are transmembrane proteins, which regulate the flow of ions along their electrochemical gradient. This gradient is orientated perpendicular to the membrane. Once an action potential is induced, the changing ion concentration and the corresponding potential changes will open channels in the neighbourhood. In this way, the action potential propagates along the axon.

The connections between neurons are called synapses (see Fig. 2.3). If a neuron sends a signal across a synapse, it has become standard nomenclature to refer to the sending neuron as the presynaptic cell and to the receiving neuron as the postsynaptic

[1]The channels are highly selective to the ion type, parameters steering this selectivity are the ions' size, the sign of its valence charge, and its hydration energy. The ions must peel off their hydration shell in order to pass the pore – the peeling process might be modulated by inner pore elements.

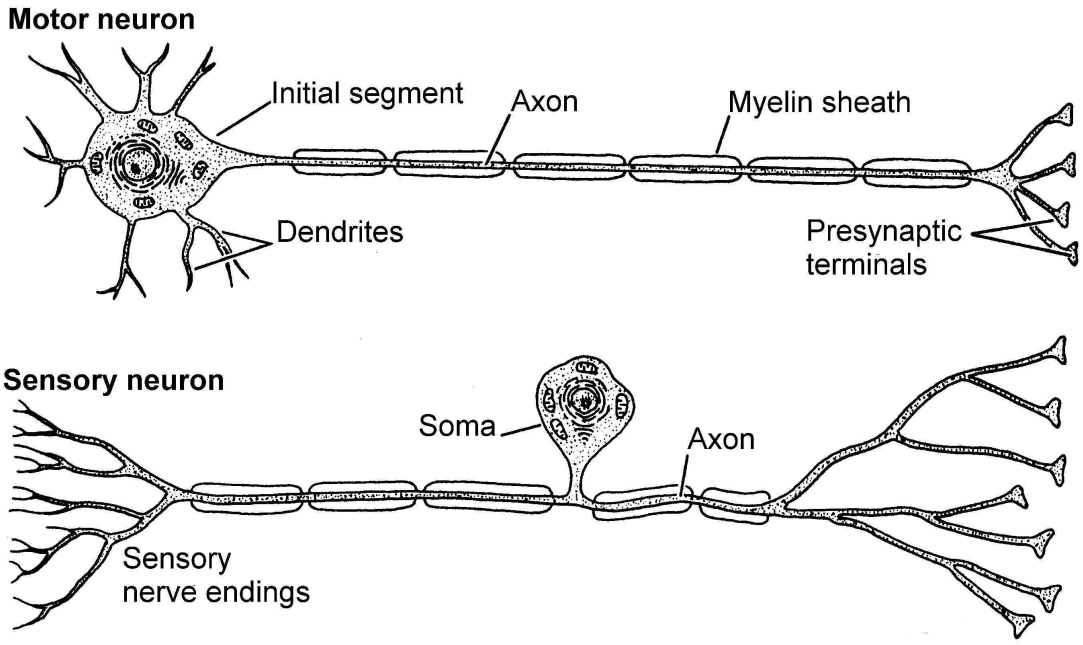

Figure 2.2: **Functional parts of three types of neurons.** *Top* A vertebrate motor neuron which activates muscle cells. The dendrites are located around the soma where a single axon extends from the cell body and finally splits into several presynaptic terminals. *Bottom* A vertebrate sensory neuron which conveys sensory information centrally from the periphery. Here, the soma is located in the middle of the neuron. The illustration has been taken from Z.W. Hall; *An introduction to molecular neurobiology,* page 23 [6].

cell. A neuron can be connected through synapses to a number of other neurons ranging from a few to up to hundreds of thousands. The most common type of synapses in vertebrate brains is the chemical synapse. Here, the axon terminal comes very close to the postsynaptic dendrite or soma, leaving only a tiny gap between pre- and postsynaptic cell membranes, which is called the synaptic cleft. Synaptic clefts usually have a diameter in the range of 20-200 nm. With an action potential arriving at a chemical synapse, calcium-ions enter the presynaptic terminal through voltage-dependent channels. This triggers a chain of biochemical processes, which ultimately lead to the release of neurotransmitter molecules from the presynaptic terminal into the synaptic cleft. As soon as the transmitter molecules reach the postsynaptic side, they are detected by specialised receptors in the postsynaptic membrane. Then pores are opened and allow ions from the extracellular fluid to flow into the postsynaptic terminal. The ion flux, in turn, leads to a change of the membrane potential at the postsynaptic neuron. The voltage response of the postsynapse to any presynaptic action potential is called the postsynaptic potential. Neurons can also be coupled with each other through electrical synapses, which are known as gap junctions. Here, specialised transmembrane pro-

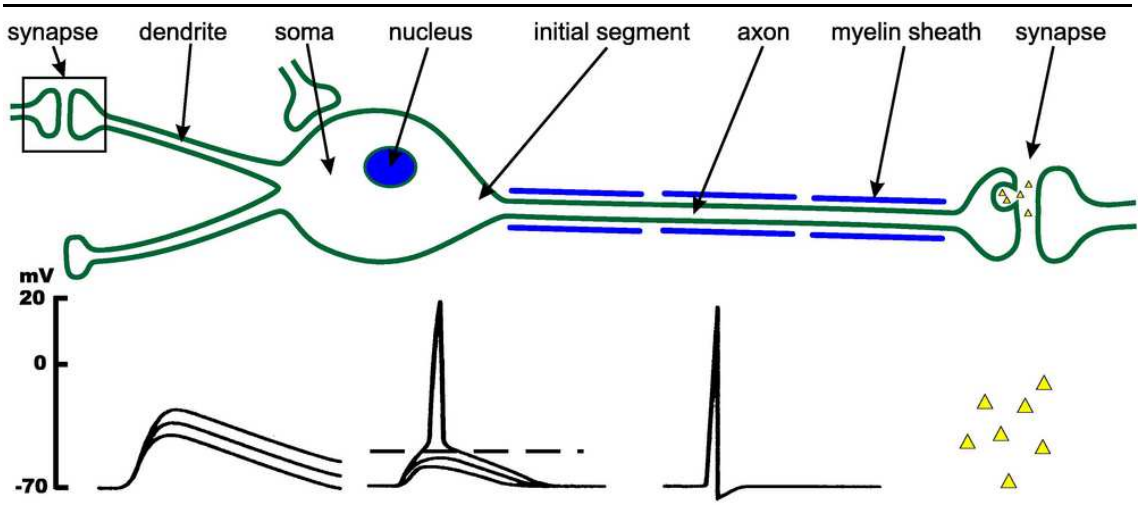

Figure 2.3: **The process of signal transmission in neurons.** A synaptic input signal evokes a gradual synaptic potential (*lower left* graph). If all incoming and integrated potentials exceed a certain threshold at the initial element, an action potential is triggered (*lower middle* graph), which travels along the axon (*lower right* graph). At the axon terminal of the synapse, the action potential triggers the release of neurotransmitter (yellow) into the synaptic cleft. The illustration has been taken from M. Graupner; *A theory of plasma membrane calcium pump function and its consequences for presynaptic calcium dynamics*, page 9 [10].

teins electrically connect the two neurons in a direct way. However, in the framework of this thesis they will not be considered, since neuronal signals are mainly transmitted by chemical synapses.

To summarise: Both the synaptic transmission and the propagation of action potentials and postsynaptic potentials in neurons themselves are achieved by ion fluxes through specific ion channels. These channels are formed by transmembrane proteins and exhibit a voltage and time dependent opening dynamics.

2.2 The importance of calcium

One of the most universal signalling agents in animal cells is the calcium-ion. That fact has winking been paraphrased by O. Loewy in 1959: "Ja, Kalzium, das ist alles!" (found in [11]). On the level of individual cells, calcium originates from external and internal sources. External calcium enters the cell from the outside by passing through transmembrane channels. Alternatively, internal calcium-stores release calcium-ions through other types of transmembrane channels; in this case, the channels cross the membranes of intracellular organelles. In general, a prolonged increase in the calcium-concentration can be lethal for cells, whereas moderate calcium-fluxes trigger vital processes within or around cells. The signal transmission summarised in Fig. (2.4) features characteristics which are sensitive to both the spatial and the temporal resolution of the

corresponding underlying calcium-dynamics [11, 12, 13, 14]:

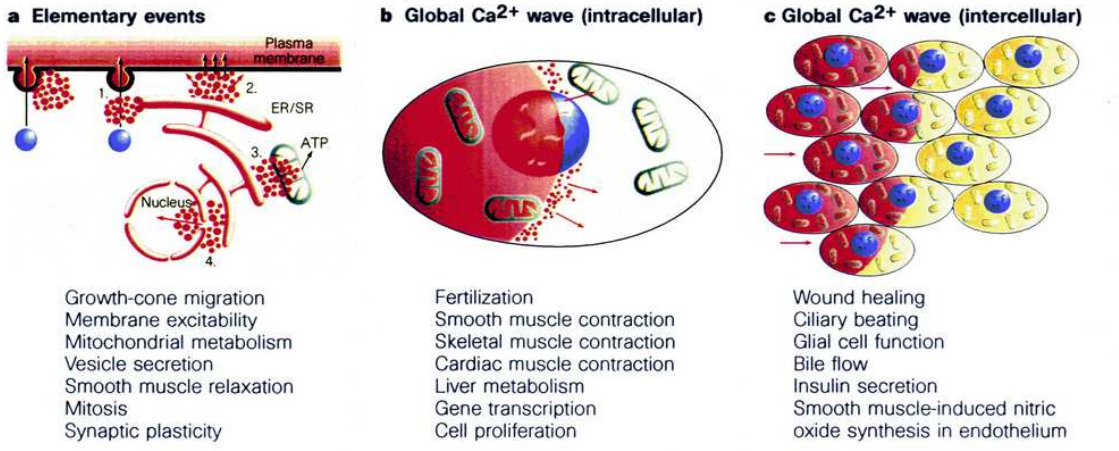

Figure 2.4: **Spatiotemporal aspects of calcium signalling.** *a* Elementary events (red) result from the entry of external calcium across the plasma membrane or release from internal stores in the endoplasmic or sarcoplasmic reticulum (ER/SR). They generate localised concentrations of calcium that can activate many processes, including export of cellular material (1), opening of potassium channels (2) and metabolism in the mitochondria (3). The calcium signal can also enter the nucleus (4). All of these processes respond to the very high concentrations of calcium, that build up within the sub-domain of the elementary events. *b* Global calcium signals are produced by coordinating the activity of elementary events to produce a calcium wave, which spreads throughout the cell. *c* The activity of neighbouring cells within a tissue can be coordinated by an intercellular wave that spreads from one cell to the next. The illustration has been taken from: M. J. Berridge et al.; *Calcium – a life and death signal,* page 645 [15].

Single calcium-peaks are used to activate certain cellular processes, such as secretion of cellular material in membrane-bound vesicles or muscle contraction. Near the cytoplasmic face of the cell membrane, regions of extraordinary activity (often called microdomains) can emerge, related to specific processes which take place nearly exclusively in the immediate vicinity of individual channels [16]. Furthermore, calcium-oscillations occur with different periods related to different systems: 0.1-0.5 s (local in smooth muscles), 10-60 s (global in liver cells), 1-35 min (global in human oocyte), 10-20 h (local in cell division). In these examples, the word "local" refers to fluctuations in the calcium-concentration on the subcellular level. In contrast, "global" refers to mostly periodic inhomogeneities in the calcium-concentration, both spatially and temporally, on the scale of entire cells or beyond. The oscillations follow a regular pattern, waves that propagate throughout the cell or through compounds of cells up to the level of tissues. These phenomena are highlighted by the following examples:

- Fertilisation: In mammals life begins with fertilisation, when the sperm interacts with the egg to trigger a calcium-oscillation, that persists for several hours [17].

This prolonged period of repetitive calcium-pulses initiates the developmental programme by stimulating the enzymatic machinery involved in the cell-division cycle. However, the mechanism that drives this calcium-oscillator (with a period of 10-20 h) remains a mystery up to now. A popular assumption is that it may depend on periodic increases in the level of a diffusible intracellular messenger.

- Cell proliferation: A prolonged period of calcium-signalling – similar to that in fertilisation – is an important growth signal for many cells. Conversely, cell proliferation can be reduced by interfering with the generation or action of calcium-signals [18].

- Synaptic transmission: Here, calcium plays a key role in the release of neurotransmitter molecules [19, 20]. If an action potential arrives at the presynaptic terminal, the secretion of neurotransmitters is activated. Elementary calcium-signals caused by voltage-dependent channels are used to produce brief, highly localised peaks. They trigger the release of vesicles containing the neurotransmitter. This phenomenon is a prime example for a localisation of processes on the subcellular level, connected with the keyword "microdomain" mentioned above. But also in the postsynapse an increased level of the calcium-concentration occurs during repetitive stimulation. In general, the calcium-signals might exhibit a modulation, either in frequency or in amplitude, linked with different types of processes:
  Frequency modulation: Neurons use frequency modulation to select different cascades of messengers to be released. In order to rely on such frequency-coded signals, cells have developed "decoders" that respond to the frequency and longevity of the calcium-signals. Probably the best-known example is an enzyme (called calcium/calmodulin-kinase II), which regulates other messenger proteins and relies on calcium. It works by "counting" calcium-peaks and varies its activity accordingly [21]. The enzyme itself is composed of many identical subunits. They are activated to varying degrees depending on the frequency of the calcium-oscillations.
  Amplitude modulation: It has been shown that cells can interpret modest changes in the concentration of calcium. Correspondingly, different genes are activated by varying the amplitude and duration of the calcium-signals [22, 23]. The two cascades (frequency modulated and amplitude modulated) introduced above are presumably involved in phenomena which change synaptic efficacy and will be discussed in more detail in the next section.

2.3 Phenomena changing synaptic efficacy

This section is devoted to a more detailed discussion of phenomena that change synaptic efficacy, which are commonly called synaptic plasticity [24]. These phenomena are central to questions related to memory processes, in particular for short-term memory, when they are analysed in terms of temporal changes on the level of individual synapses. The underlying picture relates training effects to long-lasting changes in the efficacy of signal transmission through the network of neurons. Clear evidence for

such a picture to grasp at least the main features of the basic interrelations of the key players stems from [25]. In this experiment the production of a certain class of calcium-permeable transmembrane proteins has been suppressed. It has been argued that this suppression blocks some of the messenger cascades important for the efficacy of signal transmission. Without these proteins the learning behaviour of rats deteriorated significantly. In a counter-experiment the production of these proteins had been stimulated, leading to an improved learning behaviour.

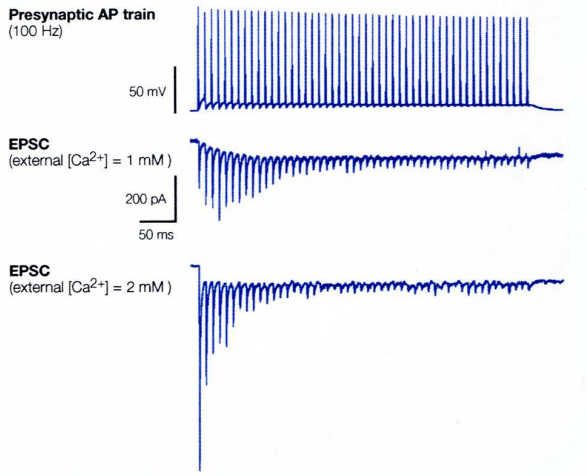

Figure 2.5: **Short-term depression (STD) and facilitation (STP) in a Calyx-of-Held-type synapse.** Presynaptic action potentials (APs; *top panel*) and excitatory postsynaptic currents (EPSCs) during a 100-Hz train at an extracellular Ca^{2+}-concentration of 1 mM (*middle panel*) or 2 mM (*bottom panel*) in a brainstem slice from a 9-day-old rat. At 1 mM $\left[\mathrm{Ca}^{2+}\right]$, EPSCs are initially facilitated; depression is observed later in the train. At 2 mM $\left[\mathrm{Ca}^{2+}\right]$, severe short-term depression is observed. The presynaptic pipette contained a low concentration of an exogenous $\left[\mathrm{Ca}^{2+}\right]$-buffer (50 M BAPTA). The illustration has been taken from: H. von Gersdorff and J.G.G. Borst; *Short-term plasticity at the Calyx of Held*, page 57 [26].

The efficacy changes take place both on the level of amplitude and slope of the postsynaptic potential at onset and can be measured as changes in quantal parameters of the postsynaptic response [27]. Quantal in this context refers to the fact that the peak of the postsynaptic current can be interpreted as a quantised signal which corresponds to the fixed number of neurotransmitter molecules within vesicle. In general, the effects of plasticity can be classified according to their duration and to their amplifying or dampening effect. The latter is usually known as potentiation or depression, respectively. In potentiation (depression), the efficacy of synaptic transmission is enhanced (decreased), due to a barely known combination of two possible reasons: On the presynaptic side the number of released neurotransmitters is increased (reduced), on the postsynaptic side, the number and and/or permeability of activated ion channels

is raised (lowered). The following types of plasticity effects exist in dependence from their duration: Short-term potentiation (STP), short-term depression (STD), long-term potentiation (LTP), long-term depression (LTD).

A feature common to all potentiation or depression effects is that their induction is correlated to a changed calcium-influx into the pre- and/or the postsynapse compared to the single action potential synaptic transmission. A high-frequency induction stimulus opens channels, through which calcium-ions flows into the presynapse and – after the signal has been transmitted through the neurotransmitters – also into the postsynapse. This causality has been exemplified for LTP through: LTP induction is suppressed when a chelator is added to the cytoplasm which binds calcium-ions [28]. Furthermore, LTP can be induced by an experimentally induced calcium release into the cytoplasm [29]. In the following, the different potentiation and depression modes and their induction mechanisms will be shortly highlighted. It is thought as an presentation of the most important features. Nevertheless, an excellent introduction into this area of research is given in [30].

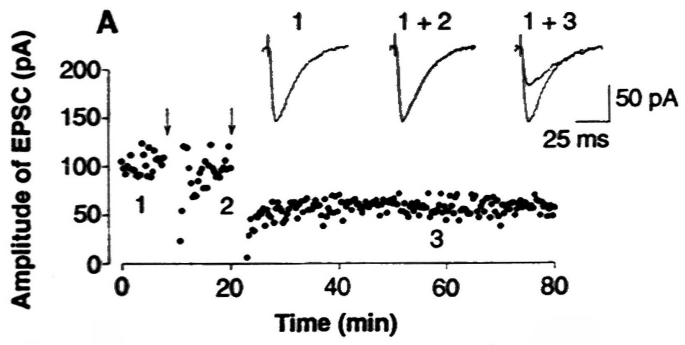

Figure 2.6: **The induction of Long-term depression (LTD) and its dependency on postsynaptic depolarisation and intracellular Ca^{2+}-concentration.** Excitatory postsynaptic currents (EPSCs) have been recorded before and after applying a LTD stimulus (*Top*). LTD has been induced by stimulating the Shaffer collateral pathway at 5 Hz for 3 to 4 min in current clamp mode (arrow 2 in the *lower* graph). The same stimulation was used during voltage-clamp conditions at -70 mV (arrow 1 in the *lower* graph). The pipette contained a standard intracellular solution (0.4 mM Ca^{2+} and 1.1 mM EGTA). The illustration has been taken from: V.Y. Bolshakov and S.A. Siegelbaum; *Postsynaptic induction and presynaptic expression of hippocampal long-term depression*, page 1149 [31].

STP and STD: Short-term refers to manipulations lasting for tens of milliseconds up to seconds [26]. All synapses show some form of short-term potentiation (often called facilitation), short-term depression or a mixture of both, which is induced by the application of a stimulus with a frequency of roughly 10-500 Hz. During application of the stimulus the following changes in the amplitude of the postsynaptic response can be

measured (illustrated in Fig. 2.5): STP is observed as an increase in the amplitude of the postsynaptic response caused by the first individual action potentials. It is directly followed by STD – a continuous decrease in the amplitude of the postsynaptic response, which saturates during stimulation. The extent of STP or STD varies at a given synapse depending on stimulus frequency, type of neuron, the stage of development, and neuromodulation. Within a particular frequency range, some synapses show extensive potentiation or strong depression, whereby both effects may arise from both presynaptic and postsynaptic mechanisms. In general, the efficacy of the presynapse during synaptic transmission depends on the number of vesicles and/or neurotransmitter molecules within the vesicles, that are available for release, on their calcium sensitivity, and on the properties of the calcium-peaks themselves, to which the pool of vesicles is exposed. The efficacy of the postsynapse during synaptic transmission depends on the sensitivity of the ion-permeable receptor to the neurotransmitter and the overall number of active receptors.

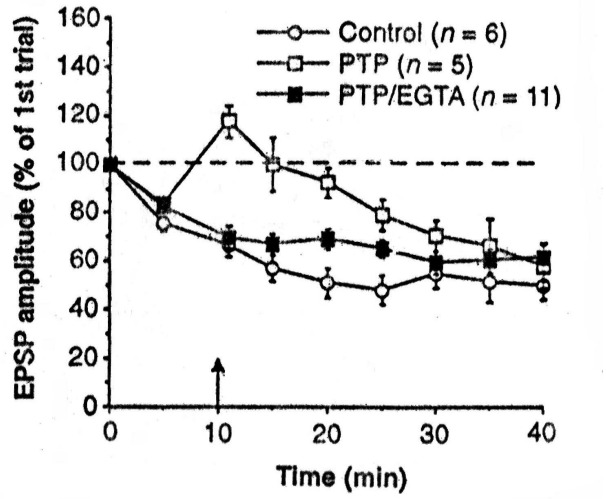

Figure 2.7: **The induction of post-tetanic potentiation (PTP) and its dependency on calcium.** PTP and PTP/EGTA of excitatory postsynaptic potentials (EPSPs) caused by a tetanus (20 Hz for 2 s) applied at time 10 min (arrow). PTP is reduced by presynaptic injected Ca^{2+}-buffer EGTA. The illustration has been taken from: J.X. Bao et al.; *Involvement of pre- and postsynaptic mechanisms in posttetanic potentiation at Aplysia* synapses, page 970 [32].

In the case of STP, the residual calcium within the presynapse is thought to combine with calcium that enters during the next AP, leading to an increase in release. Because of the limited speed of the calcium clearance mechanism, the intra-terminal calcium-concentration will remain elevated for some ms. Accordingly, STP is dominantly caused by presynaptic mechanisms. In contrast, STD could be caused by both pre- and postsynaptic mechanisms: Here, a depletion of the pool of releasable vesicles occurs within

the presynapse during continuous stimulation whereas the neurotransmitter receptors into the membrane of the postsynapse will become desensitised and/or saturated. Of course, other mechanisms may also influence the above effects, such as inactivation of the calcium currents, replenishment of the vesicle pool, heterogeneity of the release probability, or inactivation of the release sites.

LTP and LTD: Long-term effects at synapses of several types of neurons play a role on the time-scale of hours or even days. They can be measured experimentally by the following procedure:

1. Pre-pulse – recording of the postsynaptic potential caused by a presynapse-induced action potential
2. Induction – application of a train of action potentials characterised by frequency and duration
3. Post-pulse – continuous recording of postsynaptic potentials induced by presynaptic action potentials and comparison with the pre-stimulus recording.

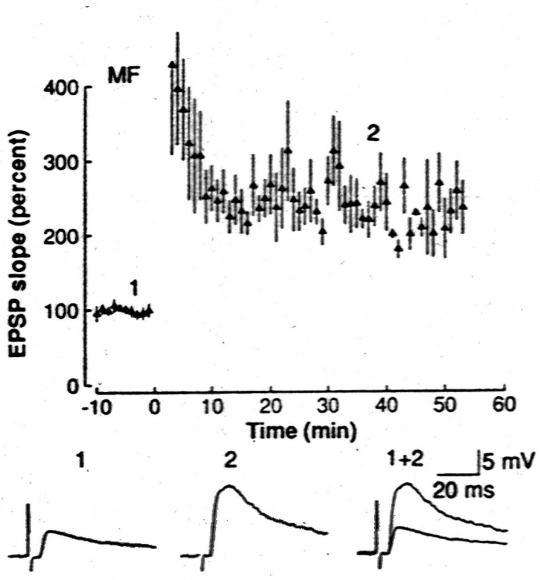

Figure 2.8: **The induction of long-term potentiation (LTP) in mossy fiber-type synapses.** At time 0 the mossy fiber pathway has been stimulated by two trains of action potentials of 1 s duration each at 100 Hz and 10 s intervals. The slope of the excitatory postsynaptic potentials (EPSPs) shows a significant and long-lasting increase (*upper* graph). *Below* the graph individual EPSPs are displayed which show an increase in the amplitude of the EPSPs. The time course of LTP in mossy fiber has been recorded in normal Ringer solution. The illustration has been taken from: R.A. Zalutsky and R.A. Nicoll; *Comparison of two forms of long-term potentiation in single hippocampal neurons*, page 1620 [33].

LTD (see also Fig. 2.6) is induced by a low-frequency stimulus of around 2-10 Hz, lasting for several minutes, whereas LTP (see also Fig. 2.8) is triggered by a single or repeated stimulus (lasting for a couple of seconds) with a frequency of around 20-200 Hz. Interestingly, at some types of neurons the synapses can be switched from an LTP-state into an LTD-state and vice versa. This behaviour shows that the synapses can respond very dynamically to different stimulus patterns. Again, the common induction key for both long-term effects is that channels in the presynapse and, indirectly, receptors in the postsynapse (this receptor will be described in Sec. 3.1) are opened such that calcium-influx is enabled. LTP is definitely induced by both pre- and postsynaptic mechanisms. But it can be hypothesised that, in principle, the same types of messenger cascades (in both, pre and postsynapse) but with different consequences play a significantly role for the induction of LTP. These messenger cascades can be split into two phases:

1. The early phase of LTP is reversible (see also Fig. 2.7), which means that the synapse returns slowly (in the range of minutes) to its ground state. It has been argued, that the calcium-peaks within the pre- and postsynapse couple to a messenger protein[2]. It usually remains inoperative for single action potential stimuli and is activated depending on the frequency of the stimulus, equivalent to the frequency of the calcium-peaks. The messenger protein activates a protein kinase which in turn enables additional transmembrane ion-channels in the postsynapse [34] or more proteins responsible for neurotransmitter release from the presynapse [35, 36]. This messenger cascade probably plays the dominant role for moderate stimulation frequencies (20-50 Hz) and is more correlated to the frequency of the stimulus than to the peak amplitude.

2. The late phase of LTP leads to an long-lasting enhancement of the synaptic efficacy. It has been hypothesised that calcium couples to one or more additional messenger proteins[3], which are activated depending on the amplitude of the calcium-concentration. When operative, this messenger protein finally facilitates the enhanced production of proteins amplifying the release of neurotransmitter in the presynapse or the production of ion channels in the postsynapse [34]. It should be stressed that as a well-established fact LTP exhibits threshold behaviour with respect to the frequency. To support or falsify the hypothesis of amplitude dependence has been one of the goals of this thesis. The corresponding results can be found in Sec. (5.3.3) and Sec. (5.3.4).

[2]Calmodulin is an important messenger which can bind calcium to its four binding sites. Depending on the number of bound calcium ions, the calcium/calmodulin complex can activate the calcium/calmodulin-dependent protein-kinase II. The latter possibly leads to a phosphorylation of target proteins, i.e. a phosphor group is attached to the protein [8]. This manipulation activates the target protein, for example an ion channel. In general, a large number of proteins can be either activated or inactivated by phosphorylation or dephosphorylation.

[3]For example the calcium/calmodulin-dependent protein kinase IV which may regulate the synthesis of ion channels into the postsynapse [34] or the activity of a further messenger protein, calcineurin may regulate the number of releasable vesicles [37].

Chapter 3

The synapse

The goal of this chapter is to discuss the dynamics of synaptic transmission in detail, i.e. including pre- and postsynaptic terminals which connect two neurons through the corresponding synapse. In a first step, a membrane model of the overall system will be introduced. Then, flux dynamics of various ions through the presynaptic terminal are addressed, before buffering mechanisms in the presynapse are dealt with. Finally, the use of fluorescence indicators for measurement of calcium concentrations and distributions is discussed.

3.1 Synaptic transmission

In order to develop a membrane model for the dynamics underlying synaptic transmission a toy system is introduced. This system serves as a starting point, because it provides an intuitive idea about its ground state. It consists of a volume filled with water, separated from a surrounding water bath through a membrane in which specific channel proteins are embedded. Within the water, a number of different ions, in particular sodium, potassium, calcium, and chloride, are dissolved. They can traverse the membrane in both directions through the channels. The specific permeability of the channel proteins, however, is different for each ion type. The electrochemical gradient of the ions is responsible for net fluxes through the membrane. Therefore, the equilibrium state of this system is characterised by the balance of thermal fluctuations and the

Ion	Extracellular concentration	Intracellular concentration
Na^+	145 mM	10 mM
K^+	5 mM	140 mM
Cl^-	110 mM	17 mM
Ca^{2+}	2 mM	100 nM

Table 3.1: **Free ion concentrations of the 4 major ion-types in mammalian neurons.**

electrical and chemical gradients resulting from charge and concentration differences of the solvent ions (see also Fig. 3.1).

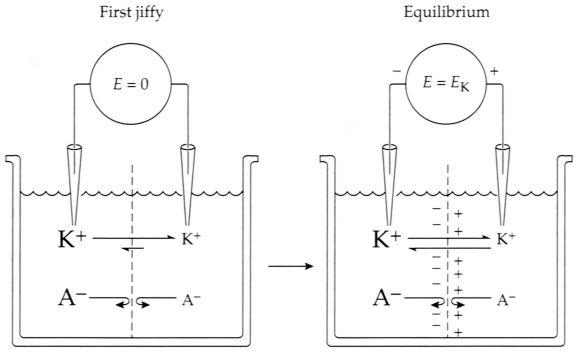

Figure 3.1: **Diffusion Potentials in Pores.** A membrane with perfectly K^+-selective pores separates solutions with different concentrations of a potassium salt, (KA). A voltmeter records the potential across the porous membrane. When the salt solutions are poured in, there is no membrane potential ($E = 0$). However, as few K^+ ions diffuse from the left side to the right, a potential develops, with the right side becoming positively charged. Eventually, the membrane potential reaches the Nernst potential for K^+-ions ($E = E_{\mathrm{K}}$). The illustration has been taken from: B. Hille; *Ion channels of excitable membranes*, page 13 [38].

Consequently, an equilibrium membrane potential can be defined as the potential difference between inside and outside of the volume. This equilibrium potential is connected to the equilibrium concentration gradients of the different ion types. The composition of these different concentration gradients as well as the equilibrium potential for each single type of ion is temperature dependent and can be described by the Nernst equation, confer Eq. (4.38). In order to map this toy system to neurons it is sufficient to take a closer look at the ground state parameters: The outside medium, i.e., the extracellular space, is defined to be at ground potential (0 mV). Hence, the membrane potential is simply given by the intracellular potential, typically values being situated between -40 and -95 mV in equilibrium. Typical ion concentrations are presented in Tab. (3.1).

The equilibrium state described above can be perturbed by action potentials. As outlined before, these are short electrical pulses travelling along the neuron's axon. Action potentials are depolarisations of the membrane potential and when an action potential reaches a presynaptic terminal, this depolarisation opens voltage-dependent calcium-permeable ion channels in the membrane (for an illustration, see also Fig. 3.2). This allows calcium-ions to flow into the presynaptic terminal, since the electrochemical calcium-gradient points inwards, confer Tab. (3.1). The increased intracellular calcium-concentration is responsible for the release of neurotransmitters into the synaptic cleft. The underlying reaction cascade in the presynaptic terminal is called exocytosis and proceeds in the following way:

1. First of all, before calcium influx takes place, the vesicles fill with neurotransmitter molecules. Vesicles are intracellular nearly spherical closed membranes. They consist of the same material as the cell membrane, namely lipids. The filling procedure actually mainly takes place some distance away from the presynaptic terminal, and, hence, the vesicles have to travel there.

2. Still before calcium influx, the vesicles are transported by motor proteins [39] along cytoskeleton filaments towards regions on the membrane, where the neurotransmitter can be released. Within this "active zone" the release of neurotransmitters takes place. Before, the vesicle is caught by large protein complexes, which exist only in the active zone. Afterwards, the vesicle is docked to the membrane.

3. The docked vesicles are "primed", i.e. they are equipped with proteins that can bind to membrane-bound proteins themselves in order to prepare them for release. Within this state the vesicles become sensitive to calcium: A calcium-signal brings the membranes of vesicle and cell-terminal into close proximity, such that they fuse in order to minimise their surface energy. When the vesicle fuses with the membrane of the terminal the inner-vesicle space becomes extracellular thus expelling a defined quantity of neurotransmitter into the synaptic cleft.

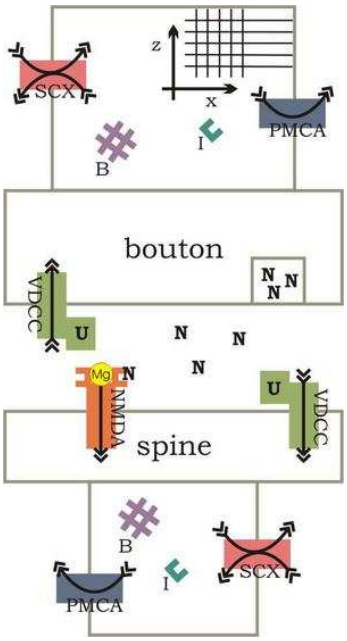

Figure 3.2: **Schematic illustration of important calcium-dependent mechanisms of synaptic function.** If an action potential enters the presynapse (bouton), voltage-dependent calcium channels (VDCC) open and calcium-ions flow into the bouton. The incoming calcium-ions bind to endogenous buffer molecules (B) and – if added – to exogenous buffer molecules (I). In addition, calcium-ions trigger the release of neurotransmitters (N) which diffuse through the synaptic cleft. The neurotransmitters bind to postsynaptic (spine) receptors (not shown), generating the postsynaptic potential. During repetetive stimulation the spine cumulatively depolarises. Then, calcium-permeable recepetors (NMDA) can open. This is caused by a conjunction of two processes: Binding of neurotransmitters to the NMDA-receptor and detaching a voltage-dependent magnesium-ion block from the NMDA-receptor. Consequently, calcium-ions enters the postsynapse. Finally, the surplus calcium-ions will be removed from both, bouton and spine through calcium-pumps (PMCA) and sodium/calcium exchangers (SCX).

Vesicles may be recycled by re-contracting the surplus membrane area, a process which is called endocytosis. The released neurotransmitter diffuses through the synaptic cleft and eventually binds to specific receptors located at the postsynaptic membrane. These receptors[1], however, are specific ion-permeable channels, that open once

[1]For example, the sodium/potassium permeable AMPA-receptors which can bind the neurotransmitter glutamate or the chloride permeable GABA-receptors which can bind the neurotranmsitter γ-aminobutyric acid.

the neurotransmitter molecules have bound. The channels are mainly permeable to sodium, potassium, or chloride ions. The ion flux into the postsynaptic terminal causes a depolarising (sodium and potassium – positive charge surplus) or hyperpolarising (chloride – negative charge surplus) pulse, which propagates along the dendrites to the soma of the neurons. Here, the synaptic signals are integrated (both spatially and temporally) respecting their signs. When the integrated signal passes some threshold, a new action potential will be initiated in the postsynaptic neuron. However, in some types of postsynapses there exist also voltage-dependent calcium channels and a further type of a calcium-permeable receptor[2]. This receptor opens also a pore but only when two neurotransmitter molecules have bound and simultaneously the postsynaptic membrane potential is depolarised (physiologically caused by repetitive stimulation). In their equilibrium state these specific channels are blocked by a magnesium ion, which is removed when the membrane depolarises – the channel opens. Thus, extracellular calcium may flow into the postsynapse. The postsynaptic calcium influx is involved in efficacy-changing phenomena, compare Sec. (2.3).

The calcium-ions entering the pre- and the postsynapse are subject to many interactions: For example, they can bind to intracellular buffer molecules. In addition, further release of calcium may be caused through intracellular stores that can be activated by calcium and an additional messenger cascade – a phenomenon called calcium-induced calcium-release.

The remaining calcium surplus in both the pre- and the postsynapse will be transported out of the terminal, mainly by two different transport mechanisms: Calcium-pumps are driven by adenosine triphosphate (ATP), which represents an important source of cellular energy. In addition, the sodium-calcium-exchanger proteins transport calcium by utilising the electrochemical energy of sodium ions, exchanging them with calcium ions.

For a quantitative model of the whole synaptic transmission process, a huge pool of data about all contributing sub-processes is required. Unfortunately, many parameters relevant for different sub-processes are not known up to now and can therefore only be estimated. Accordingly, a detailed model could surely verify or falsify some interesting qualitative patterns of the whole transmission but the predictive power on the level of quantitative features would be quite limited. This problem is alleviated for presynaptic terminals, since there the number of sub-processes and parameters involved is limited. Therefore, within the framework of this thesis the focus is on investigating the calcium-dynamics in presynaptic terminals. The following discussion of relevant proteins will focus on the influx of calcium through specific voltage-dependent channels, on its efflux mediated by pumps and exchangers and on its buffering through intracellular buffer proteins. Finally, a commonly applied experimental method will be discussed, which is employed in investigations of the spatiotemporal dynamics of the intracellular calcium-concentration.

[2] N-methyl-D-aspartate (NMDA)

3.2 Influx of calcium-ions into the presynaptic terminal

Within this section, calcium-permeable channel proteins, consisting of multi-subunit complexes, which form a voltage-sensitive transmembrane pore, will be discussed. The protein subunits themselves are formed by segments. These segments are α-helices built of a polypeptide chain which traverses the membrane. Some of these transmembrane segments carry a "gating charge": During depolarisation of the membrane some segments rotate and the gating charges are displaced into the external crevice. This movement favours a corresponding move of other segments, which leads to an opening of the pore. This has been verified experimentally by observing the charge current resulting from the gating charge movement and the corresponding protein conformation change [38]. The principles of this process are illustrated in Fig. (3.3) for a potassium channel.

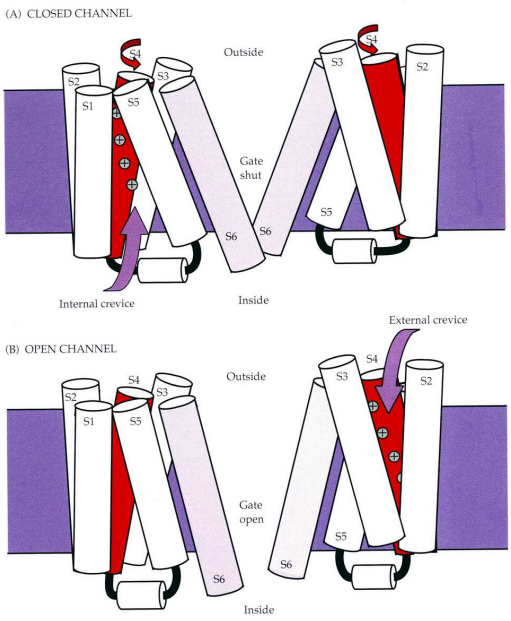

Figure 3.3: **Model for opening of a voltage-gated channel:** The model shows two of the four subunits of a potassium-channel, each with its six transmembrane helices (cylinders S1 to S6). The S4-segments are displayed in red and their gating charges in yellow. The narrow selectivity filter formed by P-loops is not shown. (A) The channel is closed by the S6-segments crossed at the inner end. In a closed channel, the gating charge is mostly exposed to the inner solution via the internal crevice (arrow). (B) During depolarisation, the S4-segments rotate and the gating charges shift into the external crevice (arrow). This motion also favours a movement of the S5- and S6-segments, that opens the pore. Because of the crevices in this model, a rotation of S4 suffices for voltage sensing without any outward movement. The illustration has been taken from: B. Hille; *Ion channels of excitable membranes*, Plate 7 [38].

When the pore opens, calcium-ions flow into the neuron. The amplitude of this

ion current is determined by the electrochemical gradient of calcium. The form of a current through a single pore results from a frequent opening and closing in a stepwise manner (see Fig. 3.4 and Fig. 3.5). This opening and closing proceeds as long as depolarisation continues[3]. The average of the ion currents through the channels results from the characteristic activation dynamics of the ensemble. It can be described by voltage-dependent time constants and by voltage-dependent opening probabilities. Under the assumption of their mutual independence, an average over the dynamics of an ensemble of channels can be translated into a time-averaged dynamics of one channel.

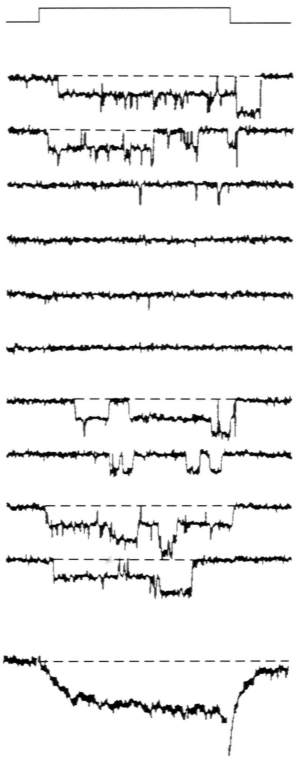

Figure 3.4: **An example for single channel calcium-currents (L-type).** Unitary currents from embryonic dorsal root ganglion cells of chick. Each panel shows 10 consecutive responses to 130-ms depolarisations (applied every 4 s), and, at the bottom, the sum of a larger number of sweeps. The on-cell patch contains at least three channels. Currents in calcium-channels have been emphasised by including 110mM Ba^{2+}, 200nM TTX in the patch pipette, and 5μM BAY K 8644 in bath. T=21°C. The illustration has been taken from: B. Hille; *Ion channels of excitable membranes*, page 13 [38].

Six types of voltage-dependent calcium-channels (VDCC) are known, classified corresponding to their pharmacological properties: They are named L-, N-, P-, Q-, and R-type for high-voltage-activated (HVA) channels and T-type for low-voltage-activated (LVA) channels. Their dynamics is primarily determined by a single subunit, namely the α_1-subunit. The genes encoding the different HVA channel types exhibit an overall matching percentage of nearly 50% [40]. In general, the calcium-influx into the presynaptic terminal is dominated by the P/Q- and N-type channels [41]. Within this thesis it is assumed that each type of VDCC has the same biophysical properties [42, 43, 44] in all kinds of tissues and animals. Because, the actual precision of the experiments, especially in view of the individual biophysical properties of different channel types,

[3]It should be noted that some channel types show inactivation during prolonged depolarisation which might be caused by ball-and-chain-like elements blocking the pore [38].

lies in the error margin of the results of this thesis and it would make no sense to distinguish different subtypes. Concerning the measurements of the P/Q- and N-type channels two additional problems exist: Most measurements have been performed with barium as carrier ion instead of calcium. For other carrier types however, the obtained conductivities differ considerably [42]. Additionally, all results refer to room temperature ($20 - 25°C$). It is well-known [45, 46], however, that biophysical properties are temperature-dependent thereby limiting the applicability of these measurements and their relevance at body temperature. Anyway, it can be expected that deviations due to these short-comings stay within the current experimental accuracy [47, 48, 49].

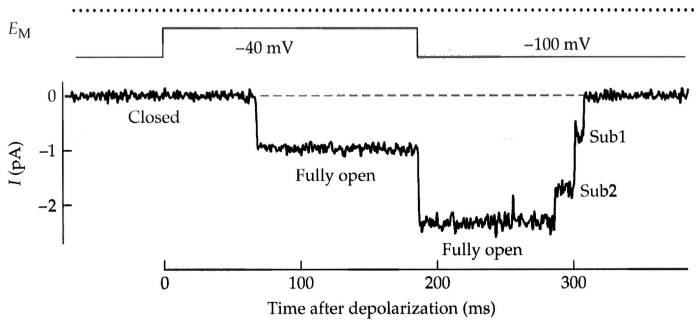

Figure 3.5: **A single channel can open and close through a series of states of lower conductance.** These experiments are designed to exaggerate the duration of sub-states. The fully open state and two smaller sub-states Sub1 and Sub2 are labelled. Current recorded from a single potassium-channel (with pore mutation) during and after depolarisation to -40 mV. One effect of the mutation is to prolong sojourn in the intermediate states, which are only fligthy in the unmutated channel. T=22°C. The illustration has been taken from: B. Hille; *Ion channels of excitable membranes*, page 601 [38].

3.3 Efflux of calcium-ions from the presynaptic terminal

Calcium-efflux from cells is mediated through two major mechanisms: The plasma membrane calcium ATPase (PMCA) and the sodium-potassium exchanger (NCX). The NCX is suited for rapid recovery from high levels of cytoplasmic calcium. Due to its large affinity and low transport rate compared to the NCX, the PMCA is of crucial importance for the fine tuning of cytoplasmic calcium-ion concentration [50, 51]. Both however, are important for the maintenance of calcium-homoeostasis.

The ATP-driven plasma membrane calcium ATPase (PMCA) PMCA acts as a pump and belongs to the P-type ATPase family. Its members utilise the energy stored in

ATP to transport calcium-ions against their electrochemical gradient across the plasma membrane [52]. ATP apparently interacts with the pump at two sites with different affinities [53, 54]. The transport cycle involves the formation and degradation of phosphorylated intermediate states of the pump. Correspondingly, the translocation step of calcium across the membrane is related to a conformation change of the pump [55, 56]. The stoichiometry between transported calcium-ions and hydrolysed ATP of the PMCA pump is most likely 1:1 [50, 53, 54, 57]. The PMCA displays a large calcium-affinity ($K_{\mathrm{d}}^{\mathrm{pm}} \approx$ 0.5-1 μM [50, 52, 53]) and a low transport rate ($\nu^{\mathrm{pm}} \approx$ 30 calcium-ions/s, [51] and private communication with [58]).

The PMCA protein has been found in all mammalian cells [56], whereby the expression level does not exceed 0.1 % of the total membrane protein [50, 54, 59, 60]. An exception is the brain, where the expression level is up to 10 times larger than in non-excitable cells [50, 56]. The PMCA can be stimulated by direct interaction with calmodulin or alternative pathways such as kinase-mediated effects[4]. Another way of stimulation consists in the exposure to acidic phospholipids or polysaturated fatty acids [52, 54]. In the latter case, the stimulation effects predominantly change the calcium-affinity, whereas calmodulin in addition changes the maximum calcium turnover rate of the pump [52, 53, 60, 61].

PMCA pumps appear in four different isoforms. The differences are encoded by four independent genes, which are indicated by numbers 1-4. PMCA1 and PMCA4 are expressed in practically all tissues; in all human tissues PMCA1 is present in a concentration larger than PMCA4 [50, 59]. PMCA2 and PMCA3 have been shown to occur in highly specialised tissues such as brain and heart [50, 59] only. The diversity of pump forms is further increased by alternative mRNA splicing variants, characterised by small letters. There exist more than 26 transcripts which differ in their regulatory properties, for instance in their affinity to calmodulin. They are distributed in a tissue-specific manner [55, 50]. The animal of origin of the pump genes is indicated by a small letter in front, for example "r" stands for rat and "h" relates to human. Referring to the available data from [61], isoform hPMCA2b will be considered in the framework of this thesis.

The sodium/calcium exchanger (NCX): The NCX can move calcium-ions either into or out of cells, depending on the coupled sodium-calcium electrochemical force on the exchanger. This driving force, and thus the net calcium-ion flux mediated by the NCX, may change direction during cell activity, for example, when the membrane potential varies and/or when the cytoplasmic calcium- or sodium-concentration is altered. Consequently, the exchanger can operate in different modes: The calcium-exit mode is defined operationally as a calcium-efflux and sodium-influx. In contrast, the calcium-entry mode is usually identified as a calcium-influx and sodium-efflux. There exist further operation modes of the exchanger which are not relevant for the aim of this thesis and will not considered here. For more details confer to the excellent review about the NCX protein [58]. The NCX protein has several binding sites for calcium- and

[4] Protein kinase A or protein kinase C.

sodium-ions, both at the intracellular and at the extracellular face of the protein. Measurements of coupled calcium- and sodium-ion fluxes yielded a coupling transport ratio of 3 Na^+ : 1 Ca^{2+} when operating in either the calcium-influx or calcium-efflux mode. If the NCX stays in the calcium-efflux mode, the underlying exchange mechanism involves the consecutive or simultaneous binding of 3 sodium-ions at the external site and 1 calcium-ion at the cytoplasmic face. Then, the exchanger may experience a conformational change such that the calcium-ion is transported to the extracellular face and the sodium-ion is released to the cytoplasm. Accordingly, for the calcium-influx mode, this process appears vice versa. The NCX protein comprises a low affinity for cytoplasmic calcium ($K_{\mathrm{d}}^{\mathrm{nc}} \approx$ 0.6-3 mM) with a large calcium-transport rate ($\nu^{\mathrm{nc}} \approx$ 1000-5000 calcium-ions/s) [50, 51].

In the case of the NCX three different coding genes (NCX1-3) and 32 different splicing variants are known [58, 62, 63]. These genes have similar overall structure and moderate amounts of sequence identity. They have been characterised in diverse mammalian species including human, rat rabbit, etc. Especially the NCX1-subtype represents the dominant exchanger gene expressed in the brain.

3.4 Buffering of calcium-ions to intracellular molecules

Intracellular calcium-buffers belong to the family of proteins with an EF-hand[5] [57, 65, 66]. Depending on the cell type they occur in different concentrations in the range 10 - 1200 μM. The buffer proteins come with different numbers of binding sites ranging from one to six. The most important proteins for calcium include parvalbumin, calretinin, calcineurin, calbindin and calmodulin [57]. Collectively, these mobile buffers absorb 95-99 % of the total intracellular calcium load, leaving only a minor fraction as free calcium-ions [7, 57]. The intracellular mobility of the buffers is defined by their comparably low diffusion constant in cytoplasm $D_{\mathrm{b}} \approx 10\ \mu\mathrm{m}^2/\mathrm{s}$. In addition, possible fixation to the cytoskeleton or to the membrane may render them immobile. Their possible attachment to the cell membrane and cytoskeleton leads to an important role of the buffering proteins for the diffusion of calcium-ions and the spatial propagation of calcium within the cytoplasm. The calcium ions can be fixed within the influx region by binding to these buffer molecules.

In general, the buffers are characterised by slow or fast kinetics with respect to the dynamics of calcium binding processes. However, only very little is known about specific kinetic schemes and the appropriate microscopic rate constants, which in turn are described by a set of essentially free parameters. To minimise the number of parameters in the framework of this thesis only calmodulin is taken into account. This choice reflects the fact that this buffer is the most important one in neuronal cells. Calmodulin contains four EF-hand motifs, or binding sites. Individual binding sites within one

[5]The classical EF-hand is a helix-loop-helix motif characterised by a sequence of usually 12 residues with a certain pattern [64]. This sequence of 3-dimensional coordinates forms a spatial loop that can accommodate calcium or magnesium with subtle differences in affinity. The participating residues comprise exposed polar binding sites in order to interact with the Ca^{2+}-ion.

protein may have different affinities for calcium ions, depending on the overall occupancy. The corresponding microscopic rate constants of the individual binding sites can vary among each other between the two extreme cases: Either all binding sites act independently (with equal microscopic forward rate constants) or the binding sites act highly cooperative (with ongoing enlarged forward rate constants relative to the number of occupied calcium ions). The calmodulin protein liganded with four calcium-ions, is capable of calcium-dependent regulation of the activities of a large array of different target proteins, including enzymes, ion pumps and channels [67].

3.5 Fluorescence indicators for detection of calcium-ions

In the previous sections it has been shown that ions such as calcium play an important physiological role in regulating a wide variety of cellular functions. For a better understanding of this role it is mandatory to measure the ion concentrations inside living cells. Fluorescence is the best of all known techniques for non-invasive measurements of the spatiotemporal dynamics of the calcium-concentration in cells [68].

Calcium ions naturally do not fluoresce. They can be visualised indirectly, however, by complexing them with fluorescent molecules. Molecules that bestow fluorescence properties on non-fluorescent species are called probes, indicators, or dyes. Fluorescent probes can be designed to exhibit a high affinity for a specific ion. The typical fluorescent dye has a single excitation and emission wavelength. Fluorescence in general proceeds in three steps:

1. Excitation of the molecule(s) in question: This is achieved by the molecules absorbing photons of a fixed wavelength $\hbar\,\omega_{\mathrm{ei}}$ corresponding to a fixed excitation energy.

2. Life-time of the excited state: This time interval usually spans 1-10 ns. During the life-time the fluorophore may experience conformational changes and interactions with its environment. These interactions may cause a loss of the excitation energy through dissipation.

3. Fluorescence emission: A photon of energy $\hbar\,\omega_{\mathrm{em}}$ is emitted. In biomolecules this energy does not need to be equal to $\hbar\,\omega_{\mathrm{ei}}$, in general, $\hbar\,\omega_{\mathrm{em}} < \hbar\,\omega_{\mathrm{ei}}$. This difference is called the Stokes shift.

The fluorescence intensity displays the calcium-concentration-dynamics through the underlying binding to the local calcium-ions. In addition to the dynamics of the calcium concentration, the fluorescence intensity becomes also dynamically by the underlying binding process of the fluorescence molecules to the calcium ions. Furthermore, it depends on several factors such as the experimental setup or the thickness of the observed volume. Therefore, the fluorescence intensity is a direct visualisation of the spatiotemporal dynamics of the calcium ions and can be utilised to calculate absolute calcium concentrations, see Sec. (4.7).

Chapter 4

The model for the system: SYNDICAD

4.1 Introduction

Several theoretical and numerical approaches exist, which describe excitable membranes and synaptic transmission. A comprehensive introduction to general aspects of single neuron modelling can be found in [69]. A precise mathematical analysis of single neurons as well as of neuronal network models is given in [70]. Furthermore, [71] constitutes a practical guideline for computer simulations of Hodgkin-Huxley-like neuron models. A modelling introduction for neuronal Ca^{2+}-dynamics is given in [2] and a guideline for using Markov kinetic models can be found in [3]. More generally, questions concerning mathematical methods for the solution of reaction-diffusion systems have been discussed in [70]. A introduction to pure diffusion approaches is given in [72]. Usually such methods involve the integration of ordinary and partial differential equations to describe large numbers of ions. Sometimes, also Monte Carlo and Green's Function Monte Carlo approaches are applied in order to investigate the behaviour of a limited number of ions.

Many theoretical studies investigate selected phenomena, which are related to the Ca^{2+}-dynamics in presynaptic or postsynaptic terminals in response to different patterns of stimuli. Traditionally, the first approaches towards a quantitative analysis of the intracellular Ca^{2+}-dynamics have been triggered by the question concerning the importance of Ca^{2+}-ions for the induction of long-term potentiation. For example, in [5] the dynamics of Ca^{2+}-ions in postsynaptic terminals in response to such stimuli has been investigated. Further studies, such as [73], have considered the importance of special Ca^{2+}-influx pathways for the induction of long-term potentiation. The next level of modelling – see for example [74] – takes into account different messenger cascades, which may induce long-term potentiation. In addition, different aspects of the neurotransmitter release at presynaptic terminals and the associated short-term plasticity have been investigated in a considerably number of studies: In [4] the importance of

local Ca^{2+}-inhomogeneities for the paired-pulse facilitation has been discussed in detail. An extended model of the neurotransmitter release cycle, has been presented in [75], it may account for some aspects of short-term depression. Furthermore, the role of intracellular organelles with the capability to store and release calcium and their relevance for long-term potentiation have been analysed in [76, 77]. Indeed, most of the incoming calcium ions are bound to intracellular buffers [78], which emphasises the importance of this issue. This effect constitutes a significant discovery. It has triggered extensive investigations about the role of slow and fast as well as mobile and immobile intracellular buffers [79].

As shown in Sec. (2.2), Ca^{2+}-ions represent an important cellular messenger. The messenger cascades in general can be activated by different dynamics and amplitudes of the concentration of the same ion. Thus, a detailed analysis of the Ca^{2+}-fluxes is of great interest. Unfortunately, many properties of the Ca^{2+}-dynamics in cells are concealed in a complex interaction of proteins which in turn determine the Ca^{2+}-fluxes. To be able to design a realistic model of intracellular ion activity, which provides quantitative predictions, a precise description of the properties of these proteins has to be incorporated.

In the past decades, data covering ion fluxes through single-proteins and the time-dependence of the corresponding activation dynamics had not been available in sufficient detail. To overcome this lack of experimental data, investigations were performed which were based on models with some questionable assumptions and unmeasurable parameters. However, the situation has improved significantly: Information concerning single-protein characteristics has become increasingly available. With the emergence of both quantitatively and qualitatively improved results the experiments have started to challenge the various models. SYNDICAD is an attempt to base a model for Ca^{2+}-dynamics on experimental single-protein data. Hence, one of the major questions addressed in this thesis is whether this is possible at all at the moment. In other words, it remains to be tested, whether the current information on single-protein properties is sufficient in order to explicitly describe the activation and activity of each protein involved in transmembrane as well as intracellular Ca^{2+}-fluxes.

As outlined in Ch. (2), the processes underlying activation and activity of the single-proteins are in fact determined through a complex set of chemical reactions and through conformation changes of the protein structure. Evidently, at this stage it is not in the realm of our abilities or our knowledge to design a model which is based on complete microscopic mechanisms of protein behaviour. In contrast, single-step kinetics, which has been the method of choice, intrinsically is too simplistic to provide a true dynamical understanding of the Ca^{2+}-fluxes. However, a first step towards a correct description of the Ca^{2+}-dynamics is to merely reproduce the experimental results of protein activation and activity. In SYNDICAD this is attempted through a macroscopic and therefore reductive ansatz, namely by simple and physically falsifiable kinetics.

The link between the single-protein characteristics and those properties, which define the ion dynamics in a given volume, is missing. This link is far from being trivial and subject to modelling. Only comparison with experimental data allows to deter-

mine whether this kinetic model is up to the task of describing the intracellular Ca^{2+}-dynamics. In SYNDICAD, the connection of single-protein dynamics and its effect on the large-scale properties of the cell is provided by considering the macroscopic behaviour of the proteins, in particular their surface densities. Due to the lack of direct measurements of protein surface densities and because their values are expected to strongly depend on the cell under consideration, the densities are fitted to fluorescence measurements, which will be demonstrated in Sec. (5.3.1). In addition, constant external conditions, such as temperature, are taken into account.

Of course, local inhomogeneities of the Ca^{2+}-concentration play a crucial role for some important phenomena, like the release of neurotransmitters, which is coupled to local Ca^{2+}-peaks near the Ca^{2+}-influx zone. Hence, any model aiming at describing such phenomena must account for the spatiotemporal behaviour of the Ca^{2+}-ions. In SYNDICAD the Ca^{2+}-concentration is subject to intracellular diffusion processes which eventually result in local inhomogeneities. This enables SYNDICAD to provide a physical model of a large set of intracellular phenomena.

A further aim of this thesis has been to design a model which clearly separates between properties common to all types of neurons and those which are specific for them. In principle, SYNDICAD is universally applicable to any type of neuron by adjusting the type-specific parameters only.

4.2 The main model equations

A presynaptic part of the synaptic signal transmission cascade is described by using a coupled reaction-diffusion differential equation (DEq) system. This is a system of partial DEqs, which are of first order with respect to temporal and of second order with respect to spatial coordinates. The system focuses on the spatiotemporal free Ca^{2+}-dynamics in a presynaptic terminal due to a predefined, time dependent membrane potential. The model geometry consists of a reaction volume which is situated in a homogeneous extracellular space. A cylindrical symmetry of the reaction volume is assumed. However, for single compartments, the results remain valid for other shapes provided that the surface to volume ratio is conserved.

The static boundary conditions of the equation system are set by the cell membrane which separates the extracellular space from the intracellular space. Source and sink terms of the intracellular Ca^{2+}-concentration are embedded into this membrane and correspond to the specific action of membrane proteins. The model represents these terms by a set of DEqs. In addition, reactions triggered by proteins inside the cell are included; they are also represented by a set of DEqs. More precisely, the model includes the following processes:

- *Influx* of Ca^{2+}-ions through voltage dependent Ca^{2+}-channels caused by time dependent changes of the membrane potential.
- *Buffering* of Ca^{2+}-ions caused by intracellular buffer molecules as well as fluorescence indicators.

- *Efflux* of Ca^{2+} ions caused by plasma membrane Ca^{2+}-ATPase as well as $\mathrm{Na}^{+}/\mathrm{Ca}^{2+}$-exchangers

- *Diffusion* of free Ca^{2+}-ions, and buffer molecules, as well as indicator molecules within the presynaptic terminal.

Reaction-diffusion equation: Starting from a cell in equilibrium, the application of a depolarising, time-dependent membrane potential U induces a Ca^{2+}-ion current between the reaction volume and the extracellular space through voltage dependent Ca^{2+}-channels. This leads to a change of the intracellular free Ca^{2+}-concentration $C(\vec{r},t) = \left[\mathrm{Ca}^{2+}_{\mathrm{free}}\right]$, whose spatiotemporal dynamics is represented by the partial DEq

$$\frac{\partial}{\partial t} C(\vec{r},t) = D_{\mathrm{c}}\, \vec{\nabla}^2\, C(\vec{r},t) + f_{\mathrm{s}}\left[U(t), C(\vec{r},t), t\right] + f_{\mathrm{b}}\left[C(\vec{r},t), t\right]. \tag{4.1}$$

The first term on the right hand side of Eq. (4.1) describes the diffusion of Ca^{2+}-ions within the presynaptic terminal. The diffusion constant is assumed to be constant, i.e. all local inhomogeneities of the cytoplasm are neglected. Instead, an average diffusion constant is considered which lumps together all intracellular barriers into one effective parameter.

The term f_{s} takes care of the sources and sinks of the Ca^{2+}-concentration at the boundary of the reaction volume. It defines the influx into the volume and the efflux from the volume and therefore depends explicitly on the membrane potential U, the Ca^{2+}-concentration C, and on the time t. The second reaction term f_{b}, denotes the buffering processes within the volume and does not depend on the membrane potential.

Boundary conditions: Static boundary conditions of the diffusion term are determined, which is realised in particular by the requirement that the cell membrane acts as the boundary of the reaction volume, through which the Ca^{2+}-ions can not leave the terminal. This requirement is enforced by the von-Neumann boundary condition, which are imposed in the integral of Eq. (4.1) over the whole volume of the presynaptic terminal. Through the Gaussian theorem this leads to

$$\begin{aligned}\frac{\partial}{\partial t}\int\limits_{V} C(\vec{r}\,',t)\,\mathrm{d}^3\vec{r}\,' &= D_{\mathrm{c}} \oint\limits_{\partial V} \vec{\nabla}\, C(\vec{r}\,',t)\cdot \mathrm{d}\vec{f}\,' \\ &+ \int\limits_{\mathrm{V}} f_{\mathrm{s}}\left[U(t), C(\vec{r}\,',t), t\right]\,\mathrm{d}^3\vec{r}\,' + \int\limits_{\mathrm{V}} f_{\mathrm{b}}\left[C(\vec{r}\,',t), t\right]\,\mathrm{d}^3\vec{r}\,',\end{aligned} \tag{4.2}$$

where the loop integral is integrated over the surface ∂V of the volume V. According to the von Neumann boundary conditions, the gradient of the Ca^{2+}-concentration within the first term on the right hand side of Eq. (4.2) must be constant

$$\vec{n}(\vec{r})\cdot\vec{\nabla}\, C(\vec{r},t)\Big|_{\partial V} = \text{constant} \equiv 0\,, \tag{4.3}$$

where $\vec{n}$ denotes the normal vector on ∂V. Since the membrane fluxes are treated as reaction terms, the diffusion flux through the boundary is assumed to be zero for the case considered here. The sources and sinks f_{s} of the Ca^{2+}-concentration are connected to ion-fluxes through the surface of the volume, coming from or going into the extracellular space. According to the continuity equation corresponding to Eq. (4.1),

$$\frac{\partial}{\partial t} C\left(\vec{r},t\right) + \vec{\nabla}\cdot\vec{j_{\mathrm{d}}}\left[C\left(\vec{r},t\right)\right] + \vec{\nabla}\cdot\vec{j_{\mathrm{s}}}\left[U\left(t\right),C\left(\vec{r},t\right),t\right] = f_{\mathrm{b}}\left[C\left(\vec{r},t\right),t\right] \tag{4.4}$$

f_{s} can be defined by the gradient of surface current densities through

$$f_{\mathrm{s}}\left[U\left(t\right),C\left(\vec{r},t\right),t\right] = -\vec{\nabla}\cdot\vec{j_{\mathrm{s}}}\left[U\left(t\right),C\left(\vec{r},t\right),t\right] . \tag{4.5}$$

The term $\vec{\nabla}\cdot\vec{j_{\mathrm{d}}}$ represents those current densities which carry the diffusion process.

Discretisation: The reaction-diffusion system introduced above forms a large set of DEqs. The reaction terms are represented by sets of mostly nonlinear ordinary DEqs. The diffusion terms are represented by a coupled set of parabolic DEqs. In most cases the individual equations are easy to solve analytically. But any analytical approach to solve the whole reaction-diffusion system simultaneously is bound to fail. Therefore, in this thesis the DEq system has been solved by a numerical approach, namely by discretisation. Many different strategies for explicit or implicit discretisation of partial differential equations in space and time exist. For instance, the Euler method (explicit) or the Crank-Nicholson method and the Alternation-Direction-Implicit method (both implicit) are the most commonly used finite difference techniques. These methods and their applicability are mainly characterised by the truncation error, the numerical stability and the computational requirement on CPU time and memory. A detailed introduction into the methodology is given in [72] and for questions concerning implementation issues, confer [80] .

Due to the large number of involved DEqs, a simple-minded finite difference technique has been used in the framework of this thesis in order to conserve lucidity at the implementation level. The algorithms are defined by the following forward-in-time and centered-in-space explicit discretisation. Apart from its simplicity, the main advantage of the method chosen is the independency of the diffusion equation from the compartmentalisation geometry of the volume. Starting from the reaction-diffusion system

$$\frac{\partial}{\partial t} C\left(\vec{r},t\right) = D_{\mathrm{c}}\,\vec{\nabla}^2\, C\left(\vec{r},t\right) - \vec{\nabla}\cdot\vec{j_{\mathrm{s}}}\left[C\left(\vec{r},t\right),U\left(t\right),t\right] + f_{\mathrm{b}}\left[C\left(\vec{r},t\right),t\right] , \tag{4.6}$$

the observable C and the terms f_{b} and $\vec{\nabla}\cdot\vec{j_{\mathrm{s}}}$ will be discretised in space and time with homogenous compartments of volume V_i at time t^n. The homogeneity is represented through an integration over the volume of each single compartment and time step

$$C_i^n = C\left(V_i,t^n\right) = \frac{1}{V_i\,\Delta t}\int\limits_{V_i}\int\limits_{\Delta t} C\left(\vec{r}\,',t\,'\right)\,\mathrm{d}^3\vec{r}\,'\,\mathrm{d}t\,' \tag{4.7}$$

Furthermore, the reaction-terms will be integrated over the volume

$$(f_{\mathrm{b}})_i^n = \frac{1}{V_i}\int\limits_{V_i} f_{\mathrm{b}}\left(C_i^n, t^n\right)\,\mathrm{d}^3\vec{r}\,' = f_{\mathrm{b}}\left(C_i^n, t^n\right)\,, \tag{4.8}$$

$$\begin{aligned}(f_{\mathrm{s}})_i^n &= -\frac{1}{V_i}\int\limits_{V_i}\vec{\nabla}\cdot\vec{j}_{\mathrm{s}}\left[C_i^n, U\left(t^n\right), t^n\right]\,\mathrm{d}^3\vec{r}\,' \\ &= -\frac{1}{V_i}\oint\limits_{\partial V_i}\vec{j}_{\mathrm{s}}\left[C_i^n, U\left(t^n\right), t^n\right]\cdot\mathrm{d}\vec{f}\,' = -\frac{A_i}{V_i}\,j_{\mathrm{s}}\left[C_i^n, U\left(t^n\right), t^n\right]\,,\end{aligned} \tag{4.9}$$

where n is the temporal index and V_i is the spatial discretisation label. The integration over f_{b} in Eq. (4.8) can be executed easily, since all variables f_{b} depend on are assumed to be spatially constant within the compartment V_i. For the integration over the source- and sink-surface-current densities, again the Gaussian theorem has been used. This integration is performed under the assumption that the current densities are homogeneously distributed over the boundary of the terminal. Furthermore, the current is assumed to be perpendicular to the membrane surface, which finally leads to a geometry factor A_i/V_i with the influx area A_i of the compartment[1] V_i. Expressing the left hand side of Eq. (4.6) through discrete values and using Eqs. (4.7), (4.8), and (4.9) yields

$$\begin{aligned}\frac{C_i^{n+1}-C_i^n}{\Delta t} &= \frac{D_{\mathrm{c}}}{V_i}\int\limits_{V}\vec{\nabla}^2\,C\left(\vec{r}\,', t^n\right)\,\mathrm{d}^3\vec{r}\,' + (f_{\mathrm{b}})_i^n + (f_{\mathrm{s}})_i^n\,, \\ &= \frac{D_{\mathrm{c}}}{V_i}\oint\limits_{\partial V_i}\vec{\nabla}\,C\left(\vec{r}\,', t^n\right)\,\mathrm{d}\vec{f}\,' + (f_{\mathrm{b}})_i^n + (f_{\mathrm{s}})_i^n\,, \\ &\simeq \frac{D_{\mathrm{c}}}{V_i}\sum_{k\epsilon NN(V_i)}\frac{C_k^n - C_i^n}{|\vec{r}_i - \vec{r}_k|}\,A_{ik} + (f_{\mathrm{b}})_i^n - \frac{A_i}{V_i}\,j_{\mathrm{s}}\left[C_i^n, U\left(t^n\right), t^n\right]\,.\end{aligned} \tag{4.10}$$

In the transformation above, the Gaussian theorem has been used for the integration over the surface of the volume V_i. In Eq. (4.10) the integration is translated into a sum over all next neighbours NN of the compartment V_i. The quantity A_{ik} represents the contact surface between the compartments V_i and V_k, whereas $|\vec{r}_i - \vec{r}_k| = r_{ik}$ stands for the distance between the midpoint of the two compartments V_i and V_k. Finally, after all manipulations outlined above, the discretised differential equation assumes the form

$$C_i^{n+1} = C_i^n + D_{\mathrm{c}}\,\Delta t\sum_{k\epsilon NN(V_i)}\frac{C_k^n - C_i^n}{r_{ik}}\,\frac{S_{ik}}{V_i} + \Delta t\,\left[(f_{\mathrm{b}})_i^n - \frac{A_i}{V_i}\,j_{\mathrm{s}}\left[C_i^n, U\left(t^n\right), t^n\right]\right]\,. \tag{4.11}$$

This has been used in the framework of this thesis.

Influx and efflux: Ca^{2+}-ions enter the presynaptic terminal through openings of specific transmembrane proteins. This is triggered by changes in the membrane potential: Such proteins open a pore in the cell membrane and the Ca^{2+}-ions follow their elec-

[1] Of course, the source and sink terms are different from zero, only if the compartment V_{i} is a boundary compartment.

trochemical gradient. Also, the clearance of the presynaptic terminal from the Ca^{2+}-surplus is achieved by specific transmembrane proteins. They pump Ca^{2+}-ions against the electrochemical gradient depending on the Ca^{2+}-concentration and time by using different forms of energy. Taken together, the source and sink terms of the Ca^{2+}-concentration from and into the reaction volume are determined by

$$j_{\mathrm{s}}\left(U,C,t\right)=\frac{1}{2F}\,j\left(U,C,t\right)-\frac{1}{N_{\mathrm{a}}}\,\nu\left(U,C,t\right)+L\,, \tag{4.12}$$

where j is the influx current density per membrane surface. It is caused by voltage-dependent Ca^{2+}-channels and represents the source of the Ca^{2+}-ions entering the reaction volume. In order to describe the influx current density through single-protein properties, j is defined as

$$j\left(C,U,t\right)=\rho_{\mathrm{vd}}\,i_{\mathrm{vd}}\left(U,C,t\right)\,. \tag{4.13}$$

With that, the current density is split into an average single channel current i_{vd} and a surface density ρ_{vd} of the voltage dependent channels. Such a subdivision offers the possibility to differentiate between universal properties of classes of single-proteins on the one hand and surface densities on the other hand. This renders the adaption of the model to different types of neurons a simple task, which will be demonstrated in Sec. (5.2). The dependencies and the dynamics of the single channel current are introduced in detail in Sec. (4.3).

The term ν in Eq. (4.12) represents the efflux rate-density per membrane surface unit caused by plasma membrane Ca^{2+}-ATPase pumps and Na^{+}/Ca^{2+}-exchangers, divided by Avogadro's constant

$$\nu\left(C,U,t\right)=\rho_{\mathrm{pm}}\,\nu_{\mathrm{pm}}\left(C,t\right)+\rho_{\mathrm{nc}}\,\nu_{\mathrm{nc}}\left(C,U,t\right), \tag{4.14}$$

where ρ_{pm} and ρ_{nc} are the surface densities of the ATPase pumps and the exchangers, respectively. Their single-protein Ca^{2+}-transport rates depend on time, on the free intracellular Ca^{2+}-concentration and the membrane potential. They are described in detail in Sec. (4.4) and Sec. (4.5). L in Eq. (4.12) represents the leakage-surface current density, which is in balance with the equilibrium current densities caused by the sources and sink terms.

Equilibrium: Any realistic model must allow the system under consideration to recover a stable equilibrium state after some stimulation. In the model of this thesis it is enforced by the requirement that in the equilibrium state of the neuron (defined by the equilibrium membrane potential U_0 and the free equilibrium Ca^{2+}-concentration C_0) the leak conductivity of the membrane L exactly compensates the net current densities resulting from the sum of voltage dependent Ca^{2+} channels, plasma membrane ATPase pumps and exchangers.

Buffering: The main part of the incoming Ca^{2+}-ions will bind to intracellular buffer molecules [78]. In addition, fluorescence indicators, which are used for calcium visu-

alisation are acting as buffers, too. Accordingly, the term $f_{\mathrm{b}}(C,t)$ in Eq. (4.2) stands for the action of endogenous buffers and of fluorescence indicators which bind to and disengage from the free Ca^{2+}-ions. Both forms of the buffers, the bound and the free ones, are subject to diffusion. This is described by the following partial DEqs for the bound $B_{\mathrm{ca}}(\vec{r},t) = [\mathrm{B}_{\mathrm{ca}}(\vec{r},t)]$ and the free $B(\vec{r},t) = [\mathrm{B}(\vec{r},t)]$ buffer concentration:

$$\frac{\partial}{\partial t} B(\vec{r},t) = D_{\mathrm{b}} \vec{\nabla}^2 \cdot B(\vec{r},t) + f_{\mathrm{b}}(C,t) \;, \tag{4.15}$$

$$\frac{\partial}{\partial t} B_{\mathrm{ca}}(\vec{r},t) = D_{\mathrm{b}} \vec{\nabla}^2 \cdot B_{\mathrm{ca}}(\vec{r},t) - f_{\mathrm{b}}(C,t) \;, \tag{4.16}$$

where the diffusion constant D_{b} is fixed to be identical for both types of buffer[2]. The binding and un-binding dynamics of the Ca^{2+} ions, represented by f_{b}, are introduced in detail in Sec. (4.6). The difference in sign in front of f_{b}in both equations above is due to the fact that the source term for the bound buffers is identical to the sink term of the free buffers.

Fitting algorithm: In order to adapt the model to experimental results, a fitting procedure is necessary fixing the free parameters. The Powell algorithm [80], which is a multi-dimensional extension of parabolic interpolation, has been found to do the best job in minimising the difference between model results and experimental data. SYNDICAD has been used as a function of the Powell algorithm, that can be called with different parameters p_i in order to minimise the function F_Δ (the relative fluorescence changes, see Sec. 4.7 and Sec. 5.3.1)

$$\chi^2[p_i] = \sum_{\text{datapoints}} \left(F_\Delta|_{\text{syndicad}}[p_i] - F_\Delta|_{\text{experiment}} \right)^2 , \tag{4.17}$$

by implicitly assuming that the experimental errors are equal for every data point. Powell's algorithm is a purely deterministic algorithm which implies the possibility that it will terminate within a local minimum. This has been taken into account by starting the algorithm at different initial values and checking for its convergence to the same final parameter set.

4.3 Voltage-dependent Ca^{2+}-channel

Voltage-dependent ion channels of biological membranes are formed by pore-like single-proteins that penetrate through the cell membrane. They provide the most important influx pathway for the Ca^{2+}-ions. VDCCs participate in many important processes occurring in living cells. For example, they are crucial for the phenomenon of synaptic transmission [20]. In terms of their functionality, two elements of the macroscopic current through the VDCCs can be distinguished. First, there must be a device that opens or closes discretely the voltage-dependent gate of the pore. The underlying mech-

[2]Here it is assumed that the calcium binding state represents no drastic volume changes of the comparably large buffer protein.

anism is denoted as gating mechanism. Second, if the VDCCs are in an open state the Ca^{2+}-flux through the pore is characterised by a pore-specific current-voltage relation. Taken together, the macroscopic current through an ensemble of VDCCs expressed as an average single VDCC current is given by

$$i_{\mathrm{vd}}\left(U,C,t\right) = O\left(U,t\right)\, i_{\mathrm{op}}\left(U,C\right)\,. \tag{4.18}$$

The term i_{vd} represents the average single-channel current and O denotes the average open probability, which depends on membrane potential U and time t. The quantity $i_{\mathrm{op}}\left(U,C\right)$ represents the current through an opened single-channel, which depends on the membrane potential U as well as on the free intracellular calcium concentration C.

Gating mechanism: The opening of a voltage-dependent ion channel is accompanied by a charge movement across the membrane. The charge movement produces a conformational change in the channel molecule, which opens the pore. The huge amount of published works (see for example [3, 38, 81, 82]) concerning the gating mechanism demonstrates that this process is of vast complexity rather than of easy nature. The detailed mechanisms of the gating process on a molecular level currently are under active discussion. It can be anticipated that this problem will be solved through a detailed analysis of measurements on the single channel (gating) currents, channel fluctuations and on the crystal structure of the protein.

It must be stated clearly that it would go beyond the scope of this thesis to deduce a realistic first-principle model of the whole gating process. Instead, it has been the goal of this thesis to find a description of the gating mechanism, which reproduces the experimental investigations on VDCCs in detail. Such a description can be introduced by the simplest discrete-state Markov model

$$\mathrm{W_c} \underset{\beta\left(U\right)}{\overset{\alpha\left(U\right)}{\rightleftharpoons}} \mathrm{W_o} \tag{4.19}$$

The quantity $\mathrm{W_o}$ denotes the probability of a channel to be in the open state, whereas $W_{\mathrm{c}} = 1 - \mathrm{W_o}$ is the probability of a channel to be in the closed state. The rates α and β represent the forward and backward transitions respectively, which depend on the membrane potential. The inactivation of the VDCC channel is not included here, because its effect for the duration of stimulation considered here is negligible. The kinetic scheme can be translated into an ordinary differential equation by using total probability conservation,

$$\frac{d}{dt}W_{\mathrm{o}} = \alpha - \left(\alpha+\beta\right)\, W_{\mathrm{o}}\,. \tag{4.20}$$

In order to replace the parameters of Eq. (4.20) with corresponding numbers determined from experiment, Eq. (4.20) can be converted into

$$\frac{d}{dt}W_{\mathrm{o}} = \frac{1}{\tau}\,\left(W_{\mathrm{o}}^{\infty} - W_{\mathrm{o}}\right) \tag{4.21}$$

with the steady-state open probability

$$W_{\mathrm{o}}^{\infty} = \frac{\alpha}{\alpha + \beta} \tag{4.22}$$

and the relaxation time constant

$$\tau = \frac{1}{\alpha + \beta}\,. \tag{4.23}$$

According to Eyring's theory of reaction rates [3], the rate of transition between two states exponentially depends on the free energy barriers $E_\alpha\,(U)$ and $E_\beta\,(U)$

$$\alpha = \exp\left(\frac{-E_\alpha}{kT}\right), \tag{4.24}$$

$$\beta = \exp\left(\frac{-E_\beta}{kT}\right). \tag{4.25}$$

Eqs. (4.24) and (4.25) can also be interpreted by using statistical mechanics. From the Boltzmann equation it can be found that they represent the probability for the gating sensor to dispose of the extra energy needed to reach the activated or in-activated state, respectively. In general, the functions $E_\alpha\,(U)$ and $E_\beta\,(U)$ are very difficult to ascertain, and may involve both linear and nonlinear components arising from interactions between the channel and the membrane electrical field. Nevertheless, this dependence can be expressed without additional assumptions on underlying molecular mechanisms by a Taylor series expansion [3], i.e., exemplified for $E_\alpha\,(U)$

$$E_\alpha\,(U) = a_0 + a_1\,U + a_2\,U^2 + \cdots\,, \tag{4.26}$$

where the various a_0, a_1, a_2 etc. represent constants specific for the transition. The constant a_0 corresponds to energy differences that are independent of the applied field; the linear term corresponds to the translation of isolated charges or rotation of charged channel subunits, all other terms are of higher order, which are negligible for small variations of the membrane potential. Thus, both reaction rates take the form

$$\alpha\,(U) = \tilde{a}_0\,\exp\left(\frac{a_1}{kT}\,U\right) + \mathcal{O}\left(U^2\right), \tag{4.27}$$

$$\beta\,(U) = \tilde{b}_0\,\exp\left(\frac{-b_1}{kT}\,U\right) + \mathcal{O}\left(U^2\right). \tag{4.28}$$

This simple formulation predicts that forward rates will increase with depolarisation and backward rates will increase with hyperpolarisation of the membrane potential. Putting Eqs. (4.27) and (4.28) into Eq. (4.22) results in

$$W^{\infty}\,(U) = \frac{1}{1 + \frac{\tilde{b}_0}{\tilde{a}_0}\,\exp\left[\frac{-(a_1+b_1)}{kT}\,U\right]}; \tag{4.29}$$

and putting the same equations into Eq. (4.23) yields

$$\tau\left(U\right)=\frac{1}{\tilde{a}_0\,\exp\left(\frac{a_1}{kT}\,U\right)+\tilde{b}_0\,\exp\left(\frac{b_1}{kT}\,U\right)}\,. \tag{4.30}$$

Usually, equations like the ones above are in good agreement with practically all exper-

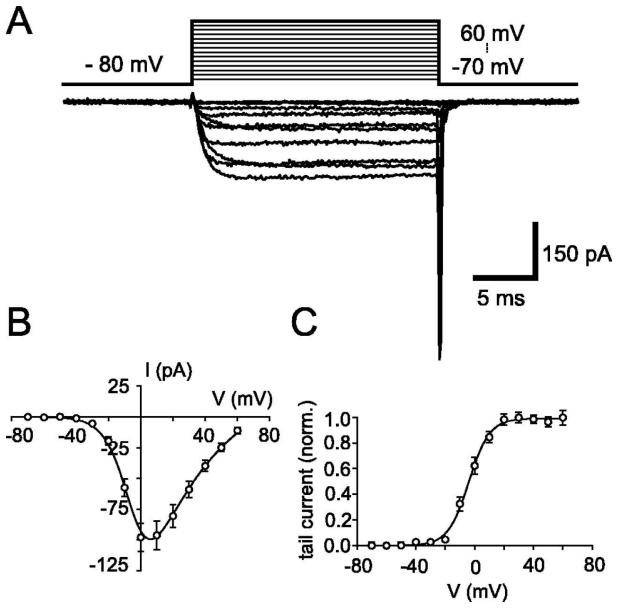

Figure 4.1: **Presynaptic voltage-gated Ca^{2+}-currents in Mossy Fiber presynaptic terminals.** *A*, Voltage-clamp recording of Ca^{2+}-currents evoked by 20 ms voltage pulses from a holding potential of -80 mV to potentials of -70 to 60 mV. *B*, The maximum current amplitude during the pulses is plotted against pulse potential. *C*, The steady-state activation curve. The illustration has been taken from: J. Bischofberger et al.; *Timing and efficacy of calcium channel activation in hippocampal mossy fiber boutons*, page 10595 [83].

imental studies on VDCC and are commonly used as fitting functions. Such a study is illustrated by a measurement of calcium-currents in a presynaptic terminal of a mossy-fiber type neuron in Fig. (4.1). Unfortunately, the measurement of the gating mechanism of VDCC [83], which is used for the SYNDICAD simulation is not in full agreement with the simple model above. Instead of the four parameters introduced in the model above, that measurement needs at least six parameters for a correct description of the gating mechanism. The appropriate fitting functions are given by

$$W^{\infty}\left(U\right)=\frac{1}{1+\exp\left[\frac{1}{U_{\mathrm{sl}}}\,\left(U_{0.5}-U\right)\right]} \tag{4.31}$$

and

$$\tau\left(U\right)=\frac{1}{k_1\,\exp\left(\frac{1}{U_1}\,U\right)+k_2\,\exp\left(\frac{1}{U_2}\,U\right)}\,, \tag{4.32}$$

with the potential of half-activation $U_{0.5}$, the potential steepness factor U_{sl}, as well as the coefficients k_1, k_2 and the time steepness factors U_1, U_2. Eqs. (4.31) and (4.32) has been used in the SYNDICAD simulation. The discrepancy of the number of parameters needed and the introduced simplest Markov model is most likely caused by the fact that more than the two states are needed in order to describe the gating mechanism correctly. This has been verified in [83], where a five-state Markov model has been employed, which is described by 12 parameters.

Current through the opened pore For the following considerations the channel will be assumed to rest in the open state, and the current through the pore driven by the electrochemical gradient will be discussed. Two phenomena determine the permeation process. First, the nature of the permeation process defines the approach to model the current: the differences of a passive transport through a hole in the channel as compared with an active transport of the carrier ions by specific binding sites into the channel must be properly reflected. A multitude of ion-flux measurements as well as more recent works on the crystal structure of the ion channels have shown that the permeation process is realised by a passive flux through a hole in the channel. Second, ion channels are highly permeable to some but not to all types of ions. This selectivity is governed by two factors, namely by the partioning into the membrane and by the mobility of the ions once they are inside the compartment. The derivation of the ion flux through the pore starts with the one dimensional Nernst-Planck equation for fluxes through membranes. The current carried by an ion depends on the concentration gradient and the electric field and reads

$$i_{\mathrm{op}} = 2\,F\,\tilde{D}_{\mathrm{c}}\,\left(\frac{d}{dx}C\left(x\right) + 2\,\frac{F}{R\,T}\,C\left(x\right)\,\frac{d}{dx}\psi\left(x\right)\right), \tag{4.33}$$

whereby the variable x directs along the pore (perpendicular to the membrane). i_{op} represents the current through the open transmembrane channel which depends on the gradient of the free Ca^{2+}-concentration C and the gradient of the electrical potential profile ψ along the inner pore distance x, respectively. The effective diffusion coefficient $\tilde{D}_{\mathrm{c}}$ describes the mobility of the Ca^{2+}-ions within the pore. F denotes the Faraday constant. R stands the molar gas constant, and T represents the absolute temperature.

To assist the integration across the membrane of thickness l, both sides are multiplied by an integrating factor and simplified

$$\begin{aligned} & i_{\mathrm{op}}\left\{\frac{1}{\tilde{D}_{\mathrm{c}}}\,\exp\left[2\,\frac{F}{R\,T}\,\psi\left(x\right)\right]\right\} \\ = 2\,F\,\tilde{D}_{\mathrm{c}}\,&\left\{\frac{1}{\tilde{D}_{\mathrm{c}}}\,\exp\left[\frac{2\,F}{R\,T}\,\psi\left(x\right)\right]\right\}\,\left[\frac{d}{dx}C\left(x\right) + 2\,\frac{F}{R\,T}\,C\left(x\right)\,\frac{d}{dx}\psi\left(x\right)\right] \\ & = 2\,F\,\frac{d}{dx}\left\{C\left(x\right)\,\exp\left[2\,\frac{F}{R\,T}\,\psi\left(x\right)\right]\right\}. \end{aligned} \tag{4.34}$$

In a next step the concentration just inside the edges of the membrane is assumed to be C_0 at $x = 0$ and C_{ex} at $x = l$ by simple equilibrium partitioning. Then integrating

Eq. (4.34) from $x = 0$ to $x = l$, yields

$$i_{\mathrm{op}} = -2\,F\,\frac{C_0\,\exp\left[2\,\frac{F}{RT}\,\psi\,(l)\right] - C_{\mathrm{ex}}\,\exp\left[2\,\frac{F}{RT}\,\psi\,(0)\right]}{\int_{x=0}^{l}\left\{\frac{1}{\tilde{D}_{\mathrm{c}}}\exp\left[2\,\frac{F}{RT}\,\psi\,(x)\right]\right\}\,dx}\,. \tag{4.35}$$

Eq. (4.35) integrates straightforwardly. Under the assumptions that the membrane

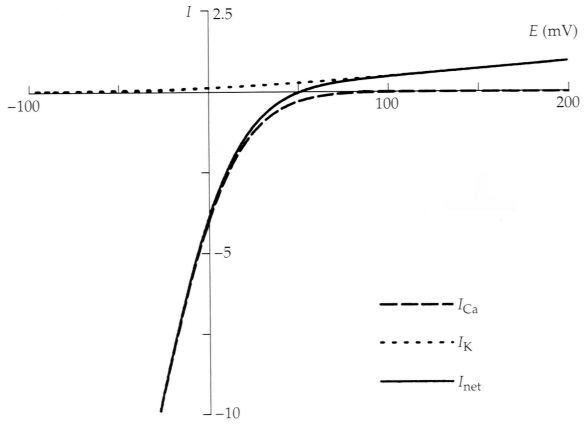

Figure 4.2: **Theoretical I-E curve for open calcium channels:** The GHK-equation predict nonlinear I-E relations whenever the concentration of permeant ions does not equal on the two sides of the membrane. The rectification is completed over a narrower voltage range. Curves of calcium-, potassium-currents, and their sum are drawn for a channel permeable to calcium-ions and very slightly permeable to potassium-ions with an assumed permeability ratio of 0.001. The assumed ion concentrations are C_{ex} = 2 mM, C = 100 nM for calcium and K_{ex} = 2 mM, K = 100 mM for potassium. The theoretical reversal potential here is at U_{k} = 52 mV, far less positive than the thermodynamic single calcium reversal potential, which is U_{ca} = 124 mV. The illustration has been taken from: B. Hille; *Ion channels of excitable membranes*, page 122 [38].

is homogenous with a constant diffusion coefficient $\tilde{D}_{\mathrm{c}}$ and that the potential drops linearly from $\psi\,(0) = U$, to $\psi\,(l) = 0$ with the membrane potential U this results in the Goldman-Hodgkin-Katz (GHK) current equation [38]. Taking into account that C as well as U are time-dependent within the SYNDICAD model and by generalising C_0 to any C thus finally results in

$$i_{\mathrm{op}}\,(U, C) = \frac{(z\,F)^2}{RT}\,p\,U\,\frac{C - C_{\mathrm{ex}}\,\exp\left(-\frac{2\,F}{RT}\,U\right)}{1 - \exp\left(-\frac{2\,F}{RT}\,U\right)} \tag{4.36}$$

with the permeability $p = D_{\mathrm{c}}/l$. Eq. (4.36) represents a convenient tool for reproducing the measurements of single channel ion fluxes required here (see also Fig. 4.2). However, the Goldman-Hodgkin-Katz current equation can not give a guide to the physical structure of the channel because the large complex structure within the channel is lumped into one permeability parameter. The channel is assumed to be homogenous and the ions are assumed not to interact physically or electrostatically – surely wrong

assumptions when going into detail.

To summarise: The gating mechanism of the VDCC in the framework of this thesis is determined by Eqs. (4.21), (4.31) and, (4.32). The current through the opened channel is determined by Eq. (4.36). Together, they offer the possibility to quantitatively reproduce the Ca^{2+}-currents into presynaptic terminals.

Ohm's law: A large fraction of studies employs Ohm's law to describe currents in ion channels. Then, the Ca^{2+}-current due to the membrane potential gradient is approximated by a voltage-current relation with open pore conductivity g

$$i_{\mathrm{op}} = g\,(U_{\mathrm{c}} - U)\ , \tag{4.37}$$

where U_{c} denotes the Ca^{2+} reversal potential. Usually the latter incorporates the Ca^{2+}-concentration gradient over the membrane through Nernst's equation [84]

$$U_{\mathrm{c}} = \frac{R\,T}{z\,F} \ln\left(\frac{C_{\mathrm{ex}}}{C}\right)\ . \tag{4.38}$$

This value of U_{c} then has to be modified by introducing a constant correction factor ΔU_{eff} in order to recover the exact current for I=0:

$$U_{\mathrm{c}} = \frac{R\,T}{z\,F} \ln\left(\frac{C_{\mathrm{ex}}}{C}\right) - \Delta U_{\mathrm{eff}}\,. \tag{4.39}$$

This is partially justified for physiologically relevant membrane potentials for which the VDCC current-voltage relation has been found to be nearly linear in a certain range of voltages (for example in [44] – the range below 20 mV). Nevertheless, this approximation seems to be critical, because the measured relation as such is non-linear. Providing a linear fit to some range of the voltage is perfectly justified as long as the relevant voltages fall into this region; applying the approximation everywhere will surely misrepresent the exact relation. This is highlighted by the finding that efflux Ca^{2+}-currents through VDCC at voltages above the reversal potential are negligible [38] in striking contrast to the linear approximation.

4.4 Plasma membrane Ca^{2+}-ATPase (PMCA)

PMCA represents an excellent example for those components of the cell which transport Ca^{2+}-ions against their electrochemical gradient out of the cytoplasm [53, 58]. This transport proceeds in the following way: The PMCA binds Ca^{2+}-ions to its two intracellular Ca^{2+} binding sites. Then, the Ca^{2+}-ions will be moved one by one through the protein to the extracellular surface of the cell membrane. This is achieved through a conformational change of the PMCA protein by de-phosphorylation of an ATP molecule. Finally, the transported Ca^{2+}-ions will be released from the PMCA. The overall process

can be expressed in the following kinetic scheme

$$\mathrm{P^{in}} + 2\,\mathrm{Ca^{2+}} \underset{k_-^{\mathrm{pm}}}{\overset{k_+^{\mathrm{pm}}}{\rightleftharpoons}} \mathrm{P^{in}_{ca}} \underset{\beta^{\mathrm{pm}}}{\overset{\alpha^{\mathrm{pm}}}{\rightleftharpoons}} \mathrm{P^{ex}_{ca}} \underset{m_-^{\mathrm{pm}}}{\overset{m_+^{\mathrm{pm}}}{\rightleftharpoons}} \mathrm{P^{ex}} + 2\,\mathrm{Ca^{2+}_{ex}}\,. \qquad (4.40)$$

with ATP $\downarrow$ attached to $\mathrm{P^{in}_{ca}}$, ADP $\downarrow$ attached to $\mathrm{P^{ex}_{ca}}$, and $\downarrow \gamma^{\mathrm{pm}}$ $\mathrm{P^{in}}$ attached to $\mathrm{P^{ex}}$.

$\mathrm{P^{in}}$ and $\mathrm{P^{ex}}$ represent the PMCA proteins. $\mathrm{P^{in}_{ca}}$ and $\mathrm{P^{ex}_{ca}}$ denote the $\mathrm{Ca^{2+}}$-bound mode of the PMCA protein. The superscripts "in" and "ex" symbolise the intracellular or the extracellular position of the $\mathrm{Ca^{2+}}$-ion binding sites of the PMCA protein, respectively. $\mathrm{Ca^{2+}}$ and $\mathrm{Ca^{2+}_{ex}}$ denote the free intracellular as well as free extracellular $\mathrm{Ca^{2+}}$-ions. It has been assumed that always two $\mathrm{Ca^{2+}}$-ions will be transported per reaction cycle, denoted by the number 2. ATP and ADP denote Adenosintriphosphate and Adenosindiphosphate, respectively, the energy source to the reaction cycle. k^{pm} and m^{pm} represent the rate constants for the forward (subscript "+") and backward (subscript "−") binding and releasing of the intracellular $\mathrm{Ca^{2+}}$-ions, respectively. Finally, α^{pm} is the forward and β^{pm} is the backward transition rate denoting the conformational change during the $\mathrm{Ca^{2+}}$-ion transport. Finally, the PMCA returns to its ground state (transition rate γ^{pm}). The expression above can be simplified by the following assumptions:

1. The ATP concentration is constant, and the rate under which the PMCA protein absorbs ATP is adjusted instantaneously to its level of $\mathrm{Ca^{2+}}$-transportation. This most probably holds true for physiological conditions , because the homoeostasis of the cell tries to maintain a constant ATP-level.

2. Since the conformation change is fast compared to all other reaction steps of the PMCA, it is assumed to be instantaneous. Conformational changes occur on a time scale of nanoseconds, in contrast the time scale for a full ion transport cycle is in a millisecond range.

3. The release of the $\mathrm{Ca^{2+}}$-ions at the extracellular face is irreversible. In fact, this might be a valid assumption, since so far no measurement has found any indication of a reverse mode of the PMCA. As a result, the $\mathrm{Ca^{2+}}$-ions can only be transported from cytoplasm to the extracellular space but not vice versa.

4. For every reaction cycle, two $\mathrm{Ca^{2+}}$-ions are to be transported through the PMCA protein. This assumption is in contradiction with a measured stoichiometry between transported $\mathrm{Ca^{2+}}$ and hydrolysed ATP of 1:1 [53]. However, the measurement of the Hill coefficient to be equal to 2 [85] for the activity of the PMCA in equilibrium with the ions supports this assumption. In principle, this apparent contradiction of data may be resolved by assuming that 2 ATP molecules are dephosphorylated during one pumping cycle.

5. The possibility of the PMCA to be in both an activated as well as in an in-activated

state (for instance driven by activation through calmodulin) with apparently altered kinetic properties is not considered.

With the resulting simplifications the kinetic scheme sketched above can be reduced to the well-known Michaelis-Menten enzyme model

$$\mathrm{P} + 2\,\mathrm{Ca}^{2+} \underset{k_-^{\mathrm{pm}}}{\overset{k_+^{\mathrm{pm}}}{\rightleftharpoons}} \mathrm{P}_{\mathrm{ca}} \xrightarrow{\nu_{\mathrm{max}}^{\mathrm{pm}}} \mathrm{P} + 2\,\mathrm{Ca}_{\mathrm{ex}}^{2+} \quad . \tag{4.41}$$

It can be translated into a set of 4 ordinary DEqs by using the law of mass action. They can be reduced further by employing the conservation of the total concentration of PMCAs $P_0 = P + P_{\mathrm{ca}}$. The resulting set of DEqs reads:

$$\frac{d}{dt}P_{\mathrm{ca}} = k_+^{\mathrm{pm}}\,C^2\,P_0 - \left(k_+^{\mathrm{pm}}C^2 + k_-^{\mathrm{pm}} + \nu_{\mathrm{max}}^{\mathrm{pm}}\right)\,P_{\mathrm{ca}}\,, \tag{4.42}$$

$$2\,\frac{d}{dt}C = -k_+^{\mathrm{pm}}\,P_0 + \left(k_+^{\mathrm{pm}} + k_-^{\mathrm{pm}}\right)\,P_{\mathrm{ca}}\,, \tag{4.43}$$

$$\frac{d}{dt}C_{\mathrm{ex}} = \nu^{\mathrm{pm}} = \frac{1}{2}\,\nu_{\mathrm{max}}^{\mathrm{pm}}\,P_{\mathrm{ca}}\,. \tag{4.44}$$

The implicit time dependence of C in Eq. (4.42) stems from the Ca^{2+} main equation Eq. (4.1), whereas the explicit Ca^{2+}-binding dynamics related to the PMCA is described by Eq. (4.43). Eq. (4.44) defines the transport rate ν^{pm} of the Ca^{2+}-ions and thus represents the observable of interest. The Ca^{2+}-concentration dependency of ν^{pm} is illustrated by an measurement shown in Fig. (4.3). Accordingly, Eqs. (4.42) and Eq. (4.44) are used in SYNDICAD in order to describe the Ca^{2+} transport rate of the PMCA protein. In the following it will be elaborated on the connection between the experimental observable and the parameters k_+^{pm}, k_-^{pm}, and $\nu_{\mathrm{max}}^{\mathrm{pm}}$ of the dynamics above.

Experimental observable: To discuss the experimental observable, first a stationary state of Eq. (4.42) is investigated. This implies a constant transport rate Eq. (4.44), which then becomes a Hill equation characterised by a Hill coefficient of 2

$$\nu^{\mathrm{pm}} = \frac{C^2\,P_0}{\left(k_-^{\mathrm{pm}} + \nu_{\mathrm{max}}^{\mathrm{pm}}\right)\left(k_+^{\mathrm{pm}}\right)^{-1} + C^2}\,\nu_{\mathrm{max}}^{\mathrm{pm}}\,. \tag{4.45}$$

The Hill equation describes the activity of the PMCA and the parameter $\nu_{\mathrm{max}}^{\mathrm{pm}}$ can be interpreted as the overall maximum rate of one PMCA protein. Furthermore, the term $\left(k_-^{\mathrm{pm}} + \nu_{\mathrm{max}}^{\mathrm{pm}}\right)/k_+^{\mathrm{pm}}$ represents the square of the concentration at half activation $\left(K_{0.5}^{\mathrm{pm}}\right)^2$. Both values are well determined by recent experimental investigations on PMCA proteins. Unfortunately, one of the three parameter remains free. Eq. (4.42) will be analysed by rearranging them in order to fix k_+^{pm} or k_-^{pm},

$$\frac{d}{dt}P_{\mathrm{ca}} = \frac{1}{\tau^{\mathrm{pm}}}\,\left(P_{\mathrm{ca}}^{\infty} - P_{\mathrm{ca}}\right)\,, \tag{4.46}$$

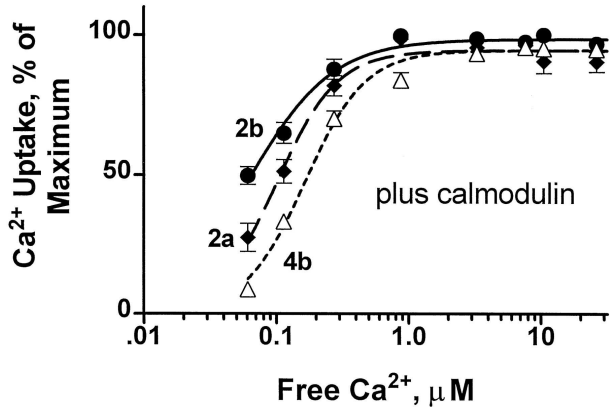

Figure 4.3: **Calcium-transport activity of different PMCA-types:** The PMCA activity is drawn as a function of free Ca^{2+}-concentration. The lines represent the best fit to the data given by the Hill equation. The concentration of half activity $K_{0.5}$ were: hPMCA4b $K_{0.5}$ = 0.16 μM; rPMCA2a $K_{0.5}$ = 0.09 μM; rPMCA2b $K_{0.5}$ = 0.06 μM. The illustration has been taken from: N.L. Elwess et al.; *Plasma membrane calcium pump isoforms 2a and 2b are unusually responsive to calmodulin and ca*, page 17983 [61].

where $1/\tau^{\mathrm{pm}}$ represents the time constant which can be determined as

$$(\tau^{\mathrm{pm}})^{-1} = k_{+}^{\mathrm{pm}}\, C^2 + k_{-}^{\mathrm{pm}} + \nu_{\mathrm{max}}^{\mathrm{pm}}\,. \tag{4.47}$$

P_{ca}^{∞} denotes the stationary state value of P_{ca}

$$P_{\infty} = \frac{C^2\, P_0}{\left(k_{-}^{\mathrm{pm}} + \nu_{\mathrm{max}}^{\mathrm{pm}}\right)\left(k_{+}^{\mathrm{pm}}\right)^{-1} + C^2}\,, \tag{4.48}$$

which is indeed equivalent to the Hill equation in Eq. (4.45). Formally speaking, it represents a boundary condition of Eq. (4.46). Now, Eq. (4.47) yields the possibility to determine the last free parameter through a concentration-dependent relaxation time constant.

4.5 $\mathrm{Na}^{+}/\mathrm{Ca}^{2+}$-exchanger (NCX)

A further important extrusion mechanism is represented by the NCX proteins. They can transport Ca^{2+}-ions in both directions, either out of or into the cytoplasm. The direction depends on the prevailing electrochemical driving forces of Ca^{2+}- and Na^{+}-ions. Compared to the PMCA, the NCX has a nearly ten times higher turnover rate but its affinity is nearly 10 times lower. This suggests that the NCXs act as a kind of "fire brigade" for the clearance of highly increased Ca^{2+}-concentrations. The transport process can be represented by the following kinetic scheme, which is similar to the PMCA scheme

$$\begin{array}{ccccccc} & & 3\,\mathrm{N^{in}} & & & & \\ & \overset{k_+^{\mathrm{nc}}}{\rightharpoonup} & \downarrow & \overset{\alpha^{\mathrm{nc}}}{\rightharpoonup} & & \overset{m_+^{\mathrm{nc}}}{\rightharpoonup} & \\ \mathrm{X^{in}} + \mathrm{Ca^{2+}} & \rightleftharpoons & \mathrm{X_{ca}^{in}} & \rightleftharpoons & \mathrm{X_{ca}^{ex}} & \rightleftharpoons & \mathrm{X^{ex}} + \mathrm{Ca_{ex}^{2+}} \\ & \underset{k_-^{\mathrm{nc}}}{\leftharpoondown} & & \underset{\beta^{\mathrm{nc}}}{\leftharpoondown} & \downarrow & \underset{m_-^{\mathrm{nc}}}{\leftharpoondown} & \downarrow \gamma^{\mathrm{nc}} \\ & & & & 3\,\mathrm{N^{ex}} & & \mathrm{X^{in}} \end{array} \quad . \tag{4.49}$$

Here, $\mathrm{X^{in}}$ and $\mathrm{X^{ex}}$ denote the numbers of NCX proteins, where the superscripts "in" and "ex" symbolise the intracellular and the extracellular $\mathrm{Ca^{2+}}$ binding site position of the the exchanger, respectively. $\mathrm{X_{ca}^{in}}$ and $\mathrm{X_{ca}^{ex}}$ represent the number of the NCX proteins in the $\mathrm{Ca^{2+}}$ bound state. Intracellular $\mathrm{Ca^{2+}}$-ions $\mathrm{Ca^{2+}}$ will be transported to the extracellular space where it will be released as $\mathrm{Ca_{ex}^{2+}}$. This transport is enabled through the counter-transport of extracellular $\mathrm{Na^+}$-ions $\mathrm{N^{ex}}$ which will be released into the cytoplasm $\mathrm{N^{in}}$. The rate constants k^{nc} and m^{nc} represent the forward (subscript "+") and backward (subscript "−") binding and releasing process of the $\mathrm{Ca^{2+}}$-ions respectively. The transition rate constants α^{nc} (forward) and β^{nc} (backward) denote the conformational change during the ion transport. Finally, the NCX returns to its ground state (transition rate γ^{nc}). In analogy to the PMCA protein, that expression can be also simplified by some assumptions:

1. The $\mathrm{Na^+}$-concentration is constant.
2. The dynamics of $\mathrm{Na^+}$-transport is not considered, the transport proceeds instantaneously
3. Since the conformation change is fast compared to all other reaction steps of the NCX, it is assumed to be instantaneous.
4. The possibility of the NCX to be both in an activated and in an in-activated state (for instance driven by phosphorylation) with apparently altered kinetic properties is not considered.
5. Further exchange modes and their effects in the kinetic scheme are neglected.

With these simplifications, the kinetic scheme above can again be mapped onto the Michaelis Menten enzyme model

$$\mathrm{X} + \mathrm{Ca^{2+}} \underset{k_-^{\mathrm{nc}}}{\overset{k_+^{\mathrm{nc}}}{\rightleftharpoons}} \mathrm{X_{ca}} \overset{\nu_{\mathrm{max}}^{\mathrm{nc}}}{\rightharpoonup} \mathrm{X} + \mathrm{Ca_{ex}^{2+}} \quad . \tag{4.50}$$

Following the same steps as for the case of PMCA, a set of three DEqs emerges for the NCX

$$\frac{d}{dt} X_{\mathrm{ca}} = k_+^{\mathrm{nc}}\, C\, X_0 - \left(k_+^{\mathrm{nc}} C + k_-^{\mathrm{nc}} + \nu_{\mathrm{max}}^{\mathrm{nc}}\right) X_{\mathrm{ca}}\,, \tag{4.51}$$

$$\frac{d}{dt} C = -k_+^{\mathrm{nc}}\, X_0 + \left(k_+^{\mathrm{nc}} + k_-^{\mathrm{nc}}\right) X_{\mathrm{ca}}\,, \tag{4.52}$$

$$\frac{d}{dt} C_{\mathrm{ex}} = \nu^{\mathrm{nc}} = \nu_{\mathrm{max}}^{\mathrm{nc}}\, X_{\mathrm{ca}}\,, \tag{4.53}$$

with a total concentration $X_0 = X + X_{\mathrm{ca}}$ of NCXs. Again, the implicit time dependence of C in Eq. (4.51) stems from the main equation Eq. (4.1), whereas the explicit dynamics of Ca^{2+}-binding to the NCX is described by Eq. (4.52). Eq. (4.53) again defines the rate ν^{nc} of the transported Ca^{2+}-ions and thus represents the observable of interest. Accordingly, Eqs. (4.51) and (4.53) are used in SYNDICAD in order to describe the rate of the NCX.

Experimental observable In full parallel with the PMCA, a steady state of Eq. (4.51) is investigated; again, the transport rate is given by a Hill equation, but with a Hill coefficient of 1

$$\nu^{\mathrm{nc}} = \frac{C\,X_0}{\left(k_-^{\mathrm{nc}} + \nu_{\max}\right)\left(k_+^{\mathrm{nc}}\right)^{-1} + C}\,\nu_{\max}^{\mathrm{nc}}\,. \tag{4.54}$$

The quantities $\left(k_-^{\mathrm{nc}} + \nu_{\max}^{\mathrm{nc}}\right)/k_+^{\mathrm{nc}}$ has the same interpretation as above, only with NCX replacing PMCA. The concentration of half activation $K_{0.5}^{\mathrm{nc}}$ can be determined by recent experimental investigation on NCX proteins. The remaining third parameter is determined also in the same way as for the PMCA. In contrast, here the maximum rate $\nu_{\max}^{\mathrm{nc}}$ of the exchanger depends on additional factors, which will be discussed in the next section.

Maximum rate $\nu_{\max}^{\mathrm{nc}}$ of the NCX: As mentioned above, Ca^{2+}-ions can be transported via the NCX protein in both directions, into and out of the cytoplasm. The maximum rate is governed by the difference between the membrane potential and the reversal potential of the NCX as well as by the conductance of individual exchangers [58]

$$\nu_{\max}^{\mathrm{nc}}\left(C,N\right) = \frac{1}{2e}\,g_{\max}^{\mathrm{nc}}\,\left[U - U_{\mathrm{nc}}\left(C,N\right)\right]\,. \tag{4.55}$$

It is assumed that the maximum transport rate is proportional to the difference of the membrane potential U with the exchanger reversal potential U_{nc} and to the maximum conductance $g_{\max}^{\mathrm{nc}}$ of one individual NCX protein. The Ca^{2+}-ion charge is represented by the twofold elementary charge e. The reversal potential U_{nc} of the exchanger is determined by the electrochemical gradient of Ca^{2+} and Na^{+}. For the transport system in stationary state, the flux of one Ca^{2+}-ion is coupled to the counterflow of 3 Na^{+} ions. Then the relationship between the two electrochemical gradients is

$$\Delta\overline{\mu}_{\mathrm{c}}\left(U_{\mathrm{nc}}\right) = 3\,\Delta\overline{\mu}_{\mathrm{n}}\left(U_{\mathrm{nc}}\right)\,. \tag{4.56}$$

The two electrochemical gradients are defined as

$$\Delta\overline{\mu}_{\mathrm{n}}\left(U\right) = F\,\left(U_{\mathrm{n}} - U\right) = R\,T\,\ln\left(\frac{N^{\mathrm{ex}}}{N}\right) - F\,U\,, \tag{4.57}$$

where N^{ex} and N denote the extra- and intracellular sodium concentration, and

$$\Delta\overline{\mu}_{\mathrm{c}}\left(U\right) = 2\,F\,\left(U_{\mathrm{c}} - U\right) = R\,T\,\ln\left(\frac{C^{\mathrm{ex}}}{C}\right) - 2\,F\,U \tag{4.58}$$

with the reversal potential of sodium U_{n} and the reversal potential of calcium U_{c}. Combining Eqs. (4.56-4.58), the reversal potential reads

$$U_{\mathrm{nc}} = \frac{RT}{F}\left[3\,\ln\left(\frac{N^{\mathrm{ex}}}{N}\right) - \ln\left(\frac{C^{\mathrm{ex}}}{C}\right)\right]. \tag{4.59}$$

Eqs. (4.55) and (4.59) are used in SYNDICAD in order to describe the maximum rate of the exchanger. The mode of the exchangers is defined by the polarity of the electrical driving force $(U - U_{\mathrm{nc}})$. For equilibrium conditions ($U \approx$ -70 mV and $C \approx 0.1$ μM) the exchangers act in the Ca^{2+}-outward mode; in contrast, for highly positive membrane potentials, the exchangers switch to the Ca^{2+}-inward mode. More light will be shed on this finding in Sec. (5.2). It should be noted that the NCX proteins may have more than these two working modes. The authors of [58] report a $\mathrm{Ca}^{2+}/\mathrm{Ca}^{2+}$-exchange mode as well as a $\mathrm{Na}^{+}/\mathrm{Na}^{+}$-exchange mode depending on the external and internal ion concentrations. The $\mathrm{Ca}^{2+}/\mathrm{Ca}^{2+}$-exchange mode results in a zero net flux of Ca^{2+} and thus can be neglected here. The same holds true for the $\mathrm{Na}^{+}/\mathrm{Na}^{+}$-exchange mode, because this exchanger mode does not affect the Ca^{2+}-flux.

4.6 Endogenous and exogenous buffers

The major fraction of the intracellular Ca^{2+} is bound to endogenous buffers [78, 86, 87]. In the rest state of the neuron the amount of free buffers is still large enough to allow most of the incoming free Ca^{2+}-ions to bind to these buffers [78] during stimulation. The continuous binding and dissociation of Ca^{2+} ions and buffers strongly influences the resulting free Ca^{2+}-dynamics. This does apply not only to the phase of growing Ca^{2+}-concentration during stimulation but also to the return of the Ca^{2+}-concentration to its equilibrium level.

In addition, also the fluorescence indicators used in experiments act as an exogenous buffer system [88]. They are employed to visualise the spatiotemporal dynamics of the Ca^{2+}-dynamics into the cytoplasm, which is described in detail in Sec. (3.5) and Sec. (4.7). The indicators influence the Ca^{2+}-dynamics significantly, clearly an unwanted but unavoidable side effect, which has to be corrected for. For the correction a tool is necessary, which allows to disentangle the fundamental Ca^{2+}-dynamics from the additional impact of fluorescence measurements. In fact, SYNDICAD is well suited for this task, its capabilities will be presented in more detail in Sec. (5.3.2).

The dynamics of the buffers can be described explicitly by using the first order kinetic scheme for the endogenous and exogenous buffer presented in [77, 89, 90]. The scheme is based on the assumption that all multiple binding sites of the buffers act independently from each other and can be represented as

$$\mathrm{Ca} + \mathrm{B} \underset{k_-}{\overset{k_+}{\rightleftharpoons}} \mathrm{B_{ca}}\,, \tag{4.60}$$

whereby Ca denotes the free Ca^{2+}-ions and $\mathrm{B}, \mathrm{B}_{\mathrm{ca}}$ denotes the free and the Ca^{2+}-bound buffer molecules, respectively. By using the law of mass action it can be mapped onto two ordinary DEqs, namely

$$\frac{d}{dt}B_{\mathrm{ca}} = +k_+ C\, B - k_- B_{\mathrm{ca}} \tag{4.61}$$

$$f_{\mathrm{b}}(C,t) = \frac{d}{dt}B = -k_+ C\, B + k_- B_{\mathrm{ca}}\,. \tag{4.62}$$

The concentration of bound buffer sites is represented by B_{ca} and the concentration of free buffer sites is represented by B. The forward k_+ and the backward k_- binding rate constants determine the dissociation constant $K_{\mathrm{d}} = k_-/k_+$. Eqs. (4.61) and (4.62) are used in SYNDICAD to simulate the binding dynamics of the buffers. The buffer dynamics itself and, in particular, its influence on the dynamics of the Ca^{2+}-ions are discussed in detail in Sec. (5).

Fast buffer approximation: Unfortunately, no experimental values for the rate constants k_+ and k_- are available. This problem can be circumvented by the assumption that the buffer dynamics takes places on short time scales compared to the Ca^{2+}-dynamics, i.e., that the buffer dynamics is always in a quasi-stationary state. The time dependence in Eq. (4.61) is then given by the implicit time dependence of C in Eq. (4.61) only. The result of this assumption is known as the rapid buffer approximation [78, 79, 91]. It has two important consequences. First, on short time scales the bound endogenous and exogenous buffer concentrations B_{ca} become constant and can be written as a function of the Ca^{2+}-concentration

$$B_{\mathrm{ca}}(C) = \frac{C\, B_0}{K_{\mathrm{d}} + C}\,, \tag{4.63}$$

where the total buffer concentration is assumed to be conserved: $B_0 = B + B_{\mathrm{ca}}$. Of course, diffusion changes this picture. However, the fast buffer approximation implies that the bound buffer concentration is instantaneously adapted to the free Ca^{2+}-concentration at each time t. Hence, the time behaviour related to the implicit Ca^{2+} time dependence can be deduced from

$$\frac{d}{dt}B_{\mathrm{ca}}(C) = \frac{d}{dC}B_{\mathrm{ca}}(C)\ \frac{d}{dt}C(t) \tag{4.64}$$

where, again, the time dependence of C is taken from Eq. (4.1). Application of Eqs. (4.63) and (4.64) results in a more compact form of the Ca^{2+}-dynamics,

$$\frac{d}{dt}C = f_{\mathrm{s}}(U,C,t)\ \frac{1}{1+T(C)} \tag{4.65}$$

as long as diffusion is neglected. T is a dimensionless correction factor which depends on the free Ca^{2+}-concentration. It is given by

$$T(C) = \frac{B_0 K_{\mathrm{d}}}{(K_{\mathrm{d}} + C)^2} \tag{4.66}$$

The great technical advantage of this approximation [90] is that Eq. (4.66) involves the dissociation constants K_d of the buffers only instead of both rate constants k_+ and k_-. These rate constants, when observed with the help of SYNDICAD, are in good agreement with some other model investigations on buffer dynamics. Unfortunately, their small values indicate that the fast buffer approximation is violated. As it will be demonstrated in Sec. (5.2), the resulting deviations are significant.

4.7 Fluorescence measurements

In this section, the focus shifts on the way, in which the measured fluorescence intensity depends on the time-dependent intracellular Ca^{2+}-concentration. The fluorescence intensity emitted at wavelength λ_1 in response to excitation at wavelength λ_2 can be expressed through the indicator concentration. Using a $1:1$ complexation ansatz [68] the dimensionless fluorescence intensity reads

$$f = y_\mathrm{b}\, B^{\,\mathrm{fl}} + y_\mathrm{ca}\, B^{\,\mathrm{fl}}_\mathrm{ca}\,. \tag{4.67}$$

The quantity f denotes the dimensionless fluorescence intensity. $B^{\,\mathrm{fl}}$ represent the free indicator concentration and $B^{\,\mathrm{fl}}_\mathrm{ca}$ represent the bound indicator concentration. The superscript "fl" is used in the following for denoting the exogenous buffer which is represented in this thesis by different fluorescence indicators. y_b represents the excitation factor for free indicator which is determined as minimum fluorescence intensity $f|_{\mathrm{c}=0} = f_\mathrm{min} = y_\mathrm{b}\, B_0^\mathrm{fl}$ for zero saturation indicator with $B^{\,\mathrm{fl}} = B_0^\mathrm{fl}$ and $B^{\,\mathrm{fl}}_\mathrm{ca} = 0$. B_0^fl is the total indicator concentration and y_ca represents the excitation factor for Ca^{2+}-bound indicator which is determined as maximum fluorescence intensity $f|_{\mathrm{c}=\infty} = f_\mathrm{max} = y_\mathrm{ca}\, B_0^\mathrm{fl}$ for full saturation indicator with $B^{\,\mathrm{fl}} = 0$ and $B^{\,\mathrm{fl}}_\mathrm{ca} = B_0^\mathrm{fl}$.

Simulation of the fluorescence intensity by SYNDICAD: Most measurements focus on relative changes of the fluorescence intensity only, defined by

$$F_\Delta = \frac{f - f_\mathrm{eq}}{f_\mathrm{eq}}\,. \tag{4.68}$$

The fluorescence intensities are recorded as time dependent fluorescence traces f. As indicated above, they will be converted into a relative change of the fluorescence intensity through normalisation with respect to f_eq, the fluorescence intensity at the equilibrium Ca^{2+}-concentration. This equilibrium intensity is given as

$$f_\mathrm{eq} = f|_{\mathrm{c}=\mathrm{c}_0} = f_\mathrm{min} + (y_\mathrm{ca} - y_\mathrm{b})\; B^{\,\mathrm{fl}}_\mathrm{ca}\big|_{\mathrm{c}=\mathrm{c}_0}\,, \tag{4.69}$$

cf. Eq. (4.67). Therefore, to compare with any simulation, the modelling of f is necessary. This is achieved by eliminating all unknown parameters by taking the ratio F_Δ. Considering the maximum and minimum value of f and assuming conservation of total

concentration yields

$$f = f_{\max} + (y_{\mathrm{b}} - y_{\mathrm{ca}})\; B^{\,\mathrm{fl}} = f_{\min} + (y_{\mathrm{ca}} - y_{\mathrm{b}})\; B^{\,\mathrm{fl}}_{\mathrm{ca}}\,. \tag{4.70}$$

Putting everything together results in

$$F_{\Delta}\,(C) = \frac{B^{\,\mathrm{fl}}_{\mathrm{ca}}\,(C) - \left.B^{\,\mathrm{fl}}_{\mathrm{ca}}\right|_{\mathrm{c=c_0}}}{B^{\,\mathrm{fl}}_{0}\left(\frac{f_{\max}}{f_{\min}} - 1\right)^{-1} + \left.B^{\,\mathrm{fl}}_{\mathrm{ca}}\right|_{\mathrm{c=c_0}}}\,. \tag{4.71}$$

This equation defines F_{Δ} in SYNDICAD. It is also used to determine the ratio $f_{\max}/f_{\min}$ in case the maximum fluorescence intensity change $(F_{\Delta})_{\max}$ for saturated concentration of indicator is provided by the experiment.

Estimate of absolute Ca^{2+}-amplitudes: From the fluorescence intensity changes above, the Ca^{2+}-concentration can be directly estimated. For that, F_{Δ} is normalised to its maximum value resulting in

$$\frac{F_{\Delta}}{(F_{\Delta})_{\max}} = \frac{f - f_{\mathrm{eq}}}{f_{\max} - f_0}\,. \tag{4.72}$$

To translate this into a direct dependence of the fluorescence intensity on the Ca^{2+}-concentration, the dependence on the buffer has to be eliminated. This is achieved by means of the first order kinetic DEq for the free indicator-dynamics (see also Sec. 4.6) given by

$$\frac{d}{dt}B^{\,\mathrm{fl}} = -k^{\mathrm{fl}}_{+}\,B^{\,\mathrm{fl}}_{\mathrm{ca}} + k^{\mathrm{fl}}_{-}\,B^{\,\mathrm{fl}}\,C\,. \tag{4.73}$$

The bound and the free indicator in Eq. (4.70) can be replaced by using the stationary state of Eq. (4.73). Then, with $K^{\mathrm{fl}}_{\mathrm{d}} = k^{\mathrm{fl}}_{-}/k^{\mathrm{fl}}_{+}$, the fluorescence intensity becomes

$$f = \frac{f_{\max}\,C + f_{\min}\,K^{\mathrm{fl}}_{\mathrm{d}}}{K^{\mathrm{ex}}_{\mathrm{d}} + C}\,. \tag{4.74}$$

From this, new $f_{\min} = f|_{\mathrm{c=0}}$, $f_{\max} = f|_{\mathrm{c=\infty}}$ and $f_{\mathrm{eq}} = f|_{\mathrm{c=c_0}}$ can be computed. Putting everything together into Eq. (4.72) finally results in

$$C = \frac{C_0 + K^{\mathrm{fl}}_{\mathrm{d}}\;(F_{\Delta})\,(F_{\Delta})^{-1}_{\max}}{1 - (F_{\Delta})\,(F_{\Delta})^{-1}_{\max}} \tag{4.75}$$

This gives a rough estimate of the total Ca^{2+}-amplitude for small values of C. It should be stressed that the fast buffer approximation, which has been used in order to derivate this equation, is violated, limiting the accuracy of the estimate. In addition, this estimate always includes the indicator buffering effect and therefore does not allow to reconstruct directly the unperturbed Ca^{2+}-amplitude.

4.8 Excitability

The neuronal signal consists of short electrical pulses and can be measured by placing a thin electrode close to the soma or axon of a neuron. The pulses, known as action potentials, are short peaks of the membrane potential. They have an amplitude of about 100 mV and typically last for 1-2 ms. Starting from the equilibrium potential defined as the inside potential (≈ -70 mV) minus the outside potential (taken to be 0 mV), any electrical stimulus beyond a typical threshold initiates an action potential that propagates along the neuron. When the action potential sweeps towards the recording electrodes, the membrane depolarises (becomes more positive), overshoots the zero line, and then re-polarises (returns to rest).

Like all electrical messages of the nervous system, the action potential is a membrane-potential change. It is caused by the flow of ions through corresponding channels in the membrane. More precisely, the action potential is caused by ionic currents through voltage-dependent Na^+- and K^+-channels. This has been shown by the important voltage-clamp measurements developed by Marmont, and Cole, and by Hodgkin, Huxley and Katz in the early fifties, for example [92]. To "voltage clamp" means to control the potential across the cell membrane.

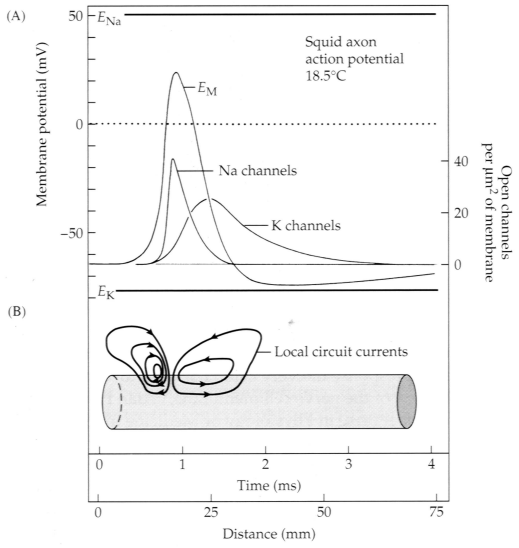

Figure 4.4: **Events during the propagated action potential:** *A,* Action potential and underlying opening of potassium and sodium channels calculated from the Hodgkin-Huxley model at 18.5 °C. *B,* Diagram of the local circuit current flows associated with propagation; inward current at the excited region spreads forward inside the axon to bring unexcited regions above firing threshold. The illustration has been taken from: B. Hille; *Ion channels of excitable membranes*, page 53 [38].

The ionic currents are caused by voltage and time dependent changes of the Na^+- and K^+-permeability, which are low at rest. During a step depolarisation, the Na^+-

permeability rises rapidly with a short delay, reaches a peak, and falls again to a low value. This behaviour has been called fast "activation" and slow "inactivation". If the membrane potential is returned to rest by these channels during the period of high conductance, the Na^+-permeability falls exponentially and very rapidly. K^+-permeability activates almost ten times slower than the Na^+-permeability, reaching a steady level without significant inactivation during depolarisation. When the potential returns to rest, the K^+-permeability falls exponentially and relatively slow. The larger the depolarisation, the larger and faster the changes of Na^+- and K^+-permeability, but for very large depolarisations both permeabilities reach a maximum value.

Because the Na^+-concentration gradient directs into the neuron, the Na^+-ions take the same route. Consequently, positive charges arrive in the cytoplasm and the membrane potential depolarises. The opposite takes place in case of K^+. Here, the K^+-concentration gradient directs out of the neuron. Accordingly, positive charges leave the cytoplasm and the membrane potential re-polarises. Hence, the action potential can be explained at the level of Na^+- and K^+-permeabilities as follows: After local stimulation currents begin to depolarise the membrane, Na^+ channels activate rapidly. Depolarisation is amplified. Before the peak of the action potential is reached, the channels are inactivated and the Na^+ permeability falls. In the mean time, this enhanced depolarisation slowly activates the K^+ channels, which in turn produce the outward current and-thus-re-polarise the membrane. For an illustration of this process see Fig. (4.4)

The equivalent circuit of an axon membrane provides an excellent starting point to translate this into a quantitative description. Hodgkin and Huxley described the membrane as an electrical circuit with four parallel branches [92]. A capacitive branch $c_{\mathrm{m}}dU/dt$ with the membrane capacitance $c_{\mathrm{m}}$and the membrane potential U represents the dielectric properties of the thin membrane. Then, three conductive branches represent sodium I_{na}, potassium I_{k}, and leak conductances I_{l} with their different electromotive forces. In this picture, the conductances of I_{na}, I_{k} vary with time and voltage arising from the opening and closing of the channels

$$c_{\mathrm{m}}\frac{d}{dt}U = -I_{\mathrm{na}}\left(U,t\right) - I_{\mathrm{k}}\left(U,t\right) - I_{\mathrm{l}}\left(U\right) + I_{\mathrm{i}}\left(t\right) . \tag{4.76}$$

Here, I_{i} represents the injected stimulation current. First, the time dependence of the K^+-channel is described. The increase of the K^+-permeability on depolarisation follows an S-shaped time course. As Hodgkin and Huxley noted in [92], such kinetics would be obtained if the opening of a K^+-channel was controlled by several independent membrane-bound particles. This can be interpreted in the following way: Suppose that there are four identical particles, each with a probability n of being in the correct position to set up an open channel. The probability that all four particles are correctly placed is n^4. Because the opening of K^+-channels depends on the membrane potential, the hypothetical particles are assumed to bear an electric charge rendering their distribution in the membrane voltage dependent. Suppose further that each particle moves between its permissive and non-permissive position with first order kinetics. As a result, the distribution of particles described by the probability n will exponen-

tially relax towards a new value, when the membrane potential is changed. Assuming the behaviour of open channels to be governed by Ohm's law, I_{k} is represented in the Hodgkin-Huxley model by

$$I_{\mathrm{k}} = n^4\, \overline{g}_{\mathrm{k}}\, (U - U_{\mathrm{k}})\ . \tag{4.77}$$

Through Ohm's law the current is driven by the maximum conductance $\overline{g}_{\mathrm{k}}$ and the difference between the membrane potential and the reversal potential U_{k} of K^+-ions. The voltage- and time dependent changes of n are given by a first order kinetic scheme

$$(1-\mathrm{n}) \quad \underset{\beta_{\mathrm{n}}(U)}{\overset{\alpha_{\mathrm{n}}(U)}{\rightleftharpoons}} \quad \mathrm{n}\ . \tag{4.78}$$

The gating particles move between the permissive and the non-permissive forms with voltage-dependent rate constants α_{n} and β_{n}. If the initial value of the probability n is known, subsequent values can be calculated by solving the ordinary DEq

$$\frac{d}{dt} n = \alpha_{\mathrm{n}}\, (1-n) - \beta_{\mathrm{n}}\, n\,. \tag{4.79}$$

An alternative to using the rate constants α_{n} and $\beta_{\mathrm{n}}$is to use the voltage-dependent time constant τ_{n} and the stationary state value n^∞, defined by

$$\tau_{\mathrm{n}} = \frac{1}{\alpha_{\mathrm{n}} + \beta_{\mathrm{n}}}\,, \tag{4.80}$$

$$n^\infty = \frac{\alpha_{\mathrm{n}}}{\alpha_{\mathrm{n}} + \beta_{\mathrm{n}}}\,. \tag{4.81}$$

The change of n with time can be calculated by solving the DEq

$$\frac{d}{dt} n = \frac{1}{\tau_{\mathrm{n}}}\, (n^\infty - n)\ . \tag{4.82}$$

This is Eq. (4.79) written in a different form.

The Hodgkin-Huxley model uses a similar formalism to describe I_{na}, with four hypothetical gating particles which undergo independent first order transitions between permissive and non-permissive positions to control the channel. However, because there are two opposing gating processes, activation and inactivation, there have to be two kinds of gating particles. Hodgkin and Huxley called them m and h. They settled on three m particles to control activation and one h particle for inactivation. Therefore, the probability that all particles are in the permissive position is $m^3 h$ and I_{na} is represented by

$$I_{\mathrm{na}} = m^3\, h\, \overline{g}_{\mathrm{na}}\, (U - U_{\mathrm{na}})\ . \tag{4.83}$$

At rest, m is low and h is high. During depolarisation, m rises rapidly and h falls slowly. After depolarisation, m recovers rapidly and h slowly to the original values. Since for the n parameter of K^+-channels, m and h are assumed to undergo first order transitions

	α [1/ms]	β [1/ms]
n	$\frac{0.01\ (10+U)}{\exp\left[\frac{1}{10}\ (10+U)\right]-1}$	$0.125\ \exp\left(\frac{1}{80}\,U\right)$
m	$\frac{0.1\ (25+U)}{\exp\left[\frac{1}{10}\,(25+U)\right]-1}$	$4\ \exp\left(\frac{1}{18}\,U\right)$
h	$0.07\ \exp\left(\frac{1}{20}\,U\right)$	$\frac{1}{\exp\left[\frac{1}{10}\ (30+U)\right]+1}$

Table 4.1: **Fit functions of the Hodgkin-Huxley model.** Fit function for a measurement of activation and inactivation of K^+- and Na^+- channel currents of a squid giant axon at 6.3 °C. That set of rate constants can explain the existence of action potentials with the underlying voltage and time dependent permeability changes of K^+- and Na^+-channels.

between permissive and non-permissive forms:

$$(1-\mathrm{m}) \underset{\beta_\mathrm{m}(U)}{\overset{\alpha_\mathrm{m}(U)}{\rightleftharpoons}} \mathrm{m} \tag{4.84}$$

and

$$(1-\mathrm{h}) \underset{\beta_\mathrm{h}(U)}{\overset{\alpha_\mathrm{h}(U)}{\rightleftharpoons}} \mathrm{h} \tag{4.85}$$

with rates satisfying the DEqs

$$\frac{d}{dt}m = \alpha_\mathrm{m}\ (1-m) - \beta_\mathrm{m}\, m = \frac{1}{\tau_\mathrm{m}}\ (m^\infty - m) \tag{4.86}$$

and

$$\frac{d}{dt}h = \alpha_\mathrm{h}\ (1-h) - \beta_\mathrm{h}\, h = \frac{1}{\tau_\mathrm{h}}\ (h^\infty - h)\ . \tag{4.87}$$

To summarise, the Hodgkin-Huxley model describes ionic current across the membrane in terms of the components

$$c_\mathrm{m}\frac{d}{dt}U = -m^3\, h\, \overline{g}_\mathrm{na}\ (U - U_\mathrm{na}) - n^4\, \overline{g}_\mathrm{k}\ (U - U_\mathrm{k}) - \overline{g}_\mathrm{l}\ (U - U_\mathrm{l}) + I_\mathrm{i}(t)\ . \tag{4.88}$$

Hodgkin and Huxley fitted their model to the measurements on a squid giant axon at 6.3 °C by using the fitting functions shown in Tab. (4.1). These functions are arbitrary with no direct or first-principles connection to the molecular mechanisms. The most important goal of the Hodgkin-Huxley work was to demonstrate that there are a certain number of independent particles moving in the electric field of the membrane, which control the independent Na^+- and K^+- permeabilities.

The first goal of this thesis is to reproduce these action potentials, which occur in the neurons of the rat brain. The model of Hodgkin and Huxley was developed on

neurons of the squid giant axons and the measured action potentials differ significant from those measured in mammalian (rat) neurons. A number of works exist, which adapt the Hodgkin-Huxley model to different types of neurons by modifying the fitting functions and/or the exponents of the coefficient n, m, h. But none of these attempts was able to provide a homogenous model of the underlying molecular mechanisms or an universal tool to reproduce action potentials in arbitrary types of neurons based on few parameters only. Therefore, for SYNDICAD a set of equations inspired by the Hodgkin-Huxley approach has been chosen, which does the best fitting job. This set is given by the following expression for the ion currents

$$c_{\mathrm{m}} \frac{d}{dt} U = -m\, h\, \overline{g}_{\mathrm{na}}\, (U - U_{\mathrm{na}}) - n\, \overline{g}_{\mathrm{k}}\, (U - U_{\mathrm{k}}) - \overline{g}_{\mathrm{l}}\, (U - U_{\mathrm{l}}) + I_{\mathrm{i}}\,(t)\ . \tag{4.89}$$

Here, the leakage conductance $\overline{g}_{\mathrm{l}}$ compensates all other currents in the equilibrium state. The time dependence of m, h, n is described in the same way as in the Hodgkin-Huxley model (Eqs. (4.82), (4.86), and (4.87). Their stationary state values, however, are different from those used in the Hodgkin-Huxley model

$$m^{\infty} = \frac{1}{1 + \exp\left[\frac{1}{U_{\mathrm{m2}}}\,(U_{\mathrm{m1}} - U)\right]}\,, \tag{4.90}$$

$$h^{\infty} = \frac{1}{1 + \exp\left[\frac{1}{U_{\mathrm{h2}}}\,(U_{\mathrm{h1}} - U)\right]}\,, \tag{4.91}$$

$$n^{\infty} = \frac{1}{1 + \exp\left[\frac{1}{U_{\mathrm{n2}}}\,(U_{\mathrm{n1}} - U)\right]}\,. \tag{4.92}$$

Here, U_2 denotes the steepness factor and the potential of half activation is denoted by U_1. Furthermore, the time constants τ_{m}, τ_{h}, τ_{n} are assumed to be constant under changes in voltage. This is, indeed, in contradiction with the measurements. However, this assumption has no visible effect on the quality of the fits.

Chapter 5

Results

5.1 Introduction

The presentation of the results of this thesis is divided into three parts: **1.** An overview of all parameters included in SYNDICAD will be given, explaining how they are determined through measurements. As far as possible, these are single-protein measurements. **2.** A quantitative analysis of synaptic functions needs well-known reference systems. Thus, SYNDICAD is initially calibrated using fluorescence measurements of the spatially averaged presynaptic Ca^{2+}-dynamics on small terminals of pyramidal neurons inside the rat's neocortex [41]. The results will be compared to corresponding experiments using different fluorescence indicator concentrations. Single action potentials as well as a 10 Hz train of action potentials have been chosen as stimulation protocols in both the experiments and the simulation. The only remaining free parameters are the protein densities, which have been adjusted as fit parameters. This procedure had to be repeated for every new experimental setup, because the surface densities are highly specific to individual terminals. Afterwards, the reliability of the model will be tested by adjusting the parameters of SYNDICAD to a measurement on a large presynaptic terminal in the rat brainstem. **3.** Finally, the most important results of this work will be discussed:

- For each experimental reference system, a prediction of protein densities for VDCC, PMCA and NCX will be given. The VDCC current and the clearance rate as well as the influence of diffusion to the spatially averaged Ca^{2+}-dynamics will be discussed.
- Ca^{2+}-measurements predominantly use fluorescence indicators in order to visualise the Ca^{2+}-concentration. These measurements involve the undesired effect of disturbing the natural Ca^{2+}-dynamics. The capability of SYNDICAD to reconstruct the physiological Ca^{2+}-dynamics without such perturbations by exogenous buffers will be demonstrated.
- Long-term potentiation (LTP) and long-term depression (LTD) are important effects of changing synaptic efficacy. It is commonly accepted that the induction of

both effects is accompanied by a prior increase of the Ca^{2+} level. This increase is induced by stimulations with both high-frequency (long-term potentiation) and low-frequency (long-term depression) trains of action potentials. But what are the differences between high- and low-frequency stimulations at the level of the Ca^{2+}-concentration? In order to answer this question, those characteristics in Ca^{2+} time courses have been studied, which are significant for different stimulation protocols.

- Many possible induction mechanisms of long-term potentiation with different Ca^{2+}-affinities are under active discussion. In order to get a preselection, an experiment will be proposed here to investigate the level of the spatially averaged Ca^{2+}-concentration, to which the induction for long-term potentiation could be sensitive. For the first time in this context, this will be facilitated by a quantitative analysis of the influence of an exogenous buffer on the Ca^{2+}-dynamics induced by the application of a train of action potentials.

- It is a well-known fact that microdomains play a crucial role for the strength of stimulus-secretion coupling. This emphasises the central importance of such local inhomogeneities of the Ca^{2+}-signal. The spatial behaviour of the incoming Ca^{2+}-flux will be investigated in order to extend the investigations about spatially averaged Ca^{2+}-peaks to the spatially resolved Ca^{2+}-dynamics near a VDCC cluster. Consequently, the local Ca^{2+}-dynamics induced by different trains of action potentials will be compared to spatially averaged Ca^{2+}-signals. Furthermore, characteristic size and typical reaction time of the microdomains will be discussed.

5.2 Determination of the model properties

Geometry: The specific geometry of a terminal is assumed to be well described by an axial symmetry. Hence, diffusion is reduced to two dimensions (l- and r- direction). Possible effects of axial inhomogeneities (for example through the surface of the endoplasmic reticulum) are neglected. However, they should not cause significant disparities anyway. Therefore, cylindrical coordinates are best suited to investigate diffusion processes within the terminal. The presynaptic terminal is determined by its radius r and its length l (in the remainder of this work, $2\,r = l$ will be assumed). The size ranges from 0.5 to 2 μm and can be deduced from corresponding fluorescence pictures of the observed regions (they were also given directly in [93]). An example for such a fluorescence image is shown in Fig. (5.1). The spatial discretisation width is computed from the calcium diffusion constant D_c = 20 $\mu m^2/s$, which results for time steps of 1 μs in a mean spatial step of Δx = 6,3 nm. Accordingly, the discretisation width is chosen as Δx = 5nm. An example configuration is given in Fig. (5.2). The VDCCs are located at the bottom of the cylinder. The PMCAs as well as the NCXs are distributed over the whole cylinder membrane. Each compartment is represented by a cylindrical ring; its height and width are given by the discretisation width Δx.

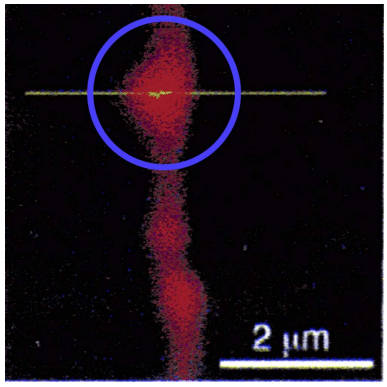

Figure 5.1: **Fluorescence scan of a presynaptic terminal.** Optical detection of a bouton (blue circle) in a pyramidal neuron with the help of a fluorescence indicator (OGB-1). The scans of fluorescence intensity changes were made along the horizontal line. The illustration has been taken from H. J. Koester and B. Sakmann; *Calcium dynamics associated with action potentials in single nerve terminals of pyramidal cells in layer 2/3 of the young rat neocortex*, page 627 [41].

Equilibrium and external parameters: The equilibrium membrane potential U_0 = -70 mV and the equilibrium concentration C_0 = 0.1 μM constitute the relevant equilibrium state parameters of SYNDICAD. Both values are taken from [41] under the implicit assumption that they represent standard values for the observed neuron types. SYNDICAD is embedded in a thermal bath. More precisely, all external conditions are set to be constant at all times. In addition, some external parameters are necessary in order to determine the dependencies of the membrane proteins on the environment:

- Unless noted otherwise, results presented in this work relate to body temperature. However, it should be kept in mind that some parameters have been obtained by single-protein experiments which were conducted at room temperature[1]. Commonly, the deviations for the parameters used are small and therefore can be neglected here.

- The external Ca^{2+}-concentration for physiological conditions is C_{ex} = 1.5 mM and determines the concentration gradient. Furthermore, the external and internal Na^{+}-concentrations N_{ex} = 145 mM, N = 12 mM are necessary to determine the exchanger transport rates. The values used in this work are taken from [38], assuming that they are nearly identical for the observed neuronal terminals.

VDCC: In CNS neurons, the Ca^{2+}-influx into the presynaptic terminal is assumed to be dominated by the P/Q- and N-type channels, see also [41]. Therefore, they are regarded as the only representative members of the channel family. The channels are pores, that can be characterised by two mechanisms: The voltage-dependent opening of the closed

[1]This holds true, e.g., for most of the experiment on VDCC, which are usually done at room temperature.

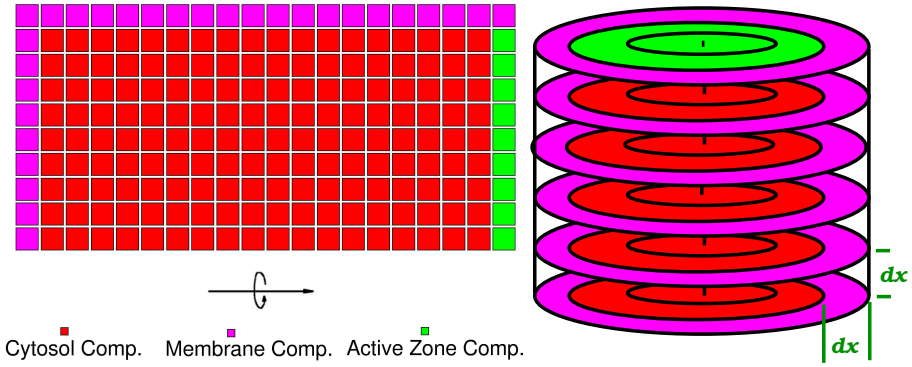

Figure 5.2: **The model geometry.** *Left:* A cut through an example configuration. Every square symbolises a ring with Δx as thickness and height. Axial symmetry of the observed volume is indicated by the black arrow. The different colours are coding the compartment types. Within the cytoplasm (red) only diffusion and buffering are allowed. The membrane compartments (magenta) constitute the boundary of the volume. Here, the PMCA's and NCX's are located. The VDCC's are located within the active zone compartments (green). *Right:* A sample configuration in a three-dimensional view.

pore as well as the current through the open pore. The parameters related to the gating mechanism Eq. (4.31) of the VDCC-pore are describing the steady-state opening probability. They are given by the half-activation voltage $U_{0.5}$ and a steepness factor U_{sl}. The voltage dependent activation time τ Eq. (4.32) is described by four parameters. All values above are determined by a measurement of Ca^{2+}-currents in Mossy Fiber presynaptic terminals [83]. It should be noted that this measurement was not resolving the specific types of channels.

The current through the open pore Eq. (4.36) depends on the Ca^{2+}-concentration gradient and on the membrane potential. Furthermore, the conductivity is determined by the single channel permeability p. A lot of single channel measurements observing these channel properties can be found in the literature, for example [44, 94]. Unfortunately, at present the ion currents through single channels are at the boundary of experimental sensitivity. A possible and widely used solution to this problem is to employ a different charge carrier with an extensively enlarged concentration gradient (in the range of 100 mM of extracellular ionic concentration). The most prominent charge carrier nowadays is Ba^{2+}. In fact, such a procedure produces measurable currents [44]. However, the single-channel permeability determined by such measurements based on the Ba^{2+}-concentration gradient results in a current which tends to be unrealistically small in the regime of truly physiological concentration Ca^{2+}-gradients. The reason for this apparent mismatch could be a mere reflection of differences inherent to the similar but still different charge carriers. In addition, non-linear effects due to large concentration gradients are well beyond current understanding. Phrased in other words: It is not clear yet whether the GHK-equation correctly describes ion current at such large concentration gradients. Taken together, the experimental setup based on the Ba^{2+} be-

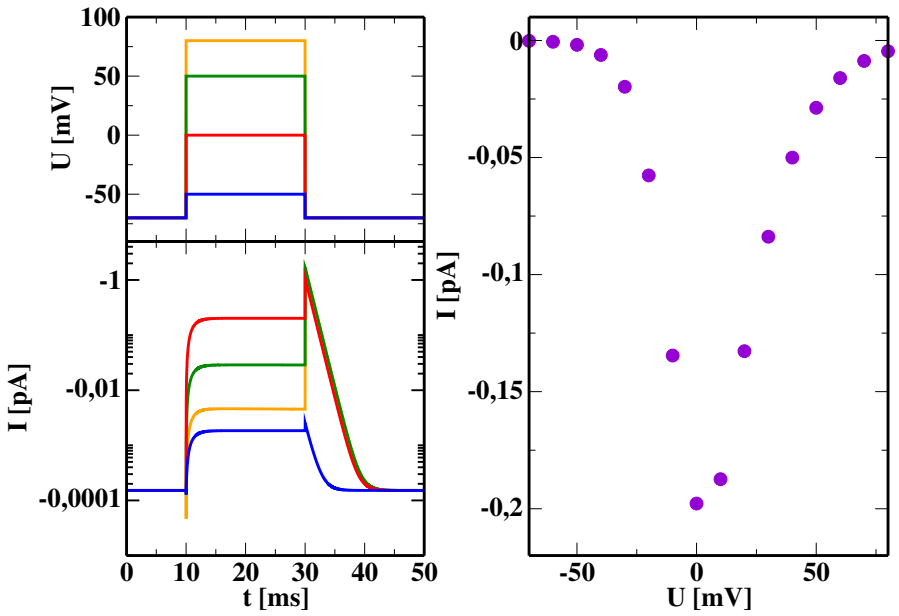

Figure 5.3: **Simulation of a voltage clamp experiment on VDCC.** The *upper left* panel shows the applied membrane potential steps. In the *lower left* panel the resulting average current through a single channel is plotted. The currents are growing to their stationary values very fast. The *right* panel shows the resulting steady state I/U - relation of a single channel.

comes un-physiological and is therefore not meaningful for the purposes of this work. To circumvent this, the conclusion of another measurement based on Ca^{2+}-ions [95] will be employed instead. It predicts a maximum peak current within a single channel, which is in the range of 0.1-0.3 pA for physiological conditions. With the help of this measurement the single channel permeability can be adjusted such that it reproduces the peak value.

The resulting I/U-relation is illustrated in the right panel of Fig. (5.3) by simulating a voltage-clamp series experiment with SYNDICAD. The bell-shaped behaviour results from the product of opening probability (falling segment) and GHK-current (growing segment) entering the stationary current. Voltage steps are applied ranging from -70 mV to +80 mV in 10 mV steps (upper left panel in Fig. (5.3) and the resulting ion current is measured. The lower left panel in Fig. (5.3) exhibits a subset of corresponding results obtained by SYNDICAD. Clearly, the resulting currents grow in a voltage dependent manner to a stationary value reflected by the plateau. The tiny peak at 10 ms in some curves is caused by the interaction of the opening probability and the current-voltage relation: The opening probability still remains in its equilibrium state (at membrane potential -70 mV), whereas, in contrast, the voltage jumps to larger values, which imply smaller currents through the open channels. Reversely, the large peak current at the end of each voltage step is caused by the cut-out current. There, the opening probability

stays in its activated state whereas the voltage jumps to the equilibrium membrane potential implying larger currents.

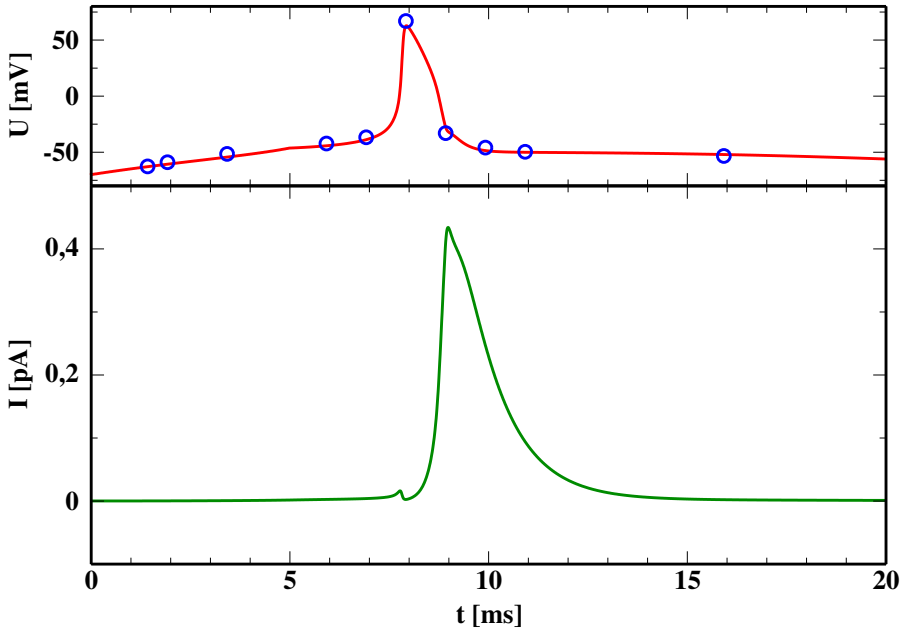

Figure 5.4: **Simulation of the average current through a single VDCC.** The VDCC-current (green) – induced by the application of a single action potential (red - simulation, blue - measurement from a rat pyramidal neuron in the neocortex) – has been depicted here. The action potential opens the VDCC very efficiently. The experimental data has been taken from H. J. Koester and B. Sakmann; *Calcium dynamics associated with action potentials in single nerve terminals of pyramidal cells in layer 2/3 of the young rat neocortex*, page 627 [41].

In order to illustrate the average current through a single VDCC under physiological conditions, the answer of this VDCC to the application of a physiological action potential is shown in Fig. (5.4). The action potential opens the channels more efficiently than a constant voltage step. Therefore, the peak value is increased compared to the maximum value of 0.2 pA shown in Fig. (5.3). The tiny peak of the current during the rising phase is due to the strong depolarising membrane-potential peak of the action potential. The membrane potential reaches up to levels, where the ion currents already start decreasing. When the depolarisation phase is finished, the current rises up to its peak value (see Fig. 5.3; range above 50 mV in the right panel).

PMCA: The PMCA2a is the dominantly expressed protein of the PMCA family in neurons [96]. Therefore, it has been chosen as the representative member of this protein class. Nevertheless more types than this single one are expressed in CNS neurons. However, the kinetic properties vary considerably [61, 97, 98] even for this type of PMCA. This is most probably due to different experimental conditions. Hence, consid-

ering more than one type of PMCA is well beyond the scope of this work and would not allow quantitative predictions.

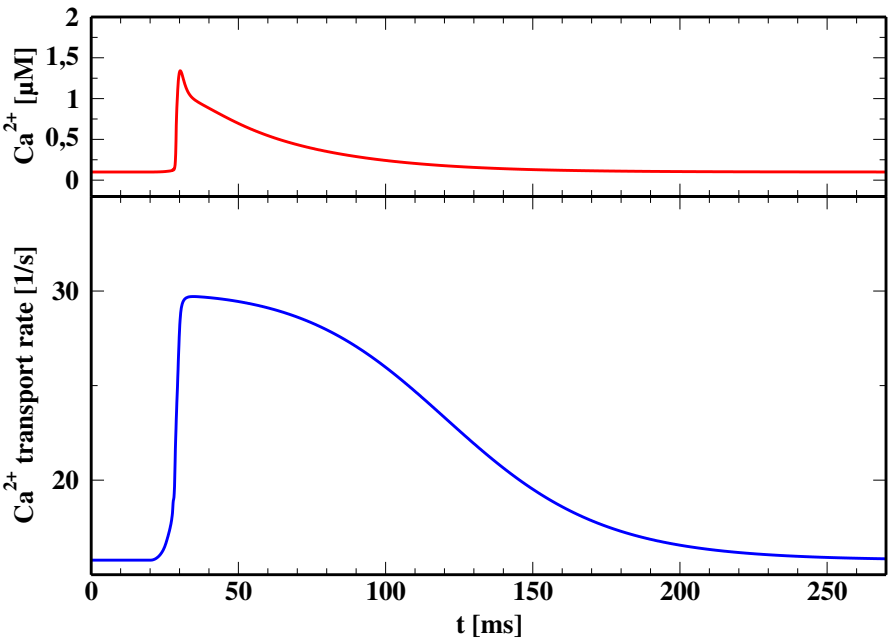

Figure 5.5: **Simulation of the dynamics of a single PMCA protein during a Ca^{2+}-peak.** The upper panel shows the Ca^{2+}-peak (red) caused by a single action potential (not shown). The lower panel shows the resulting PMCA dynamics (blue). The PMCA rate in equilibrium approximately is 15 calcium-ions/s, since the equilibrium Ca^{2+}-concentration is nearly identical with the concentration of half-activation, $K_{0.5}^{\mathrm{pm}}$ = 0.09 μM. It can be read off, that already during the Ca^{2+}-peak caused by a single action potential the PMCA activity rises to its maximum value of 30 calcium-ions/s.

The PMCA pumps Ca^{2+}-ions against the direction of the chemical gradient of Ca^{2+} by dephosphorylating ATP molecules. These proteins are characterised by a Ca^{2+}-dependent activity and a maximum pumping rate $\nu_{\mathrm{max}}^{\mathrm{pm}}$. The steady-state activity is described by the Hill-equation Eq. (4.45) with the concentration of half-activation at $K_{0.5}^{\mathrm{pm}}$ = 0.09 μM. This value has been taken from a measurement for rat PMCA [61]. The Hill-coefficient n^{pm} = 2, arises because the PMCA protein is equipped with two Ca^{2+} binding-sites and because it is assumed that always two Ca^{2+}-ions are pumped out per reaction cycle. This is in some contradiction with an observed stoichiometry of the PMCA of 1:1 [57]. Nevertheless, the measured PMCA activity [61] confirms a Hill-coefficient of n^{pm} = 2.

The rate constants of the PMCA protein k_{+}^{pm} and k_{-}^{pm} parametrise its dynamics. At present, they are not known and, hence, they are subject to an educated guess: While one of them can be expressed by the above values, the other one basically remains free. It is fixed through Eq. (4.47) with the assumption of a time constant in the range of one ms (for equilibrium Ca^{2+}-concentration).

A maximum pumping rate $\nu_{\max}^{\mathrm{pm}} = 150$ calcium-ions/s is reported in [51]. However, one of the authors (M. Blaustein, private communication) has corrected this value to $\nu_{\max}^{\mathrm{pm}}$ = 30 calcium-ions/s. This is in the same range as the results of [61], where a PMCA Ca^{2+}-uptake u^{pm} = 7.83 nmol/(mg membrane protein) has been measured. From this, $\nu = u^{\mathrm{pm}} m^{\mathrm{pm}} N_{\mathrm{a}} / p^{\mathrm{pm}} \approx 8.5$ calcium-ions/s can be approximated by assuming a PMCA fraction p^{pm} = 0.002 related to the whole membrane proteins [99] as well as an overall averaged membrane protein mass m^{pm} = 120 kDa. Therefore, the value of $\nu_{\max}^{\mathrm{pm}}$ = 30 calcium-ions/s has been used for the results obtained by SYNDICAD that will be presented in this work. The dynamics of a single PMCA protein during a Ca^{2+}-peak (caused by a single action potential) is shown in Fig. (5.5).

NCX: The NCX1 is the dominantly expressed protein of the NCX family in neurons [58]. However, no data were found concerning differences of the kinetic properties of different types of exchangers. Therefore it is impossible and irrelevant to specify the NCX type within the framework of this thesis. For the NCX the reasoning follows the same logic as the one for the PMCA protein discussed above.

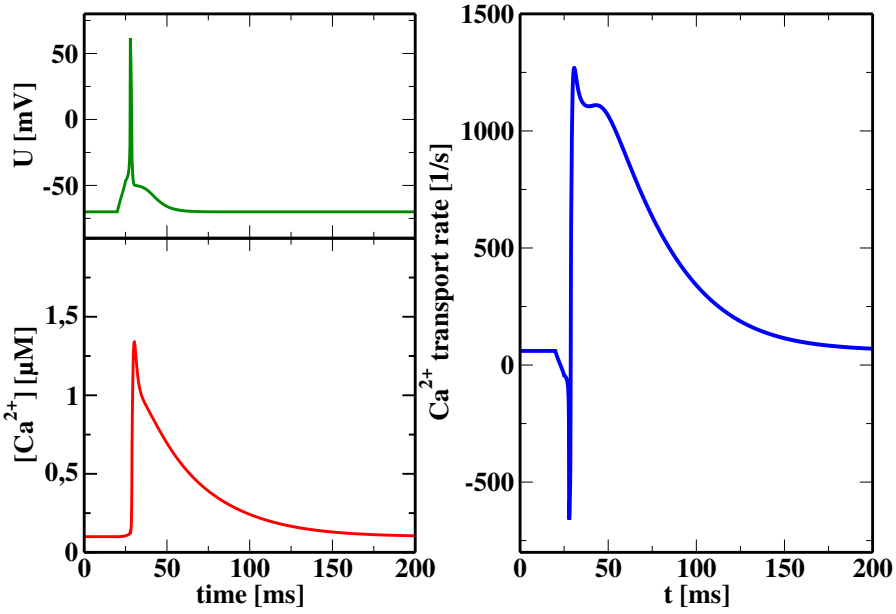

Figure 5.6: **Simulation of the transport rate of a single NCX protein.** The NCX activity is drawn (blue, right panel) during a Ca^{2+}-peak (red, lower left panel) which is caused by a single action potential (green, upper left panel). At the beginning of the stimulus, the NCX switches into a Ca^{2+}-influx mode caused by the strong depolarisation of the membrane potential. Afterwards, the NCX develops comparably large activity due to the considerable height of the Ca^{2+}-peak.

The NCX transports one Ca^{2+}-ion per reaction cycle by exchanging it with three Na^{+}-ions. Consequently, the Hill-coefficient with respect to Ca^{2+} is n^{nc} = 1. The NCX can act

in both Ca^{2+}-influx and Ca^{2+}-efflux mode depending on the membrane potential. The Ca^{2+}-activity of the NCX protein is described in the same fashion as the PMCA protein. The concentration of half-activation $K_{0.5}^{nc}$ = 1.6 μM is taken from [58].

In analogy to the PMCA, one of the rate constants of the NCX protein (k_{+}^{nc} and k_{-}^{nc}) can be expressed by the above values and the other one can be adjusted by Eq. (4.47) under the assumption of a fast time constant [100], which is in the range of 10 μs (for equilibrium Ca^{2+}-concentration).

The maximum rate of the NCX depends on the membrane potential U as well as on the reversal potential U_{nc} of Na^{+} and Ca^{2+} (Eq. 4.55). An average value of the maximum current of I_{max}^{nc} = 0.48 fA, that corresponds to ν_{max}^{nc} = 3000 calcium-ions/s (found in [51, 58]) was used in order to fix the conductivity to be g_{max}^{nc} = 21.1 fS in Eq. (4.55). Here, Ca^{2+}-concentrations of C = 0.5 μM and C_{ex} = 0.1 μM as well as Na^{+}-concentrations N = 12 mM and N_{ex} = 100 mM, as described by [100], were employed. The dynamics of a single NCX protein during a Ca^{2+}-peak (caused by a single action potential) is shown in Fig. (5.6).

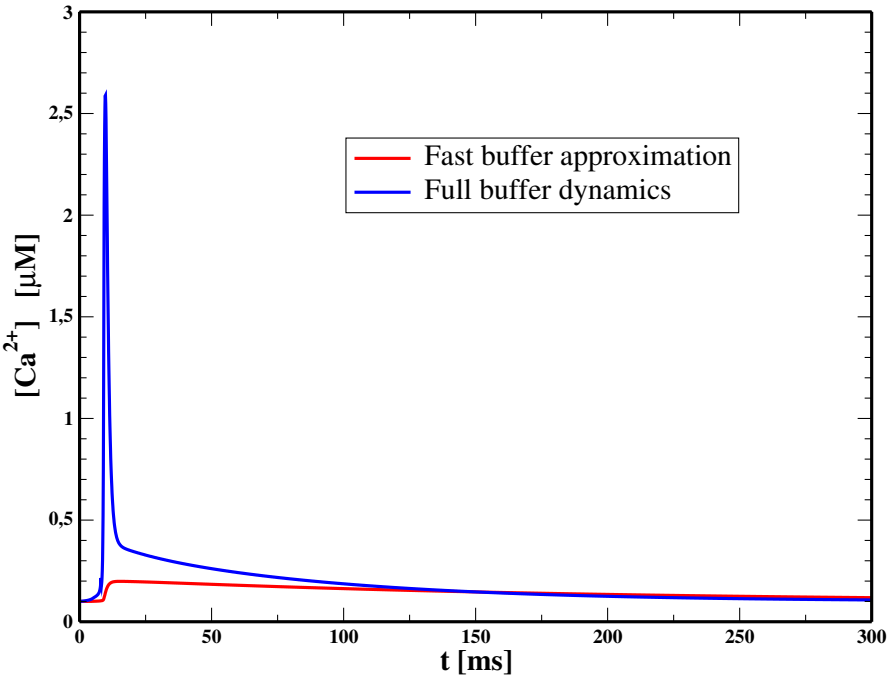

Figure 5.7: **Fast buffer approximation versus full dynamics.** The differences between the fast buffer approximation versus the full buffer dynamics are shown in comparison to the calcium peaks in the presynaptic terminal induced by a single action potential. The simulation was performed with an exogenous buffer concentration of 500 μM Magnesium Green.

Endogenous and exogenous buffers: For endogenous buffer proteins, calmodulin is the most important buffer system related to the Ca^{2+}-dynamics. Therefore it has been chosen as a representative member. The dynamics of this buffer type is described by two first order kinetic DEqs – Eqs. (4.61) and (4.62). Although the associated rate constants are unknown, estimates exist for the dissociation constant $K_d \approx 1$ μM [101], which determines their ratio. Using this estimate, the remaining free parameter has been fitted to a fluorescence measurement of [41]. The result of this fit is in good agreement with [41], stating that approximately only 1 % of the total incoming intracellular peak of the Ca^{2+}-concentration remains free. The resulting values for k_+ = 0.035 1/(μMms) and k_- = 0.035 1/ms are in the same range as values quoted by other theoretical approaches of intracellular Ca^{2+}-dynamics [5, 102]. However, it should be stressed that the values for the rate constants and the dissociation constants have been in dispute for more than one decade [73, 89]. The total calmodulin concentration B_0 = 30 μM is taken from [14] under the additional assumption that all four binding sites are acting independently.

At this point it must be stated explicitly that the prerequisites of the fast buffer approximation (Eq. 4.65), which is used in the analyses of different measurements [41, 93], are not fulfilled by the system under consideration: For such low rate constants, resulting in correspondingly high time constants, the assumption of instantaneously adapted buffer concentrations is definitively violated. The differences of the fast buffer approximation versus the full buffer dynamics are displayed in Fig. (5.7). Both shape and peak amplitude significantly depend on whether the fast buffer approximation was employed or not. Only for rate constants in the range of k_+ = 100 1/(μM*ms) and k_- = 100 1/ms, respectively, the quality of the fast buffer approximation would meet the demands of this work. Consequently, SYNDICAD does not apply the fast buffer approximation.

Several florescence indicators with different properties were used in the various results obtained in the framework of this thesis. The total indicator concentration B_0^{fl} is defined by the experimental setup of the measurements and has been taken from the corresponding publication. In addition, the experimental setup may also influence the indicator dissociation constant $K_d^{\mathrm{fl}} = k_-^{\mathrm{fl}}/k_+^{\mathrm{fl}}$. These rate constants are also a priori unknown. Again, in each case the remaining free parameter has been fitted to an appropriate fluorescence measurement regarding the dissociation constant. The relative fluorescence intensity changes F_Δ have been calculated from Eq. (4.71), where the ratio of minimal to maximum fluorescence intensity $f_{\max}/f_{\min}$ has been determined by the experimentally observed maximum of relative fluorescence intensity change $(F_\Delta)_{\max}$.

The F_Δ occurring during stimulation with a single action potential in terminals of rat pyramidal neurons are shown in Fig. (5.8). Two characteristic phases of decay are apparent: The first decay phase is dominated by the buffer dynamics whereas the second decay is determined by the sum of Ca^{2+}-buffering and efflux. It is impossible to interpret the time constants displayed in Fig. (5.8) separately, since the temporal behaviour always depends on the dynamics of all proteins participating in the reaction. In Fig. (5.9) a simulation of the dynamics of both an exogenous and endogenous buffer during a

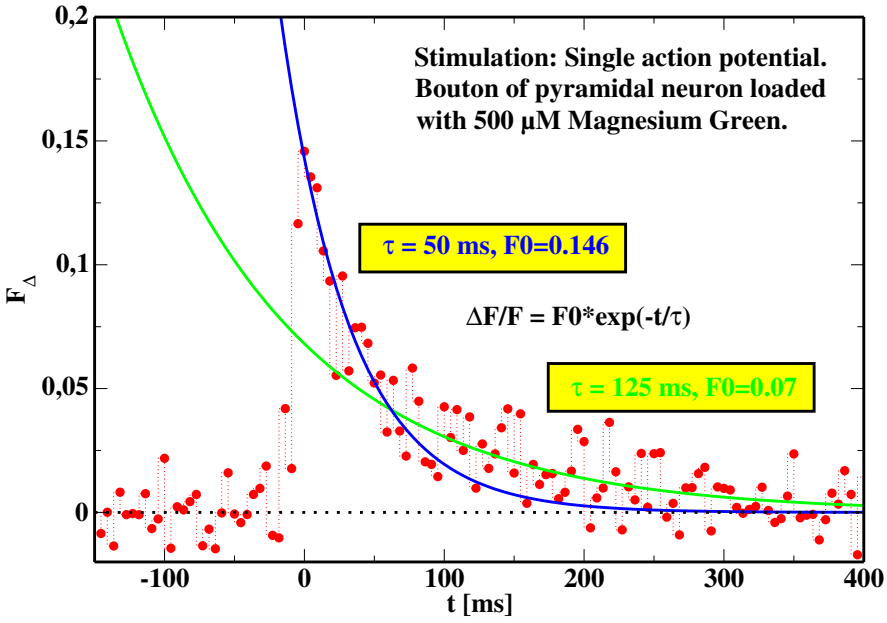

Figure 5.8: **Action potential induced fluorescence dynamics.** Fluorescence measurement in a bouton of a rat pyramidal neuron by using 500 μM Magnesium Green (data with kind permission of [41]). The bouton is stimulated by a single action potential. Short laser pulses have been used for two-photon excitation. Line scan imaging has been performed by a photomultiplier. The relative fluorescence intensity change is shown (red), which is caused by the Ca^{2+}-concentration. The decay exhibits two phases: The first phase (blue fit, below 100 ms) is dominated by the buffering process, whereas the second phase (green, above 100 ms) is determined by both buffer and efflux processes.

Ca^{2+}-peak are depicted. Obviously, the shape of the endogenous buffer concentration is considerably different from the shape of the exogenous buffer concentration. Consequently, the existence of an exogenous buffer system results in a considerably altered Ca^{2+}-dynamics. In contrast, in [41, 93] an estimate of the height of the incoming calcium peak from the relative fluorescence intensity changes via Eq. (4.75) has been calculated, which depends on the Ca^{2+}-concentration only. However, since this relation is a direct consequence of the fast buffer approximation, it seems to be sensitive to the reasoning above.

Diffusion: The importance of diffusion is demonstrated in Fig. (5.10). Here, the difference of the peak concentration between the terminals with the highest and lowest Ca^{2+}-concentration weighted by the overall peak concentration is shown as a function of the volume of the terminal with varying discretisation widths: For small volumes the normalised peak difference increases exponentially with the volume. It reaches saturation at a volume in the range of 10 μm^3. Generally, already for relatively small

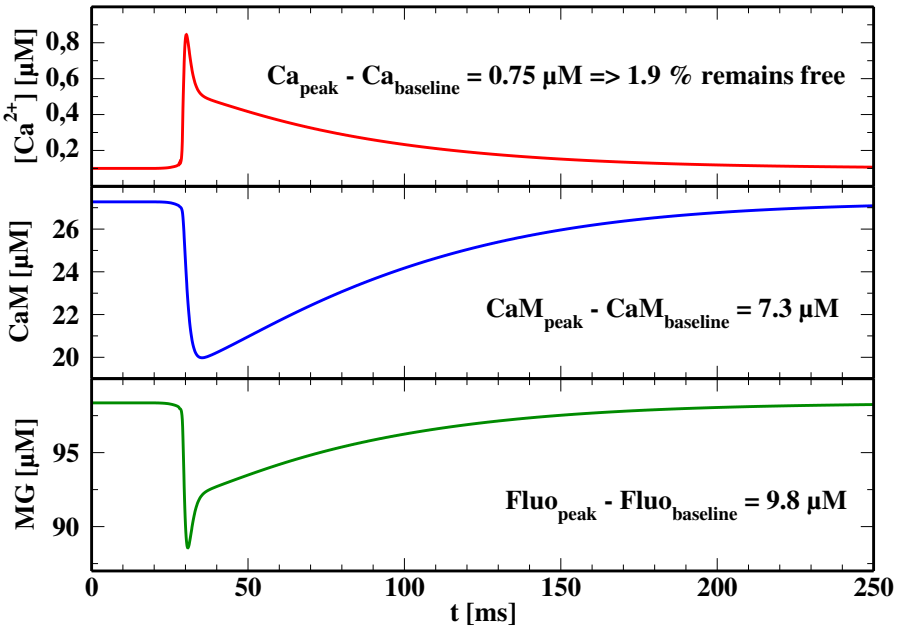

Figure 5.9: **Action potential induced buffer dynamics.** Simulation of the dynamics of a free endogenous buffer (120 μM Calmodulin CaM; blue) as well as a free exogenous buffer (100 μM Magnesium Green MG; green) caused by a Ca^{2+}-peak (red). The upper panel shows the free Ca^{2+}-peak induced by a single action potential. The dynamics of the exogenous buffer considerably changes the free Ca^{2+}-concentration dominantly in the region around 30 ms. From the peak-concentrations it can be calculated, that only 1.9 % of the total incoming Ca^{2+} remains free.

terminals with a volume of 1 μm^3 diffusion plays a significant role and has to be taken into account.

The diffusion constant D_c = 200 $\mu m^2/s$ of Ca^{2+} is based on measurements of Ca^{2+}-diffusion rates in cytoplasm [103]. This value is approximately three times smaller than in water [38] because cytoplasm is nearly twice as viscous as water. The diffusion constant D_b = 10 $\mu m^2/s$ of the endogenous buffer is estimated to be smaller due to the large volume of the protein [104, 105], whereas the diffusion constant D_b^{fl} = 200 $\mu m^2/s$ of the dye indicator is assumed to be in the same range as for Ca^{2+} [2].

Stimulation: The temporal dynamics of the membrane potential in excitable neuronal terminals is modelled by a modified Hodgkin-Huxley equation system Eq. (4.90) in order to reproduce action potentials of mammalian CNS neurons. All neuronal terminals are assumed to be iso-potential. The parameters have been adjusted such that the shape of the action potential as found in [41] is appropriately reproduced (see Fig. 5.4). This procedure is used for all further investigations on CNS action potentials.

Action potentials represent an essential basic element of the signal transduction, since the Ca^{2+}-dynamics is strongly influenced by their shape. This fact is highlighted

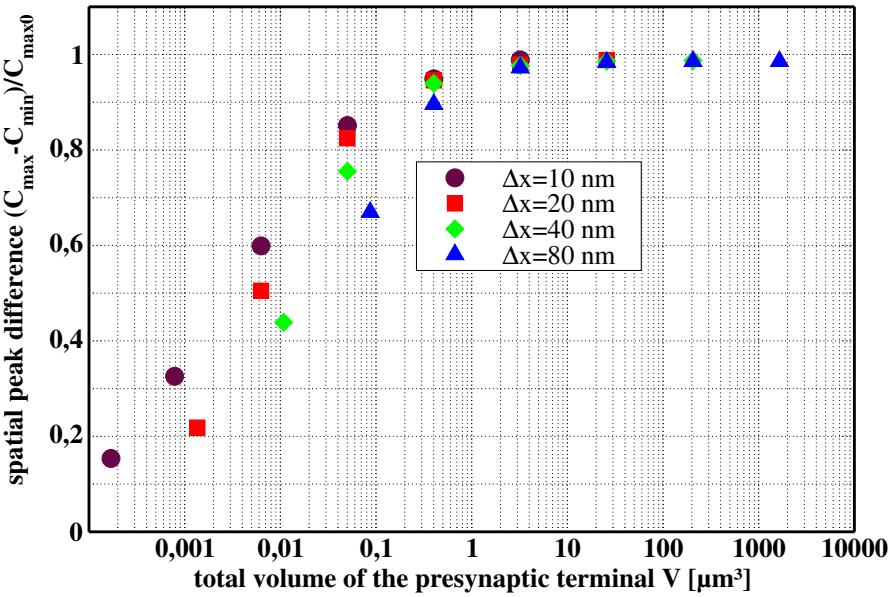

Figure 5.10: **The importance of diffusion.** Simulation of the maximum spatial calcium peak difference (induced by single action potentials) as function of the terminal volume with varying discretisation widths.

by Fig. (5.11). There, it can be seen that the total Ca^{2+}-influx is rather proportional to the area below the action potential than to its maximum absolute amplitude. Therefore, a realistic simulation of the action potential shape is of paramount importance in order to perform any quantitative study.

5.3 Spatiotemporal analysis of the Ca^{2+}-dynamics

5.3.1 Model calibration and reliability

Single action potential: To validate, whether SYNDICAD correctly describes the presynaptic Ca^{2+}-dynamics in response to single action potentials, the model is calibrated with respect to a very detailed fluorescence measurement of the Ca^{2+}-dynamics in presynaptic single terminals of pyramidal neurons in the neocortex of rats [41]. The amplitude and shape of the action potential as applied to the terminal in the experiment are reconstructed in the simulation and the free parameters are fitted such that the final result of SYNDICAD agrees well with the measured fluorescence signal evoked by a single action potential (Fig. 15C in [41]). From the experiment, both the diameter of the terminal (r = 0.5 μm) and the maximum relative fluorescence intensity change $(F_\Delta)_{\max}$ = 1.5 are known; from the simulation the rate constants of the indicator Magnesium Green have been deduced as k_+^{fl} = 0.013 1/(μMms) and k_-^{fl} = 0.078 1/ms, re-

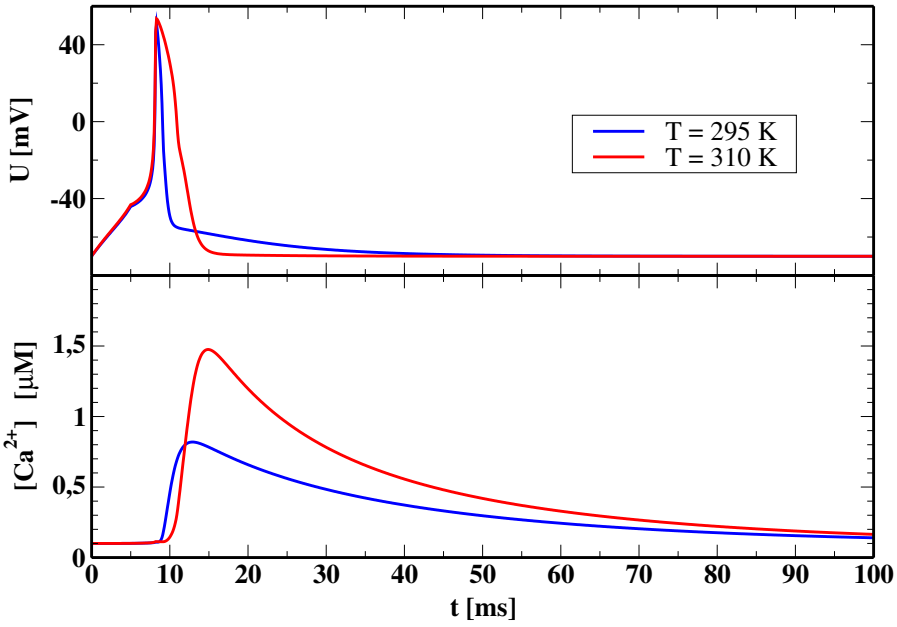

Figure 5.11: **Importance of the action potential shape**: The Ca^{2+}-dynamics is strongly influenced by the shape of the action potential. *Upper panel:* Simulation of two different shapes of action potentials due to different bath temperatures. *Lower panel:* The simulation of the resulting Ca^{2+}-dynamics displays significant differences. The total Ca^{2+}-influx is rather proportional to the area below the action potential than to its maximum absolute amplitude.

spectively.

The ratio of the NCX surface density to the PMCA density has been measured in [51]. Therefore, the only remaining free parameters are the surface densities of the VDCC ρ^{vd} and the PMCA ρ^{pm}. The surface densities of the membrane proteins (Tab. 5.1) can be interpreted as a realistic prediction for the neuron type under consideration. Note that the experiment has been conducted with B_0^{fl} = 500 μM Magnesium Green. The result of the comparison of SYNDICAD with experimental data is shown in Fig. (5.12): Obviously, amplitude and shape of the simulated fluorescence response are in good agreement with experimental data.

Different indicator concentrations: In order to test the reliability, simulations of different indicator concentrations has been compared with corresponding different experimental data sets. Fig. (5.13) shows the fluorescence pictures which have been obtained while applying the same stimulation procedure in identical set-ups but with different indicator concentrations (B_0^{fl} = 100 μM and B_0^{fl} = 2000 μM Magnesium Green). SYNDICAD reproduces the average experimental findings correctly for the different concentrations. The resulting surface densities vary over a considerable range, which is presumably due to the strong variance among the terminal sizes in the experiments. This fact is

Neuron type	VDCC	PMCA	NCX
Terminals of pyramidal neurons in the neocortex of rats (Magnesium Green)	channels/μm^2	pumps/μm^2	exchanger/μm^2
single AP B_0^{fl} = 500 μM	19.4	1822.0	61.0
single AP B_0^{fl} = 100 μM	13.7	1802.0	60.0
single AP B_0^{fl} = 2000 μM	32.7	2783.0	93.0
10 Hz train of AP B_0^{fl} = 500 μM	22.1	2953.0	98.0
Terminals of rat brainstem (MagFura-2) single AP B_0^{fl} = 400 μM	24.7	4647.0	155.0

Table 5.1: **Surface densities.** A SYNDICAD prediction for a range of the surface densities of VDCC, PMCA and NCX for two different neuron types. These values have been extracted by fitting the results of the simulation to fluorescence measurements [41, 93] using the corresponding indicator concentrations.

reflected in the limited goodness of the data: The peak intensities of the single fluorescence traces in [41] vary strongly (up to more than 100 %). All fluorescence traces are shown as averages of 13-26 different terminals[2]. This may not be enough to yield any result with statistical significance sufficient to shed light on possible short-comings of the model as implemented in SYNDICAD.

General properties of the Ca^{2+}-peaks An interesting fact is that SYNDICAD reproduces the two decay time scales very well (Fig. 5.8). They are only visible for higher indicator concentrations but not for concentrations as low as B_0^{fl} = 100 μM Magnesium Green (Fig. 5.12). The total Ca^{2+}-current into the terminal has a peak value of nearly 3 pA. Assuming a physiological single channel current of 0.4 pA results in (estimated) 8 opened VDCCs per action potential. The surface densities of 30 channels/μm^2 in the influx area yields an overall number of around 24 VDCCs per terminal. The peak values of the total Ca^{2+}-clearance rates are $170{\cdot}10^3$ calcium-ions/s for PMCA and $260{\cdot}10^3$ calcium-ions/s for NCX, respectively.

10 Hz train of action potential: The next important task is to investigate, whether the same model is able to describe Ca^{2+}-peaks evoked by more complex stimulation protocols without changing the model parameters . The fluorescence response induced by a 10 Hz train of action potentials is compared with model predictions. The experiment has been performed with 500 μM Magnesium Green. The protein surface densities have been adjusted such that the Ca^{2+}-response only to the first action potential of the train of action potentials is reproduced. Not being self-evident, the subsequent Ca^{2+}-peaks as predicted by the model turn out to be in good agreement with the fluorescence signal thus indicating the predictive power of SYNDICAD. The result is shown in Fig. (5.14).

[2]The differences could be caused, for instance, by differences in the volume of the corresponding terminals.

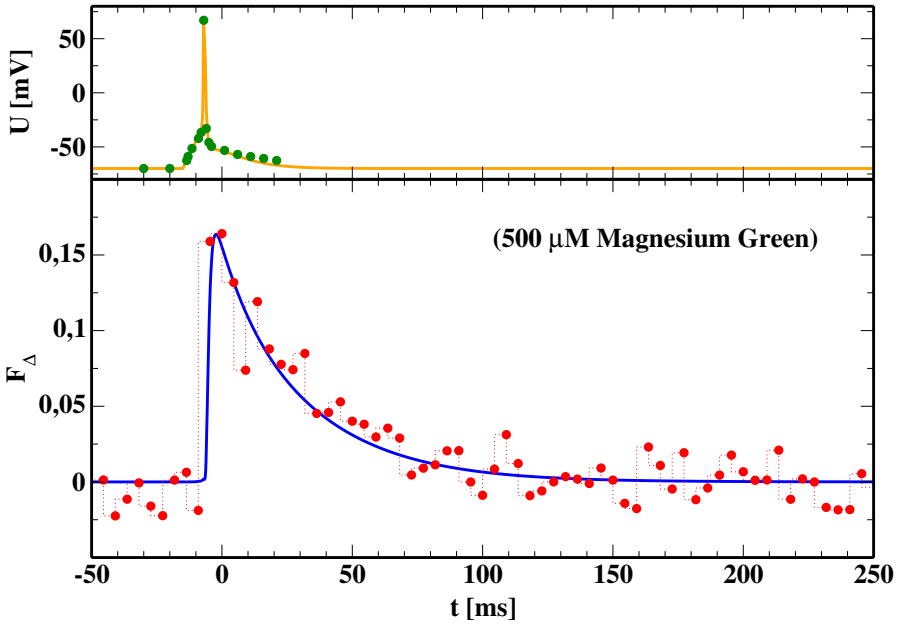

Figure 5.12: **Ca^{2+}-signal in a presynaptic terminal of the rat neocortex I.** The spatial average Ca^{2+}-peak (shown as relative fluorescence change with 500 μM Magnesium Green; average over 23 terminals in 8 cells) evoked by single action potentials in single terminals of pyramidal neurons in the rat neocortex. The upper panel shows the simulated action potential (orange) compared to the one used in experiment (green). The lower panel compares the experimental results (red, with kind permission of H. J. Koester and B. Sakmann [41], Fig. 15C) to the model results (blue).

Again, the data do unfortunately display a too large spread to allow for a more detailed comparison and more significant conclusions.

Calyx of Held: The ultimate test to SYNDICADs capability to describe any presynaptic terminal correctly on the quantitative level consists in a comparison with fluorescence measurements on large presynaptic terminals in the rat brainstem (Calyx of Held) [93]. The significance of this test is based on the fact that this system has a different geometry and size and that for the measurements a different indicator with a different affinity has been applied. The diameter of the terminals is r = 4.5 μm and as the maximum relative fluorescence intensity change (with B_0^{fl} = 400 μM MagFura-2; k_+^{fl} = 0.003 1/(μMms), k_-^{fl} = 0.058 1/ms) $(F_\Delta)_{\max}$ = 0.78 has been measured [93]. The result of the comparison of data with the simulation is exhibited in Fig. (5.15). Again, the fluorescence measurement is well reproduced by SYNDICAD. To highlight the difference in both systems it is worth to compare some values: The whole current into the terminal has a peak value of 230 pA and the overall Ca^{2+}-clearance rate lies by $322{\cdot}10^3$calcium-ions/s.

To summarise: Once the model has been calibrated with the Ca^{2+}-signal in response to single action potentials in different types of individual presynaptic terminals, it is able

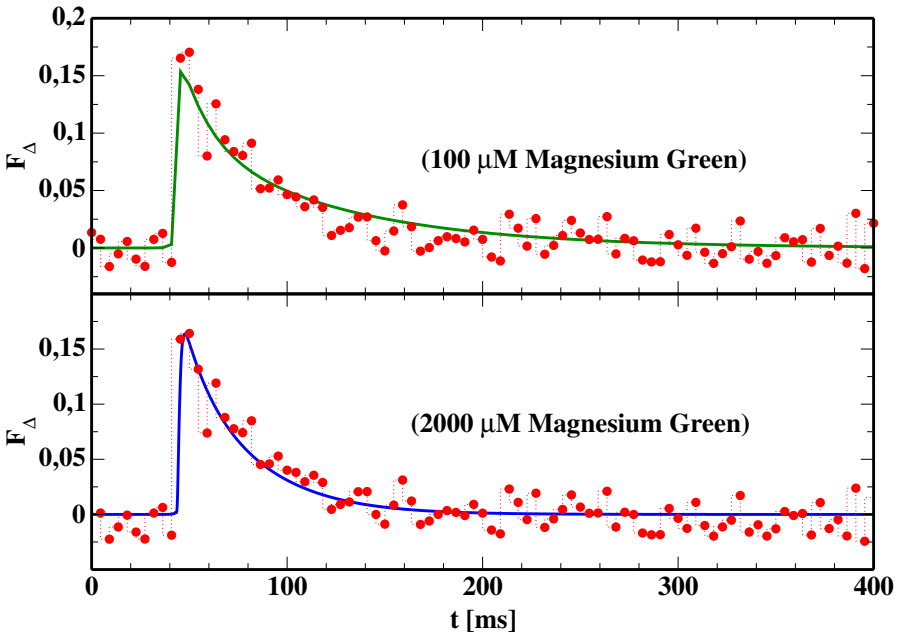

Figure 5.13: **Ca^{2+}-signals in a presynaptic terminal of the rat neocortex II.** The same experiment as in Fig. (5.12) but using different indicator concentrations: 100 μM and 2000 μM Magnesium Green (with kind permission of H. J. Koester and B. Sakmann [41], Fig. 15C). The relative fluorescence changes are shown in red (average over 16 terminals in 5 cells (100 μM MG) and 13 terminals in 3 cells (500 μM MG)). The lines represent the results of SYNDICAD for 100 μM (green) as well as 2000 μM (blue) Magnesium Green.

to describe the Ca^{2+}-signal due to different stimuli without any further changes thus giving an indication for the correctness of the model.

5.3.2 Reconstruction of the intrinsic presynaptic Ca^{2+}-dynamics from fluorescence measurements

In the following, the influence of fluorescence indicators on the Ca^{2+}-dynamics is quantified and implications for experiments using fluorescence indicators to measure Ca^{2+}-concentrations are discussed. Again, a synaptic terminal of pyramidal neurons in rat neocortex is used as the model system.

For stimulations with trains of action potentials with frequencies above some neuron-type-specific threshold frequency a new baseline of the Ca^{2+} concentration arises. In the following it will be demonstrated that the use of fluorescence indicators in experiments alters the Ca^{2+}-response and especially the emergence of a new baseline considerably. The Ca^{2+}-dynamics evoked by single action potentials with and without fluorescence indicator is compared (100 μM Magnesium Green) in Fig. (5.16). Clearly, the amplitude of the Ca^{2+}-signal decreases when a fluorescence indicator is used. In addition,

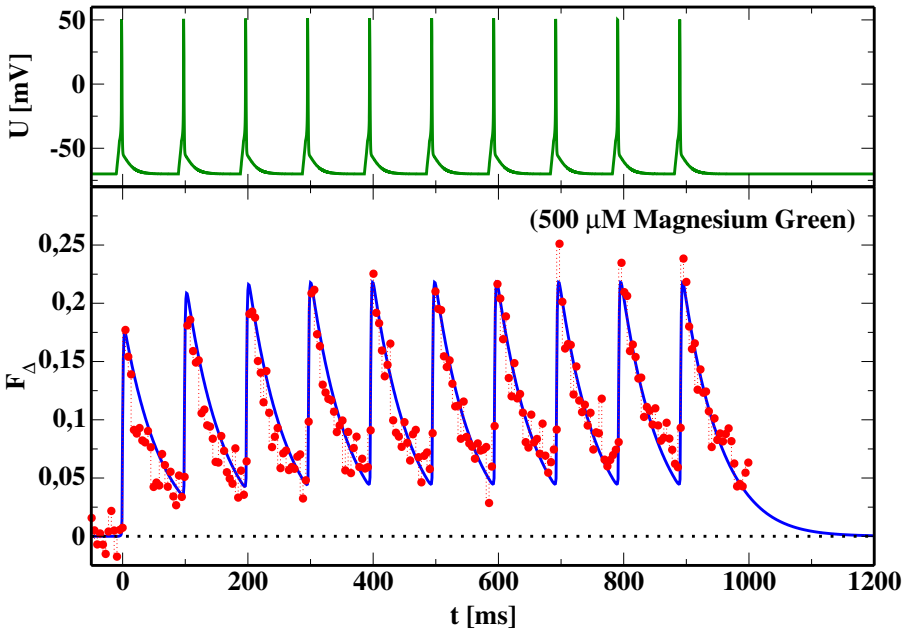

Figure 5.14: **Ca^{2+}-signals in a presynaptic terminal of the rat neocortex III.** The spatial average Ca^{2+}-concentration (shown as relative fluorescence change with 500 μM Magnesium Green) evoked by a simulated 10 Hz tetanus in single terminals of pyramidal neurons in the rat neocortex (green, upper panel) are drawn. The Ca^{2+}-signal (red, lower panel) observed in the experiment (with kind permission of H. J. Koester and B. Sakmann [41], Fig. 9) is compared to the corresponding model results (blue, lower panel).

the Ca^{2+}-relaxation time (needed to recover the rest state Ca^{2+}-concentration) becomes considerably larger in the presence of a fluorescence indicator. These findings should not be too surprising, since the indicator binds an important part of incoming free Ca^{2+}-ions and thus reduces the free Ca^{2+}-concentration. Note that the larger relaxation times are not caused by a decreased pump activity induced by the lower Ca^{2+}-peak, but by the larger extent to which intracellular Ca^{2+} binds to the buffer: The bound Ca^{2+}-ions are not subject to efflux. This has consequences for the interpretation of experiments using fluorescence indicators. SYNDICAD is able to take the effect of exogenous buffer systems into account and to predict the unperturbed Ca^{2+}-dynamics from experimental data obtained using fluorescence indicators.

5.3.3 The presynaptic Ca^{2+}-dynamics for different stimulation protocols

Investigations on effects of changing synaptic efficacy represent an important part of the neuro-physiological research. In this section, the question is addressed, whether there are characteristic differences between Ca^{2+}-peaks evoked by distinct stimulation

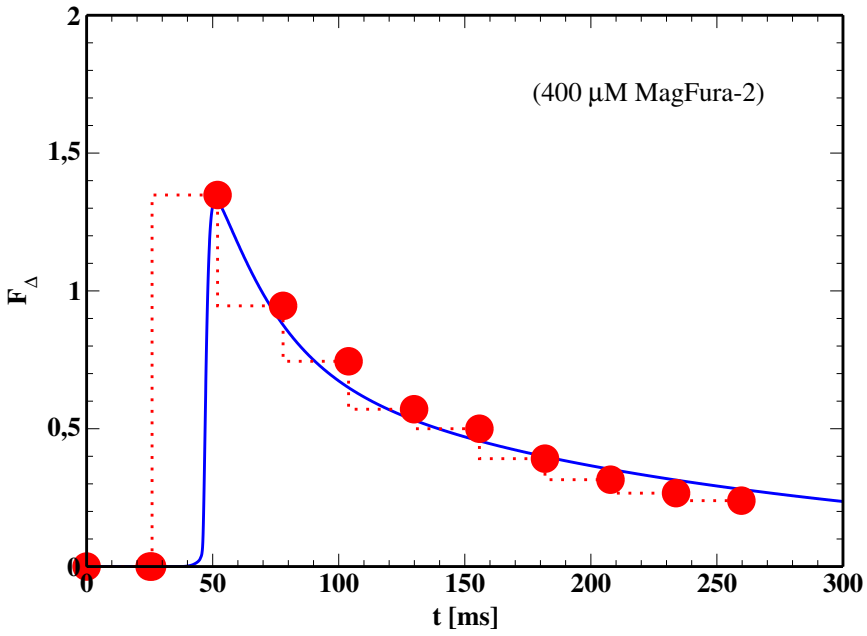

Figure 5.15: **Ca^{2+}-signals in a Calyx of Held.** The Ca^{2+}-signals during application of an action potential measured with 400 μM Mag Fura-2 in a calyx of Held are drawn. The red circles are representing the fluorescence signals (average over 20-80 sweeps) taken from the measurement [93]; Fig. 3A, Temperature: 296 K. The relative fluorescence changes have been expressed as percentage. The blue line represents the result of SYNDICAD.

protocols or not. This analysis has been performed in view of its relevance for the induction synaptic plasticity at this elementary level. A terminal of pyramidal neurons in rat neocortex has been chosen as model system, which indeed displays phenomena such as long-term potentiation.

As expected, in the low-frequency domain (2 Hz) the Ca^{2+}-response appears as a train of independent single action potential responses. This is highlighted in Fig. (5.17). The Ca^{2+}-concentration follows the activation by each action potential. Shape and amplitude of each Ca^{2+}-response remain unaltered as compared to the response to a single action potential. The stimulation frequency is in the typical range used for LTD induction [106].

For frequencies where the relaxation time of the Ca^{2+}-peaks is in the same range as the time between two subsequent action potentials (20 Hz), the baseline in the Ca^{2+}-concentration rises during stimulation. This is depicted in Fig. (5.18): The Ca^{2+}-pumps and the Na^{+}/Ca^{2+}-exchangers do not have enough time to restore the terminals rest state. This implies an overlap of the Ca^{2+}-response to subsequent action potentials. Note that this qualitative behaviour has been observed, as exemplified by experiments performed on dendritic spines of pyramidal neurons [88].

The strong increase of the peak and baseline and especially of the average Ca^{2+}-

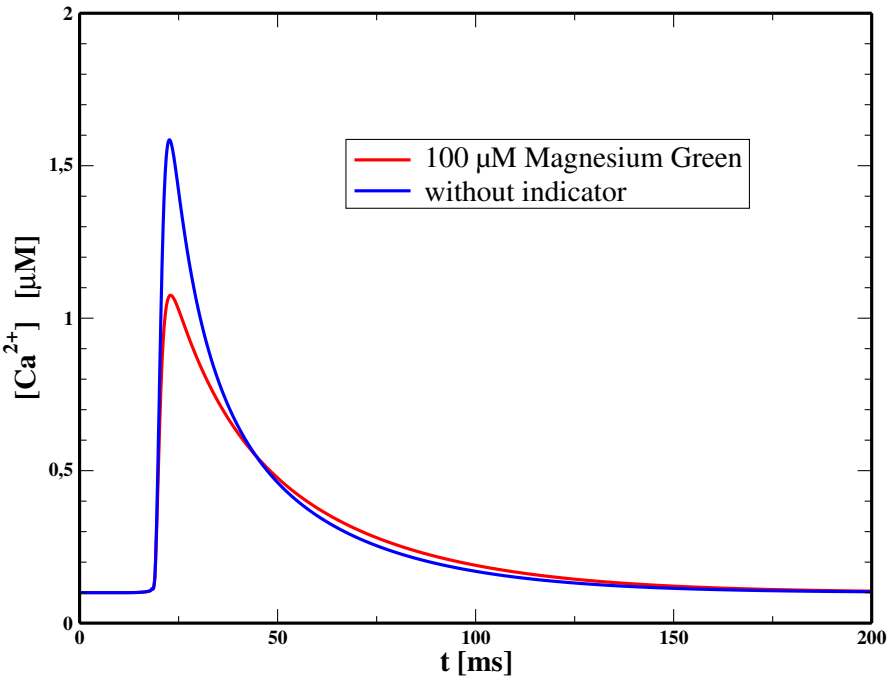

Figure 5.16: **Reconstruction of the natural Ca^{2+}-dynamics.** The spatial average Ca^{2+}-dynamics evoked by a single action potential has been drawn. The figure displays the Ca^{2+}-dynamics for a neuron with 100 μM Magnesium Green (red), and the Ca^{2+}-dynamics which would have occurred without indicator (blue). The indicator changes the amplitude and the shape of the Ca^{2+}-concentration considerably.

concentration for stimulations with larger frequencies constitutes a significant difference compared to the Ca^{2+}-response to a low-frequency train of action potential. It may be suspected that this behaviour is important for the changing synaptic efficiency. For instance, it could be shown that an accumulation of residual free Ca^{2+} is responsible for synaptic facilitation in presynaptic terminals [4, 107].

In addition, it is a well-established fact that for the induction of LTP the intensity of stimulation protocols have to overcome some threshold [106]. The strong increase of the Ca^{2+}-concentration emerges for frequencies that are in a range around this threshold [5, 108]. This hypothesis agrees well with the experimentally established fact that a modest Ca^{2+}-influx causes LTD, whereas a large Ca^{2+} influx triggers LTP [106, 109]. In general, the role of enhanced average Ca^{2+}-concentrations for changes of synaptic efficacy has been pointed out by [110]. In order to look for a significant frequency- or amplitude-modulated key of a specific induction process of one of the different forms of synaptic plasticity it has to be considered the synapse in more detail: exocytosis steps [111], buffer properties [112], diffusion effects [113] and protein kineses [114] are important elements of the induction machinery.

The qualitative behaviour of the Ca^{2+}-concentration cannot be disturbed by even

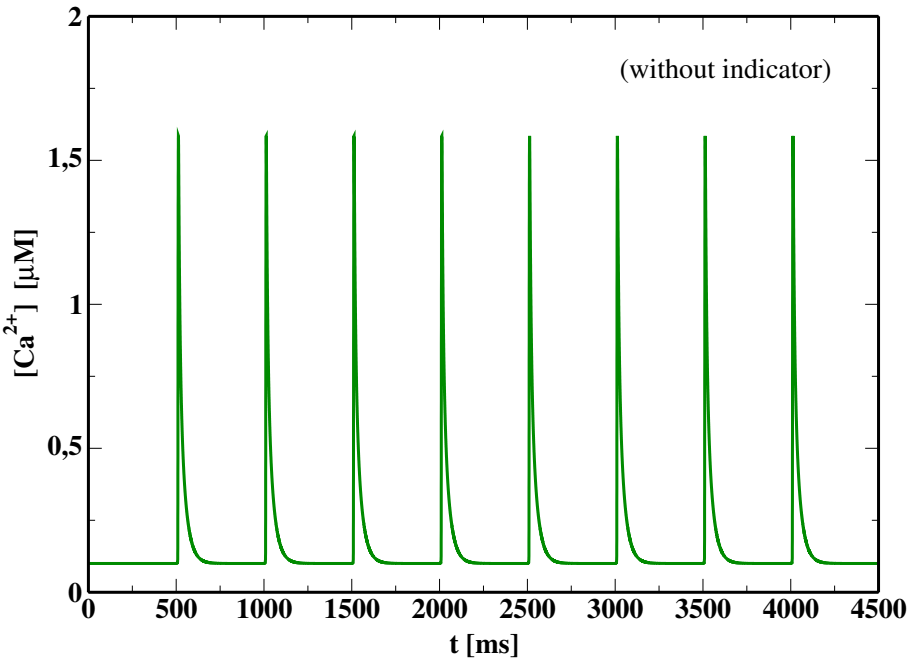

Figure 5.17: **Ca^{2+}-peaks evoked by a 2 Hz train of action potential.** This graph shows a simulation of the spatially averaged Ca^{2+}-peaks (without indicator) evoked by a 2 Hz, 3.5 s train of action potential. The Ca^{2+} responses to each action potential stimulation remain independent from each other.

larger stimulation frequencies (50 Hz): The induced Ca^{2+}-spikes remain in phase with the stimulating membrane potential. This can be seen by inspection of Fig. (5.19). There, the enhancement of the Ca^{2+}-baseline becomes even more pronounced. Again, the new baseline saturates during stimulation, but on a level which is higher compared to the 20 Hz stimulation.

The exact shape of the Ca^{2+} signal is a result of an interplay of membrane proteins and Ca^{2+}-buffers. However, some relations between the general appearance of the Ca^{2+}-signal and some specific neuron properties can be observed. Generally, the surface density of VDCC determines the amplitude of the Ca^{2+}-spikes on top of the baseline, whereas the baseline height is determined by the buffer rate constants. In contrast, the time scale, on which the Ca^{2+}-concentration returns to its rest state is governed by both the surface densities of the PMCA, NCX (efflux) and the rate constants of the buffer (buffered Ca^{2+} cannot leave the terminal). It should be emphasised that the height of the baseline levels of the Ca^{2+}-concentration increases roughly quadratically with stimulation frequencies (see Fig. 5.20) ranging up to 50 Hz.

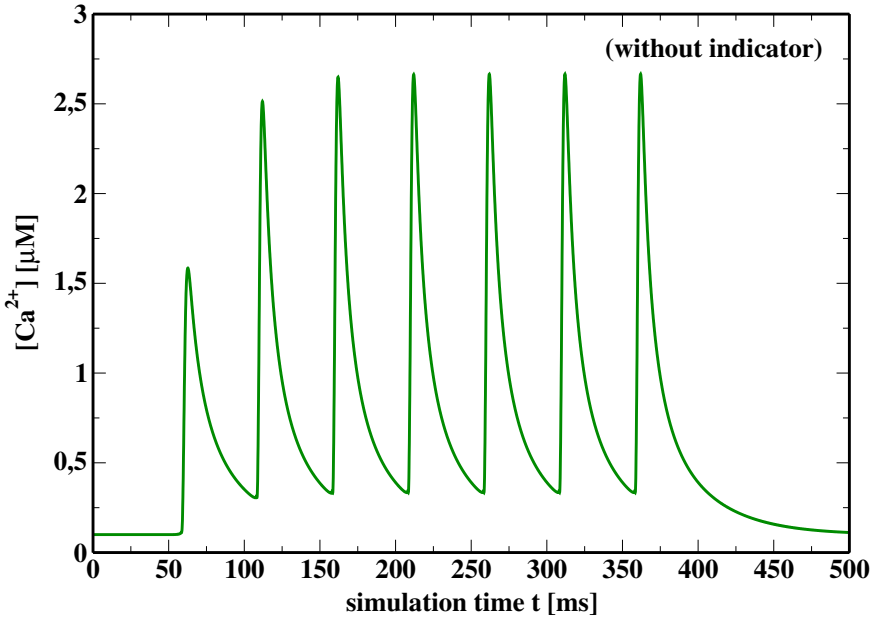

Figure 5.18: **Ca^{2+}-peaks evoked by a 20 Hz train of action potential.** The graph shows a simulation of the spatial average Ca^{2+}-concentration (without indicator) evoked by a 20 Hz, 350 ms tetanus. The baseline of the Ca^{2+}-concentration rises during stimulation. This is caused by an overlap of the Ca^{2+}-response to subsequent action potentials. The shifted baseline constitutes a significant difference compared to the Ca^{2+}-response to a low-frequency tetanus. In addition, the height of the individual peaks rises as more Ca^{2+} is bound in the buffer during stimulation, which decreases the buffer capacity.

5.3.4 The LTP induction threshold should be shifted by using exogenous buffers

The fact that exogenous buffers act as an additional intracellular buffer system changing the shape of the calcium dynamics has been pointed out before, among others by [79, 115]. In Fig. (5.21) the influence of an exogenous buffer (500 μM Magnesium Green) on the Ca^{2+}-concentration evoked by a 10 Hz train of action potential in a pyramidal neuron of the rat neocortex [41] is shown. The left panel (with exogenous buffer) clearly exhibits a shifted baseline of the Ca^{2+}-concentration, whereas the baseline remains practically unchanged in the right panel (without exogenous buffer) as would be expected for such low-frequency stimulation protocols.

Due to the longer relaxation time for the Ca^{2+}-spikes the exogenous buffer facilitates the emergence of a new baseline. Using an exogenous buffer the Ca^{2+}-spikes overlap already for lower frequencies and the baseline is significantly higher. Consequently, the threshold stimulation frequency for the emergence of a new baseline is larger for neurons without exogenous buffer compared to neurons that have been treated with indicators. In contrast, the maximum peak concentrations exhibit the opposite behaviour, see

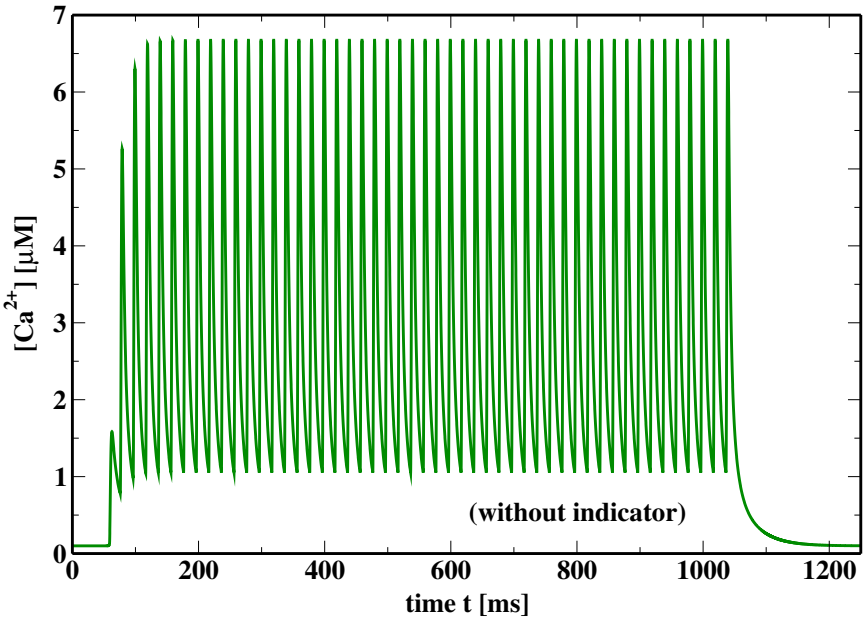

Figure 5.19: **Ca^{2+}-peaks evoked by a 50 Hz train of action potential.** This graph shows a simulation of the spatial average Ca^{2+}-dynamics (without indicator) evoked by a 50 Hz, 1 s tetanus. In comparison to Fig. (5.18), there is a more pronounced enhancement of the Ca^{2+}-baseline. Again, the new baseline saturates during stimulation but on a level which is higher compared to the 20 Hz stimulation.

Fig (5.21). By using an exogenous buffer the maximum peak concentration becomes considerably smaller than in a similar measurement without buffer. Nevertheless, it should be noted that the overall average height of the Ca^{2+}-concentration is practically unchanged with and without exogenous buffers.

The behaviour described above could be used for testing the sensitivity of LTP induction to the baseline height, the average or the maximum peak of the Ca^{2+}-concentration. The underlying hypothesis predicts a possible shift of the LTP induction threshold triggered by an exogenous buffer. Consequently, the experiment should measure the LTP induction threshold frequency without and with an exogenous buffer:

If the LTP induction threshold frequency is shifted to *lower* frequencies in the presence of an exogenous buffer, the LTP induction process should be sensitive to the baseline of the Ca^{2+}-levels. On the other hand, if the LTP induction threshold frequency is shifted to *higher* frequencies, then the LTP induction process is sensitive to the maximum peak of the Ca^{2+}-levels. If, in contrast, the LTP induction threshold frequency is unaltered, then the LTP induction process might be sensitive to the average Ca^{2+}-level or even be a frequency-coded effect. In the last case, it would be impossible distinguished between the two possibilities. To summarise: Using this procedure groups of processes of the LTP induction machinery in terms of the calcium affinity may be ruled out (compare section 5.3.3). Finally, note that the right panel in Fig. (5.21) again

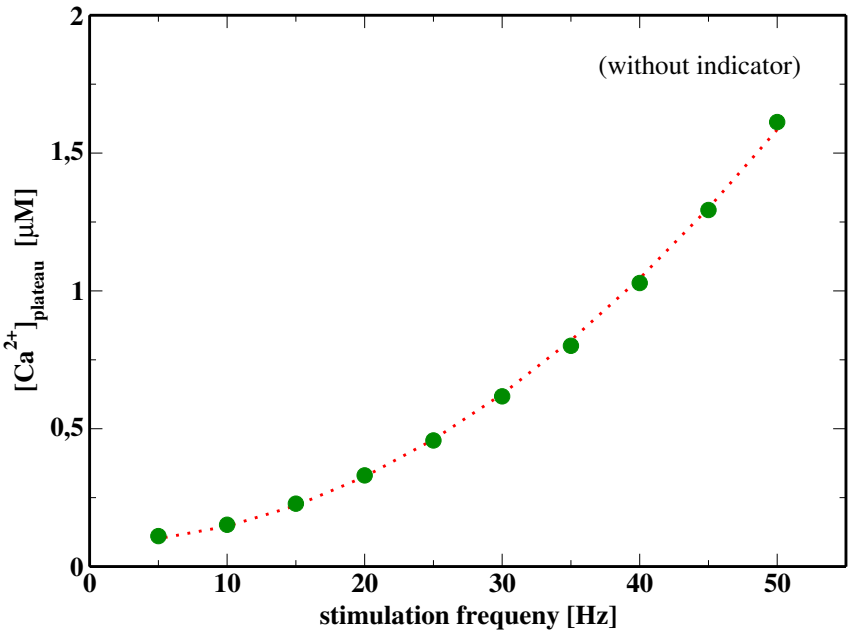

Figure 5.20: **The height of the Ca^{2+}-baseline as function of the stimulation frequency.** The height of the baseline levels of the Ca^{2+}-concentration of the simulation increases quadratically (quadratic fit with red dots) with stimulation frequencies ranging up to 50 Hz. As the bound buffer concentration saturates at large frequencies, the Ca^{2+}-relaxation depends on the linear membrane efflux only. This in turn leads to a linear behaviour of the Ca^{2+}-baseline height at large stimulation frequencies (not shown here).

provides a quantitative prediction of the Ca^{2+}-signal in the pyramidal neuron of the neocortex as it would have been without the use of an exogenous Ca^{2+}-buffer starting from the Ca^{2+}-measurement [41].

5.3.5 Properties of microdomains

It has been stated in Sec. (2.2) that the locality of the Ca^{2+}-signals within the presynaptic terminal may have an important impact for both the trigger of the neurotransmitter release [116] and further calcium induced activities within the neuron. Therefore, in this section the investigation of Ca^{2+}-signal, considering diffusion discussing only spatially averaged dynamics should be extended to a detailed view into the spatial resolved dynamics of the Ca^{2+}-ions in the region of a microdomain. In particular the question will be addressed, whether the results presented above can be confirmed for such a local view or whether significant differences exist.

Most of what is known about the temporal and spatial characteristics of Ca^{2+}-microdomains is based on model simulations [4, 117, 118, 119], because the currently available imaging technology does not simultaneously provide a sufficiently high reso-

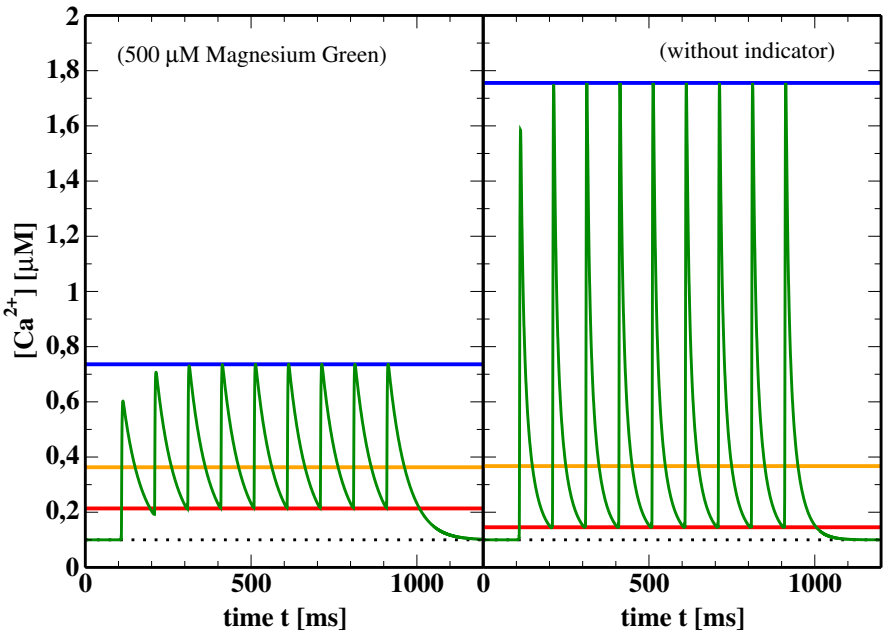

Figure 5.21: **Comparison of peak, average and baseline of the Ca^{2+}-concentration with and without a buffer.** In this graph, the simulation of the spatial average Ca^{2+}-dynamics evoked by a 10 Hz tetanus is drawn. The left panel shows the Ca^{2+}-concentration with 500 μM Magnesium Green, whereas the right panel displays the response without an exogenous buffer. The presence of an exogenous buffer changes the Ca^{2+}-signal and the height of the baseline considerably. The coloured lines represent the maximum peak values (blue) which are increased, the average concentration (orange) which is nearly unchanged and the height of the baseline (red) which is decreased in the absence of an indicator.

lution in time and space. Either the temporal resolution is suitable, which results in a sparse spatial resolution and vice versa. Recent simulation studies have shown that the properties of the microdomains are dominantly determined by the following factors:

- A microdomain consists of a cluster of VDCC. Properties such as topography of the VDCC and their overall number within a microdomain determine the dynamics of the microdomain [119, 120, 121].

- The incoming Ca^{2+}-ions are locally fixed through the presence of slow-moving buffers [122]. Therefore, both the diffusion constants of Ca^{2+}-ions and of the buffers themselves represent important factors. The influence of the buffer diffusion has been analysed by a variation of the buffer diffusion constant. Interestingly, the results show clearly that the local fixation of the Ca^{2+}-ions is only little decreased by assuming an 100fold increased diffusion constant of the buffer. This result could be changed by repetitive stimulation and corresponding enhanced accumulation of Ca^{2+}-ions to the buffer.

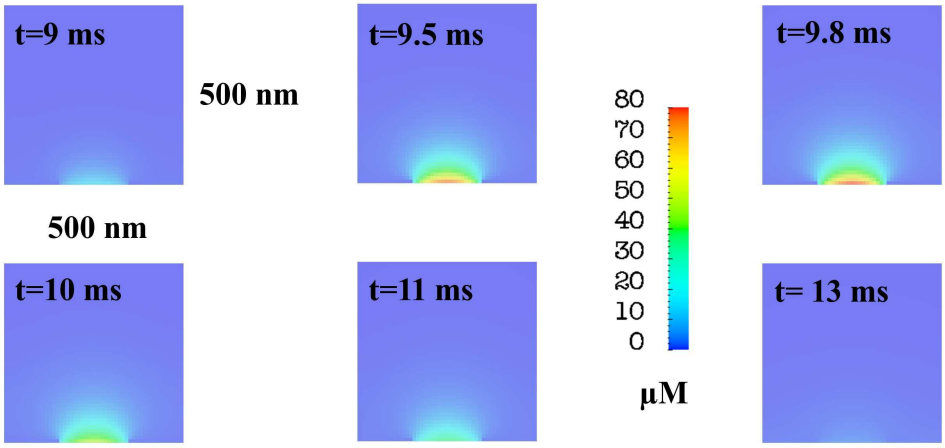

Figure 5.22: **Spatiotemporal Ca^{2+}-dynamics in a microdomain.** The simulation of the time series of the local Ca^{2+}-concentration caused by a single VDCC cluster with the diameter of 200 nm in a presynaptic terminal is drawn. The terminal was stimulated by a single action potential. The terminal has a diameter and a height of 500 nm. The Ca^{2+}-concentration develops to a peak value of 80 μM and decays in a time range of 5 ms.

- Different microdomains within a single active zone of the presynaptic terminal can interact through an overlap of the single-microdomain signals [117].
- The vesicles are assumed to be attached to the microdomains. Their distribution and overall number influences the release of the neurotransmitter [123].

First, the spatial distribution of the Ca^{2+}-ions near a single microdomain has been analysed. For this, it has been assumed that the presynaptic terminal of a pyramidal rat neuron contains only a single microdomain (which is realistic for such small terminal with a diameter of nearly 1 μm) and the whole Ca^{2+}-influx current induced by a single action potential occurs at this microdomain. The diameter of the VDCC-cluster has been measured to be approximately 200 nm. The result is shown in Fig. (5.22). The local Ca^{2+}-concentration reaches a maximum value of nearly 80 μM, which is a drastically increased value compared to the terminal averaged Ca^{2+}-concentration. The width of the microdomain is determined by the cluster width of 200 nm. In contrast, the spatial size of increased Ca^{2+}-concentration is determined by the diffusion process of both calcium and buffers and reaches a value of nearly 150 nm. The local peak decays very fast, on a time scale of approximately 5 ms.

In order to compare the local Ca^{2+}-signals with the statements above on the volume averaged Ca^{2+}-concentration, the dynamics of the Ca^{2+}-concentration within the microdomain has been analysed in dependence on different stimulation frequencies. The qualitative behaviour agrees well with the volume-averaged analysis. Also, the thresh-

old frequency for the baseline enhancement is in good agreement with the statements above. But the amplitudes of both the baseline and the peak concentration are significantly shifted to higher values. This leads to the following hypothesis: Both Ca^{2+} signals encode different processes: 1. The local Ca^{2+}-signal might be relevant for effects such as STP and STD. 2. The volume averaged Ca^{2+}-signal might be relevant for phenomena such as LTP and LTD. This hypothesis can be verified by a quantitative determination of the Ca^{2+}-sensitivity of possible induction mechanisms for short- against long-term plasticity as well as the location of the induction mechanisms within the neuron.

5.4 Discussion of results

SYNDICAD represents a well-developed tool for quantitative investigations of the spatiotemporal Ca^{2+}-peaks in presynaptic terminals of neurons including VDCC, PMCA, and NCX, as well as endogenous buffers and fluorescence indicators. These ingredients turned out to be sufficient to quantitatively reproduce all fluorescence measurements of intracellular free Ca^{2+}-peaks in response to single action potentials in pyramidal neurons of the rat neocortex. On the basis of the parameter set determined by the single action potential Ca^{2+}-peaks the model predicts, on a quantitative level, the Ca^{2+}-response for different stimulation patterns. This holds true in particular for a 10 Hz train of action potential.

The single action potential Ca^{2+}-response has been produced by fitting two parameters only: The average membrane-protein surface densities of the VDCC and the PMCA, respectively. All other parameters have been fixed either by the experiment itself or by independent single-protein measurements. The resulting values for the VDCC density are in good agreement with experimental data [44]. The PMCA density, in contrast, is found at the upper edge of values that have been observed experimentally [124]. The protein densities resulting for every neuron type can be interpreted as a prediction for average densities on the terminal. In view of the difficulties to measure such protein densities directly, their calculation with SYNDICAD provides an attractive alternative.

The general behaviour of Ca^{2+}-peaks has been investigated in response to different stimulation protocols: For a 2 Hz train of action potentials no characteristic feature of the Ca^{2+}-signal has been found, which differs from independent single action potential answers. This agrees well with the interpretation that synaptic facilitation is triggered by calcium enhancements, while synaptic depression is a consequence of reduced release-site activity [125]. A characteristic difference between Ca^{2+}-peaks in response to 2 Hz- and 50 Hz-stimulations has been found both experimentally [88] and in the simulation: Above threshold stimulation frequency, the Ca^{2+}-signal does not return to its rest state level after each spike. Instead, the baseline is shifted towards a higher level and the Ca^{2+}-spikes develop on top of this baseline. This investigation has been also presented in [126]. Indeed, the strong increase in the Ca^{2+}-signal for stimulation frequencies above some threshold can be interpreted as corresponding to the stimulation threshold for the induction of LTP [127]. Rephrased, the emergence of an enhanced baseline and, as a consequence, of an enhanced average value and increased

peak values of the Ca^{2+}-concentration constitute a necessary requirement for induction of LTP. The height of the baseline increases quadratically with increasing stimulation frequencies up to frequencies for which the buffer becomes saturated with Ca^{2+}. For higher frequencies the baseline increases only linearly.

Already on the level of calcium-dynamics averaged over the whole terminal it has been confirmed that the endogenous and exogenous buffer concentrations as well as their saturation properties crucially shift the threshold of the stimulation frequency [79, 115, 127]. It is important to realise the strong influence of fluorescence indicators on the intracellular free Ca^{2+}-signal [128, 129, 130]. Therefore, this problem has been investigated in more detail through a simulation with SYNDICAD. On the level of single action potentials, the use of indicator leads to considerably smaller Ca^{2+}-spikes, which relaxed to the rest concentration slower. This implies that the use of indicator shifts the threshold stimulation frequency mentioned above. Therefore, a quantitative evaluation of fluorescence measurements should always include the effect of the indicator, as has been done in [131, 132]. These results have been published also in [133]. Furthermore, a new test has been proposed in order to rule out possible candidates to which the LTP-induction machinery might be sensitive: The baseline, the average, or the maximum of the Ca^{2+}-peaks. Finally, the local Ca^{2+}-signals in the region of a microdomain has been compared to the volume-averaged results. SYNDICAD incorporates a specific model and provides a tool to reconstruct both the averaged or the spatial resolved Ca^{2+}-concentration as it would have been without indicator in fluorescence measurements.

Chapter 6

Summary and outlook

This thesis dealt with the simulation of synaptic signal transmission. It aimed at the development of a model, which is capable of quantitatively describing processes relevant for signal transmission on the level of single proteins. The basic idea was to incorporate all experimental findings on the single protein level and to investigate their interplay in individual synapses. In order to do this, the model had to be tested on its ability to reproduce experimental data. This thesis has focused on processes taking place on the presynaptic side of the synapse. It is clear that any fully-fledged model of the synapse will have to incorporate both sides. Consequently, the modular architecture of SYNDICAD allows for a straightforward extension towards a complete model of synaptic transmission. However, the presynapse serves as an excellent starting point for such an effort. This is especially true in view of the comparably good experimental situation for single-protein measurements within the presynapse. In general, calcium plays a dominant role in synaptic signal transmission in the pre- and the postsynapse, explaining the particular interest in its dynamics.

The resulting model for spatiotemporal calcium-dynamics in presynaptic terminals is based on ion fluxes through a membrane, which separates the intra- and extracellular space. These fluxes are triggered by external stimuli, and they are realised by transmembrane proteins, which act as pores, pumps or exchangers (voltage-dependent calcium channel – VDCC, plasma membrane calcium ATPase – PMCA, and sodium/calcium exchanger – NCX, respectively). In addition, the ion dynamics is strongly influenced by intracellular molecules acting as endogenous and exogenous ion buffers. Depending on both intracellular ion concentration and external conditions, these proteins dynamically change their behaviour with respect to ion-permeability (VDCC) and pumping rate (PMCA and NCX) or their ability to bind the ions (buffer), respectively.

The protein-ion interactions under the additional influence of complicated external conditions – e.g membrane geometry, time-dependent membrane potentials, etc. – are modelled by a system of coupled reaction-diffusion equations. These partial differential equations include the following elements: 1. Diffusion of ions and buffers is described by classical diffusion terms, first order in time second order in space. 2. The opening mechanism of VDCCs has been described by a Markov model which leads to a set

of ordinary differential equations. The ion fluxes through the open pore have been determined by the approximate Goldmann-Hodgkin-Katz solution of the corresponding electrochemical gradient problem. 3. The buffering process within a single molecule has been modelled by a first-order kinetics, which has been translated into a set of ordinary differential equations by using the law of mass action. The dynamics of PMCA and NCX has been described by a Michaelis-Menten like model and again been translated into a set of ordinary differential equations. In particular for NCX the dependence of the maximum exchanger rate on the electrochemical gradient of sodium and calcium has been taken into account.

The resulting set of differential equations and methods for their numerical solution have been implemented in terms of an object-oriented computer code – called SYNDICAD – in the modern programming language C++. The model architecture of SYNDICAD is designed to allow a differentiation between universal single-protein characteristics, which are assumed not to depend on the neuron under consideration, and specific parameters, which depend on the specific neuron type and on the specific experimental conditions. This classification allows SYNDICAD to be adjusted to different neuron types. The most important specific parameters are represented by the surface densities of VDCC, PMCA and NCX. They have been treated as fit parameters and have been determined by experimental data on the cellular level. These data stem from fluorescence measurements. Both the fluorescence dynamics and the side-effect of additional calcium buffering of these measurements have also been included into the model. SYNDICAD has been adapted to the fluorescence measurements of two neuron types, namely the pyramidal neuron of the rat neocortex and the Calyx of Held. In these measurements, the impact of different external stimuli, ranging from a single pulse to a train of action potentials, has been investigated. On the qualitative and quantitative level all relevant properties could be reproduced. In general, the adaptation of SYNDICAD to a specific neuron type allows for a prediction of the surface protein densities. The resulting values agree well with other – independent – estimates and measurements.

The above suggestion that the surface densities of VDCC, PMCA and NCX represent the most significant difference of specific neuron types certainly has to be extended to different subtypes of the proteins. However, the experimentally detected differences between protein subtypes turn out to be rather small. The differences are dominated by other uncertainties of the model parameters as for example the sensitivity of calcium transients to the shape of the action potential. Consequently, there was no possibility to consider such differences in this thesis.

SYNDICAD has been used for investigations on the contributions of single proteins to the global calcium dynamics within the presynapse:

At first, influx current caused by the VDCC in dependence on the stimulus has been discussed in detail. The influx of calcium has been shown to be more sensitive to the shape of the action potential than to its amplitude.

The central importance of endogenous buffers to the calcium dynamics in presynaptic terminals has been demonstrated. The obtained rate constants for the buffer dynamics do not justify the – elsewhere widely employed – fast buffer approximation.

It has been measured before that during a single action potential nearly 99% of the incoming calcium is bound to endogenous buffer proteins. This experimental result could be reproduced in the simulations. In contrast, during repeated stimulation with frequencies above 20 Hz, the relaxation time of the buffer coincides with the duration between two subsequent calcium responses, which consequently increases the baseline of the calcium concentration. For extremely large stimulation frequencies above 100 Hz, the bound buffer saturates, which leads to a linear dependence of the baseline shift on the stimulation frequency. Generally, the shifted calcium baseline is assumed to play an important role for synaptic memory effects such as synaptic plasticity.

It has been possible to reproduce fluorescence measurements with SYNDICAD by calculating the concentration of bound indicators and the resulting fluorescence intensity. The side-effect of these exogenous fluorescence indicators has been taken into account by calculating the complete set of reaction-diffusion equations. This allows SYNDICAD to reconstruct the unperturbed – physiological – neuronal responses which has been performed in this thesis.

In particular, the fluorescence signals have been further analysed: The maximum amplitude of the fluorescence signal depends on both the amplitude and duration of the stimulus and reflects the maximum free calcium concentration inside the neuron, which crucially depends on the VDCC activity. The decay phase of the fluorescence signal can be divided into two stages: One with a comparably steep decrease of the fluorescence intensity and one with a comparably small decrease. This behaviour is caused by the cooperative buffering by the fluorescence indicator and the endogenous buffer inside the cell. Although the overall calcium dynamics is by far more involved, the existence of two phases can be interpreted as different binding dynamics of the two buffers. Of course, the emerging fluorescence pattern also reflects the impact of the calcium extrusion mechanism realised by PMCA and NCX. The interaction of these two calcium extrusion mechanisms has been disentangled, under particular consideration of two different modes of the NCX. Earlier experimental evidence – pointing into the direction that the NCX transport dominates for the rapid reduction of large calcium concentrations – has been confirmed. In contrast, for low calcium concentrations the calcium efflux is dominantly accomplished by the PMCA.

A further purpose of SYNDICAD is to illuminate the induction mechanisms of different phenomena that are triggered by calcium in dependence on some stimulus. In the framework of this thesis this has been performed by an identification of possible mechanisms responsible for the induction of LTP on the level of the calcium concentration: The frequency domain, at which LTP can be induced by applying trains of action potentials, remarkably coincides with the frequencies that lead to a shift of the baseline of the calcium concentration. This supports the important role of the calcium concentration in LTP induction.

An experiment has been proposed that discriminates between potential calcium-related quantities that may induce LTP. The threshold frequency necessary for the induction of LTP should be measured with and without an exogenous buffer. If the LTP induction mechanism is sensitive to the baseline of the calcium concentration,

the threshold frequency will decrease in presence of an exogenous buffer. On the other hand, if the induction is triggered by the peak amplitudes, than the threshold frequency will increase.

In addition, microdomains of enhanced calcium concentration inside the neuron have been analysed. In the model microdomains have been realised by inhomogeneous VDCC distributions. Assuming all VDCC proteins to be concentrated within a cluster of 200 nm size, local calcium concentrations of up to 80 μM have been observed in the corresponding simulations. This is clearly larger than the average calcium concentrations inside a presynapse during stimulation. The large calcium concentration coincides with values obtained from independent investigations. The different calcium patterns with and without microdomains may correspond to different effects in synaptic plasticity.

These results open the way to a number of related questions for future investigations. First of all, more processes than implemented so far – involved in signal transmission through the synapse – play a role for the calcium dynamics in the presynaptic terminal. A striking example for this is the phenomenon of calcium-induced calcium release, which plays a role in some neuron types and which is triggered by internal messenger cascades. In addition, further subtypes of the involved proteins should be included after uncertainties of the protein characteristics and the overall calcium dynamics have been removed. The integration of the relevant messenger cascades in SYNDICAD – leading to the phosphorylation or the synthesis of proteins involved in synaptic transmission – may open a pathway towards a full understanding of effects as long-term potentiation.

The modular architecture of SYNDICAD represents an excellent starting point to a complete model of synaptic signal transmission, including the postsynapse. Of course, when taking into account postsynaptic receptors, at least a similar scheme of going from single-protein based experimental data to a model of the full system has to be realised. This has to be supplemented with a model dealing with the link of both terminals, i.e., processes related to the release and reception of neurotransmitters have to be simulated as well. The comprehensive system should then allow to test hypothesis about complex synaptic activity. Many of these aspects have already been prepared within SYNDICAD. This opens a lot of exciting possibilities for future research.

Appendix A

Parameters of SYNDICAD

A.1 General parameters

category	symbol	meaning	value
geometry1: Presynaptic terminal from a rat pyramidal neuron	r	radius of the terminal	0.5 μm
	l	height of the terminal	1.0 μm
geometry2: Calyx of Held	r	radius of the terminal	4.5 μm
	l	height of the terminal	9 μm
equilibrium			
	U_0	equilibrium membrane potential	-70 mV
	C_0	equilibrium Ca^{2+}-concentration	0.1 μM
external			
	C_{ex}	external Ca^{2+}-concentration	1.5 mM
	T	temperature	310 K
	N	intracellular sodium concentration	12 mM
	N_{ex}	extracellular sodium concentration	145 mM

A.2 VDCC

symbol	meaning	value
$U_{0.5}$	Half activation potential	-3.9 mV
U_{sl}	Steepness factor	7.1 mV
k_1	Activation time constant parameter	1.12 1/ms
U_1	Activation time constant parameter	31.5 1/mV
k_2	Activation time constant parameter	0.14 1/ms
U_2	Activation time constant parameter	8.6 1/ms
p	Single channel permeability	1.1 $\mu m^3/s$

A.3 PMCA

symbol	meaning	value
$\nu_{\max}^{\mathrm{pm}}$	Maximum transport rate	30 1/s
$K_{0.5}^{\mathrm{pm}}$	Half activation concentration	0.09 μM
τ^{pm}	relaxation time constant	1 ms
n^{pm}	Hill coefficient	2

A.4 NCX

symbol	meaning	value
$g_{\max}^{\mathrm{nc}}$	Maximum conductivity	21.1 fS
$K_{0.5}^{\mathrm{nc}}$	Half activation concentration	0.6 μM
τ^{nc}	relaxation time constant	1 μs
n^{nc}	Hill coefficient	1

A.5 Endogenous buffer

symbol	meaning	value
B_0	total buffer concentration	30 μM
k_+	forward rate constant	0.035 1/(μM*ms)
k_-	backward rate constant	0.035 1/ms

A.6 Indicator: Magnesium Green

symbol	meaning	value
B_0^{fl}	total indicator concentration	100-2000 μM
k_+^{fl}	forward rate constant	0.013 1/(μM*ms)
k_-^{fl}	backward rate constant	0.078 1/ms
$(F_\Delta)_{\max}$	maximum of relative fluorescence change	1.5

A.7 Indicator: Mag-Fura2

symbol	meaning	value
B_0^{fl}	total indicator concentration	400 μM
k_+^{fl}	forward rate constant	0.002 1/(μM*ms)
k_-^{fl}	forward rate constant	0.040 1/ms
$(F_\Delta)_{\max}$	maximum of relative fluorescence change	0.78

A.8 Diffusion

symbol	meaning	value
D_{c}	calcium diffusion constant	200 μm^2/s
D_{b}	endogenous buffer diffusion constant	10 μm^2/s
$D_{\mathrm{b}}^{\mathrm{fl}}$	indicator diffusion constant	200 μm^2/s

A.9 Stimulation

symbol	meaning	value
$\overline{g}_{\mathrm{na}}$	sodium maximum conductivity	330 mS/cm^2
U_{na}	sodium reversal potential	60 mV
τ_{m}	sodium activation time constant	0.1 ms
U_{m1}	sodium potential of half activation	10.0 mV
U_{m2}	sodium activation steepness factor	7.2 mV
τ_{h}	sodium inactivation time constant	0.5 ms
U_{h1}	sodium potential of half inactivation	-12.0 mV
U_{h2}	sodium inactivation steepness factor	-6.9 mV
$\overline{g}_{\mathrm{k}}$	potassium maximum conductivity	330.0 mS/cm^2
U_{k}	potassium reversal potential	-98.0 mV
τ_{n}	potassium activation time constant	0.5 ms
U_{n1}	potassium potential of half activation	0.0 mV
U_{n2}	potassium activation steepness factor	4.0 mV
U_{l}	leakage reversal potential	-71.5 mV
I_{i}	induction current	20.0 μA/cm^2
c_{m}	membrane capacity	3.6 μF/cm^2

Appendix B

Short Manual of SYNDICAD

The source code for SYNDICAD can be found in the root directory of the CD included in this thesis. In order to use the advantages of object-oriented programming, the programming language C++ has been chosen. SYNDICAD has been implemented under the operating system Linux (kernel version 2.4.21-166-smp4G) using the gcc 3.3.1 compiler of the SuSE distribution. Only the included standard libraries have been used.

In the following, the basic file structure of SYNDICAD will be described, and installation instructions will be given. In order to become acquainted with the program, its command line options as well as the syntax required for entering parameters in SYNDICADs option file will be highlighted. Afterwards, some possibilities to visualise the output files of SYNDICAD will be presented. In addition, SYNDICAD can be run by an external fitting routine that automatically adjusts predefined SYNDICAD parameters in order to minimise differences to experimental data. Finally, a brief overview of the classes and objects used in SYNDICAD will be given.

B.1 Compilation and directory hierarchy

The root directory of the enclosed CD contains the directory SYNDICAD, which hosts all source files necessary for compilation. These files include the header files:
const.h exocytosis.h memprotein.h neuron.h parameter.h potential.h pot_base.h stimulus.h syndicad.h
and the actual implementations:
exocytosis.cpp fit.cpp main.cpp memprotein.cpp neuron.cpp parameter.cc potential.cpp stimulus.cpp syndicad.cpp .
The file Makefile contains all necessary instructions for compilation. The program can be compiled by moving into the source directory and running the make utility:

```
> cd SYNDICAD
> make
```

The compilation results in an executable file called *syndicad.* The compilation options can be adapted to individual machine requirements by editing the variable **CXXFLAGS** within the file *Makefile.* In order to remove all object files, the make utility can also be called with the special option

```
> make clean.
```

All output files of SYNDICAD can be conveniently removed by calling

```
> make rmout.
```

B.2 Options and Parameters

The executable file *syndicad* requires a parameter file within its directory. If no command line option is given, the default parameter file name is *syndicad.par.* The program can be started as follows

```
> ./syndicad [PARAMETERFILE] [PARAMETERS],
```

where the optional variable **PARAMETERFILE** denotes the name of the file containing the parameters and **PARAMETERS** may contain additional parameters in the syntax **PARAMETERS** = "**-PARNAME = PARVALUE**". The program will only start when all necessary parameters have been defined in either the parameter file or in the command line options. If a parameter is defined in both the parameter file and the command line option, the value in the command line options will have higher priority. The standard parameter file *syndicad.par* contains all necessary values – adjusted to the presynaptic terminal of a pyramidal neuron. All names of the parameters and their required units are listed in the default parameter file as well. Entries in *syndicad.par* must have the following syntax:
"**PARNAME = PARVALUE**".
In every line, text occurring after the sign "#", is interpreted as a comment. If SYNDICAD is started with *syndicad.par,* as provided with this thesis, the output directories *./outputa/* and *./output/* must exist in its working directory.

B.3 Output and Visualisation

If no further changes have been performed in the used parameter file, SYNDICAD writes its output files in the directories *./outputa/* and *./output/.*

After SYNDICAD has been completed, the directory *outputa* contains the following data as time series:

averagebouton.out Spatially averaged observable such as the calcium concentration, buffer concentration, etc.

averageprotein.out Total currents and rates of the membrane proteins.

pre_u.out Membrane potential.

fluorescence.out Spatial average of the relative fluorescence intensity.

Using the shell script *mkbouton* the main features of a SYNDICAD run can be visualised:

```
> cd outputa
> ./mkbouton.
```

Note however that this script requires the visualisation program "xmgrace" (available on the SuSE distribution) to be installed on the system.

In contrast, the directory *output* contains the three relevant observable in spatially resolved form: calcium concentration, buffer concentration, and relative fluorescence intensity. These are saved in files of the form *syndicadoutxxxxx.out*, where the number *xxxxx* codes the actual simulation time. The ASCII-files can be visualised with the IBM data explorer (available on the SuSE distribution):

```
> cd output
> dx.
```

After starting the Data Explorer, the visual program file *diffusion.net* should be opened. With the Data Explorer, the spatiotemporal dynamics of the calcium concentration can be observed. In addition, the Data Explorer supports the opportunity to create movie sequences.

B.4 Fitting routine

On top of SYNDICAD, an additional program – the executable *fit* – can be used to obtain parameter sets that minimise the difference between the output of SYNDICAD and experimental data. The parameters necessary for the fitting routine must be specified in the source code file *fit.cpp*:

DIM Number of parameters to be minimised.

DATAFILE Name of the file containing the experimental data.

timestep Timestep width of the SYNDICAD simulation.

p[i] Initial values of the Parameters **i** = 0 .. **DIM** - 1.

command Here, the corresponding SYNDICAD command line options for every fit parameter must be specified.

In addition, in function **double Nfunc(double*)**, some adaptations concerning the output of the fit parameters during runtime may be necessary. The executable can be

created and started with the following commands:

```
> g++ -O3 -c fit.cpp
> g++ -O3 -o fit fit.o
> ./fit.
```

For every iteration, the program *fit* writes the parameter values and the corresponding χ^2-values to the standard output. In addition, both experimental data and the simulation output will be saved to *outputa/fitfluo.out* to enable direct comparison with "xmgrace".

B.5 Class hierarchy

SYNDICAD is based on implementations of the following major classes:

_SYNDICAD This class is responsible for controlling the main program flow of SYNDICAD: First, the parameter files are being parsed, followed by an initialisation of the diffusion compartments and a creation of all necessary objects. Second, the actual time evolution is being started. For that, member functions of all diffusion compartments – represented by individual objects – are called at every timestep, which calculate the local dynamics of the respective concentrations. At predefined intervals, the output files are updated. The variables are updated synchronously.

_NEURON An instancitiation of this class corresponds to a single volume element of the synaptic terminal. Several derived classes, such as **NEURON_CYTOPLASM, NEURON_MEMBRANE, NEURON_PRETERM, NEURON_ PRETERMEMPTY** specify the type of the individual compartment. Depending on their type, several different reaction terms and boundary conditions have been implemented in each subclass. Volume compartments situated on the membrane contain instanciations of membrane protein classes, whereas all compartments contain representations of buffer proteins. Locally, every volume compartment solves the reaction-diffusion system (4.11) and the analogous equations for the protein dynamics.

_channels Every instanciation of **_channels** represents the action of a single VDCC. Therefore, all necessary functions describing its temporal dynamics and its equilibrium state have been implemented here.

_carriers An instanciation of **_carriers** includes the combined action of both the PMCA and the NCX proteins. Consequently, their temporal and their equilibrium dynamics have been realised here.

The modular structure of SYNDICAD enables the simple insertion of additional processes, e.g., additional buffers or different subtypes of VDCCs. Structures describing

the whole synaptic transmission process – from presynaptic action potentials to postsynaptic potentials – have already been implemented in SYNDICAD, thus rendering the program a perfect starting point for further investigations in this direction. This manifests itself in the existence of additional **_NEURON**-subclasses describing compartment properties of the synaptic cleft and the postsynapse and their corresponding reaction pathways.

List of publications

Journals

1. F. Erler, P. Zahn and I. Mertig,
   Finite-size effects in giant magneto resistance - an ab initio calculation,
   Phys. Rev. B (64) 094408 (2001).

2. P. Zahn, N. Papanikolaou, F. Erler and I. Mertig,
   Evolution of Co\Cu multilayer conductivity during growth-an ab initio calculation,
   Phys. Rev. B (65) 134432 (2002).

3. F. Erler, M. Meyer-Hermann and G. Soff,
   A quantitative model for presynaptic free calcium dynamics during different stimulation protocols,
   Neurocomputing, in press.

4. M. Graupner, F. Erler, M. Meyer-Hermann,
   A theory of Plasma Membrane Calcium Pump stimulation and activity,
   arXiv:physics/0306121.

Refereed conference proceedings

1. M. Meyer-Hermann, F. Erler and G. Soff,
   Presynaptic calcium dynamics of neurons in answer to various stimulation protocols,
   in A. Deutsch, M. Falcke, J. Howard, W. Zimmermann (eds.), Function and regulation of cellular systems: experiments and models, Birkhaeuser, Basel (2004).

Poster presentations

1. P. Zahn, F. Erler, N. Papanikolaou and I. Mertig,
   Thickness dependent conductivity for finite multilayer systems,
   "Symposium on Spin Electronics"; Halle (2000).

2. F. Erler, M. Meyer-Hermann and G. Soff,
   Calcium Dynamics in Neurons,

1.MathBio Workshop "Function and Regulation of Cellular Systems: "Experiments and Models" MPI-PKS; Dresden (2001).

3. F. Erler, M. Meyer-Hermann and G. Soff,
AP- and Tetanus-induced Presynaptic Calcium Dynamics in Single Boutons of Pyramidal Neurons,
11.Neuropharmacology conference "Molecular Mechanisms of Synaptic Function" Plaza Hotel; San Diego-USA (2001).

4. F. Erler, M. Meyer-Hermann and G. Soff,
SYNDICAD - Reconstruction of intrinsic calcium signals from fluorescence measurements in neurons
1.PhD-Symposium "Horizons in Molecular Biology" GZMB; Goettingen (2003).

Acknowledgements

First of all, I would like to express my deep gratitude to the supervisor of my thesis, Prof. Dr. Gerhard Soff, for offering me the possibility to graduate in his group. His paternal guidance and continuous interest in my work has been a great encouragement over the past years.

I would like to thank especially Dr. Michael Meyer-Hermann for conceding the chance to start a collaboration with him on the subject of biophysics, before this research field had fully been established in Dresden. In the past years he spent a large amount of time and energy in order to animate my research work and to supervise the progress of my thesis. It has gained a lot from Dr. Meyer-Hermann's extraordinary expertise concerning theoretical biology and physics in general. I owe a lot to the illuminating conversation with him, both professionally and personally.

He and the other members of the research group "Theoretical Biophysics" at the Institute for Theoretical Physics, namely Christiane Berndt, Tilo Beyer, Michael Graupner, Wolfram Lorenz, and Gernot Schaller, have contributed a lot to an exciting and constructive atmosphere. In particular, I would like to thank my office-mate Gernot Schaller for technical advises and his uplifting backup. It has been a great pleasure to collaborate with the diploma students of the group, especially with Christiane Berndt and Michael Graupner. I gratefully acknowledge the other members of the group "Theory of Hadrons and Nuclei" of Professor Soff and the members of the Institute for Theoretical Physics for a pleasant environment. Especially the secretaries, Gundula Schaedlich, Gudrun Latus, and Ute Waechtler contribute a lot to this friendly atmosphere.

I'm grateful to Prof. Dr. Jonathan Howard for stimulating discussions and helpful suggestions and for admitting me to the PhD programme located at the Max-Planck Institute for Molecular biology and genetics at Dresden. It has been a great experience to get started with the field of my thesis by taking part in the two-months trainee course held at the MPI-CBG.

Finally, I would like to thank my family for their endurance, tolerance, and love.

List of Figures

List of Tables

Bibliography

[1] D. O. Hebb. *The Organization of Behavior*. Wiley, New York, 1949.

[2] E. DeSchutter and P. Smolen. *Calcium Dynamics in large neuronal Models. In: C. Koch and I. Segev, Methods in Neuronal Modeling*. The MIT Press, Cambridge MA, London, 1998.

[3] A. Destexhe, Z. F. Mainen, and T. J. Sejnowski. Synthesis of models for excitable membranes, synaptic transmission and neuromodulation using a common kinetic formalism. *J Comput Neurosci*, 1:195–230, 1994.

[4] A. L. Fogelson and R. S. Zucker. Presynaptic calcium diffusion from various arrays of single channels. Implications for transmitter release and synaptic facilitation. *Biophys J*, 48:1003–1017, 1985.

[5] E. Gamble and C. Koch. The dynamics of free calcium in dendritic spines in response to repetitive synaptic input. *Science*, 236:1311–1315, 1987.

[6] Z. W. Hall. *An introduction to molecular neurobiology*. Sinauer, Sunderland, 1992.

[7] C. Hammond. *Cellular and molecular neurobiology*. Academic Press, Paris, 1996.

[8] E. R. Kandel, J. H. Schwartz, and T. M. Jessell. *Neurowissenschaften - Eine Einführung*. Spektrum, Heidelberg, 1996.

[9] H. Reichert. *Neurobiologie*. Georg Thieme Verlag, Stuttgart, 1990.

[10] M. Graupner. A theory of plasma membrane calcium pump function and its consequences for presynaptic calcium dynamics. Master's thesis, TU Dresden, Dresden, 2003.

[11] E. Carafoli. Calcium signaling: a tale for all seasons. *Proc Natl Acad Sci U S A*, 99:1115–1122, 2002.

[12] M. J. Berridge, P. H. Cobbold, and K. S. Cuthbertson. Spatial and temporal aspects of cell signalling. *Philos Trans R Soc Lond B Biol Sci*, 320:325–343, 1988.

[13] M. J. Berridge, M. D. Bootman, and H. L. Roderick. Calcium signalling: dynamics, homeostasis and remodelling. *Nat Rev Mol Cell Biol*, 4:517–529, 2003.

[14] E. Carafoli. Intracellular calcium homeostasis. *Annu Rev Biochem*, 56:395–433, 1987.

[15] M. J. Berridge, M. D. Bootman, and P. Lipp. Calcium – a life and death signal. *Nature*, 395:645–648, 1998.

[16] G. J. Augustine and E. Neher. Neuronal Ca^{2+}-signalling takes the local route. *Curr Opin Neurobiol*, 2:302–307, 1992.

[17] C. A. Swanson, A. P. Arkin, and J. Ross. An endogenous calcium oscillator may control early embryonic division. *Proc Natl Acad Sci U S A*, 94:1194–1199, 1997.

[18] M. J. Berridge. Calcium signalling and cell proliferation. *Bioessays*, 17:491–500, 1995.

[19] B. Katz. *The Release of Neuronal Transmitter Substances*. Liverpool university press, Liverpool, 1969.

[20] R. Llinas, I. Z. Steinberg, and K. Walton. Relationship between presynaptic calcium current and postsynaptic potential in squid giant synapse. *Biophys J*, 33:323–351, 1981.

[21] P. De Koninck and H. Schulman. Sensitivity of CaM kinase II to the frequency of Ca^{2+} oscillations. *Science*, 279:227–230, 1998.

[22] H. Bito, K. Deisseroth, and R. W. Tsien. Ca^{2+}-dependent regulation in neuronal gene expression. *Curr Opin Neurobiol*, 7:419–429, 1997.

[23] G. E. Hardingham, S. Chawla, C. M. Johnson, and H. Bading. Distinct functions of nuclear and cytoplasmic calcium in the control of gene expression. *Nature*, 385:260–265, 1997.

[24] M. Baudry and J. L. Davis. *Long-Term Potentiation. (Vol.1-3)*. The MIT Press, Cambridge MA, London, 1991, 1994, 1996.

[25] J. Z. Tsien. Linking hebb's coincidence-detection to memory formation. *Curr Opin Neurobiol*, 10:266–273, 2000.

[26] H. von Gersdorff and J. G. Borst. Short-term plasticity at the Calyx of Held. *Nat Rev Neurosci*, 3:53–64, 2002.

[27] C. Stricker, A. C. Field, and S. J. Redman. Changes in quantal parameters of EPSCs in rat CA1 neurons in vitro after the induction of long-term potentiation. *J Physiol*, 490:443–454, 1996.

[28] G. Lynch, J. Larson, S. Kelso, G. Barrionuevo, and F. Schottler. Intracellular injections of EGTA block induction of hippocampal long-term potentiation. *Nature*, 305:719–721, 1983.

[29] R. C. Malenka, B. Lancaster, and R. S. Zucker. Temporal limits on the rise in postsynaptic calcium required for the induction of long-term potentiation. *Neuron*, 9:121–128, 1992.

[30] T. V. Bliss and G. L. Collingridge. A synaptic model of memory: long-term potentiation in the hippocampus. *Nature*, 361:31–39, 1993.

[31] V. Y. Bolshakov and S. A. Siegelbaum. Postsynaptic induction and presynaptic expression of hippocampal long-term depression. *Science*, 264:1148–1152, 1994.

[32] J. X. Bao, E. R. Kandel, and R. D. Hawkins. Involvement of pre- and postsynaptic mechanisms in posttetanic potentiation at aplysia synapses. *Science*, 275:969–973, 1997.

[33] R. A. Zalutsky and R. A. Nicoll. Comparison of two forms of long-term potentiation in single hippocampal neurons. *Science*, 248:1619–1624, 1990.

[34] T. R. Soderling. CaM-kinases: modulators of synaptic plasticity. *Curr Opin Neurobiol*, 10:375–380, 2000.

[35] M. Maletic-Savatic, T. Koothan, and R. Malinow. Calcium-evoked dendritic exocytosis in cultured hippocampal neurons. part II: mediation by calcium/calmodulin-dependent protein kinase II. *J Neurosci*, 18:6814–6821, 1998.

[36] G. Stefani, F. Onofri, F. Valtorta, P. Vaccaro, P. Greengard, and F. Benfenati. Kinetic analysis of the phosphorylation-dependent interactions of synapsin I with rat brain synaptic vesicles. *J Physiol*, 504:501–515, 1997.

[37] V. Beaumont, N. Zhong, R. Fletcher, R. C. Froemke, and R. S. Zucker. Phosphorylation and local presynaptic protein synthesis in calcium- and calcineurin-dependent induction of crayfish long-term facilitation. *Neuron*, 32:489–501, 2001.

[38] B. Hille. *Ionic channels of excitable membranes*. Sinauer, Sunderland, 2nd edition, 1992.

[39] J. Howard. *Mechanics of motor proteins and the cytoskeleton*. Sinauer Associates, Sunderland, 2001.

[40] L. Lacinova, N. Klugbauer, and F. Hofmann. Low voltage activated calcium channels: from genes to function. *Gen Physiol Biophys*, 19:121–136, 2000.

[41] H. J. Koester and B. Sakmann. Calcium dynamics associated with action potentials in single nerve terminals of pyramidal cells in layer 2/3 of the young rat neocortex. *J Physiol*, 529:625–646, 2000.

[42] N. M. Lorenzon and R. C. Foehring. Characterization of pharmacologically identified voltage-gated calcium channel currents in acutely isolated rat neocortical neurons. I. adult neurons. *J Neurophysiol*, 73:1430–1442, 1995.

[43] A. Tottene, A. Moretti, and D. Pietrobon. Functional diversity of p-type and r-type calcium channels in rat cerebellar neurons. *J Neurosci*, 16:6353–6363, 1996.

[44] J. C. Magee and D. Johnston. Characterization of single voltage-gated Na^+ and Ca^{2+} channels in apical dendrites of rat CA1 pyramidal neurons. *J Physiol*, 487:67–90, 1995.

[45] D. A. Coulter, J. R. Huguenard, and D. A. Prince. Calcium currents in rat thalamocortical relay neurones: kinetic properties of the transient, low-threshold current. *J Physiol*, 414:587–604, 1989.

[46] K. Takahashi, S. Ueno, and N. Akaike. Kinetic properties of T-type Ca^{2+} currents in isolated rat hippocampal CA1 pyramidal neurons. *J Neurophysiol*, 65:148–155, 1991.

[47] R. W. Tsien. Calcium channels in excitable cell membranes. *Annu Rev Physiol*, 45:341–358, 1983.

[48] B. P. Bean. Classes of calcium channels in vertebrate cells. *Annu Rev Physiol*, 51:367–384, 1989.

[49] P. Hess. Calcium channels in vertebrate cells. *Annu Rev Neurosci*, 13:337–356, 1990.

[50] L. Zylinska and M. Soszynski. Plasma membrane Ca^{2+}-ATPase in excitable and nonexcitable cells. *Acta Biochim Pol*, 47:529–539, 2000.

[51] M. Juhaszova, P. Church, M. P. Blaustein, and E. F. Stanley. Location of calcium transporters at presynaptic terminals. *Eur J Neurosci*, 12:839–846, 2000.

[52] J. T. Penniston and A. Enyedi. Modulation of the plasma membrane Ca^{2+} pump. *J Membr Biol*, 165:101–109, 1998.

[53] E. Carafoli. The calcium pumping ATPase of the plasma membrane. *Annu Rev Physiol*, 53:531–547, 1991.

[54] E. Carafoli. The Ca^{2+} pump of the plasma membrane. *J Biol Chem*, 267:2115–2118, 1992.

[55] E. Carafoli. The calcium pumping ATPase of the plasma membrane. *Annu Rev Physiol*, 53:531–547, 1991.

[56] D. Guerini. The significance of the isoforms of plasma membrane calcium ATPase. *Cell Tissue Res*, 292:191–197, 1998.

[57] W. J. Pottorf, S. P. Duckles, and J. N. Buchholz. Mechanisms of calcium buffering in adrenergic neurones and effects of ageing: testing the limits of homeostasis. *J Auton Pharmacol*, 20:63–75, 2000.

[58] M. P. Blaustein and W. J. Lederer. Sodium/calcium exchange: its physiological implications. *Physiol Rev*, 79:763–854, 1999.

[59] T. P. Stauffer, D. Guerini, and E. Carafoli. Tissue distribution of the four gene products of the plasma membrane calcium pump. *J Biol Chem*, 270:12184–12190, 1995.

[60] D. Chin and A. R. Means. Calmodulin: a prototypical calcium sensor. *Trends Cell Biol*, 10:322–328, 2000.

[61] N. L. Elwess, A. G. Filoteo, A. Enyedi, and J. T. Penniston. Plasma membrane Ca^{2+} pump isoforms 2a and 2b are unusually responsive to calmodulin and Ca^{2+}. *J Biol Chem*, 272:17981–17986, Jul 1997.

[62] E. E. Strehler. Plasma membrane Ca^{2+} pumps and Na^{+}/Ca^{2+} exchangers. *Semin. Cell Biol*, 1:283–295, 1990.

[63] R. DiPolo and L. Beauge. Metabolic pathways in the regulation of invertebrate and vertebrate Na^{+}/Ca^{2+} exchange. *Biochim Biophys Acta*, 1422:57–71, 1999.

[64] A. Lewit-Bentley and S. Rety. EF-hand calcium-binding proteins. *Curr Opin Struct Biol*, 10:637–643, 2000.

[65] R. J. Miller. Regulation of calcium homoeostasis in neurons: the role of calcium-binding proteins. *Biochem Soc Trans*, 23:629–632, 1995.

[66] C. B. Klee. Ca^{2+}-dependent phospholipid- (and membrane-) binding proteins. *Biochemistry*, 27:6645–6653, 1988.

[67] A. Persechini and B. Cronk. The relationship between the free concentrations of Ca^{2+} and Ca^{2+}-calmodulin in intact cells. *J Biol Chem*, 274:6827–6830, 1999.

[68] G. Grynkiewicz, M. Poenie, and R. Y. Tsien. A new generation of Ca^{2+} indicators with greatly improved fluorescence properties. *J Biol Chem*, 260:3440–3450, 1985.

[69] C. Koch and I. Segev. *Methods in Neuronal Modeling*. MIT Press, Cambridge, 1998.

[70] W. Gerstner and W. Kistler. *Spiking Neuron Models*. Cambridge University Press, Cambridge, 2002.

[71] J.M. Bower and D. Beeman. *The Book of GENESIS: Exploring Realistic Neural Models with the GEneral NEural SImulation System*. Springer-Verlag, New York, 1992.

[72] N. Gershenfeld. *The Nature of Mathematical Modeling*. Cambridge University Press, Cambridge, 1999.

[73] W. R. Holmes and W. B. Levy. Insights into associative long-term potentiation from computational models of NMDA receptor-mediated calcium influx and intracellular calcium concentration changes. *J Neurophysiol*, 63:1148–1168, 1990.

[74] W. R. Holmes. Models of calmodulin trapping and CaM kinase II activation in a dendritic spine. *J Comput Neurosci*, 8:65–85, 2000.

[75] J. Trommershauser, R. Schneggenburger, A. Zippelius, and E. Neher. Heterogeneous presynaptic release probabilities: functional relevance for short-term plasticity. *Biophys J*, 84:1563–1579, 2003.

[76] J. Keizer, G. D. Smith, S. Ponce-Dawson, and J. E. Pearson. Saltatory propagation of Ca^{2+} waves by Ca^{2+} sparks. *Biophys J*, 75:595–600, 1998.

[77] A. Schiegg, W. Gerstner, R. Ritz, and J. L. van Hemmen. Intracellular Ca^{2+} stores can account for the time course of LTP induction: a model of Ca^{2+} dynamics in dendritic spines. *J Neurophysiol*, 74:1046–1055, 1995.

[78] E. Neher and G. J. Augustine. Calcium gradients and buffers in bovine chromaffin cells. *J Physiol*, 450:273–301, 1992.

[79] G. D. Smith, J. Wagner, and J. Keizer. Validity of the rapid buffering approximation near a point source of calcium ions. *Biophys J*, 70:2527–2539, 1996.

[80] W. H. Press, S. A. Teukolsky, W. T. Vetterling, and B. P. Flannery. *Numerical Recipes in C*. Cambridge University Press, Cambridge, 1992.

[81] F. Bezanilla. The voltage sensor in voltage-dependent ion channels. *Physiol Rev*, 80:555–592, Apr 2000.

[82] B. Sakmann and E. Neher. *Single-Channel Recording*. Kluwer, Academic Publishers, 1995.

[83] J. Bischofberger, J. R. Geiger, and P. Jonas. Timing and efficacy of Ca^{2+} channel activation in hippocampal mossy fiber boutons. *J Neurosci*, 22:10593–10602, 2002.

[84] W. Nernst. Zur Kinetik der in Lösung befindlichen Körper: Theorie der Diffusion. *Z Phys Chem*, 3:613–637, 1888.

[85] A. J. Caride, A. R. Penheiter, A. G. Filoteo, Z. Bajzer, A. Enyedi, and J. T. Penniston. The plasma membrane calcium pump displays memory of past calcium spikes. Differences between isoforms 2b and 4b. *J Biol Chem*, 276:39797–39804, 2001.

[86] P. Belan, P. Kostyuk, V. Snitsarev, and A. Tepikin. Calcium clamp in isolated neurons of the snail helix pomatia. *J Physiol*, 462:47–58, 1993.

[87] P. V. Belan, P. G. Kostyuk, V. A. Snitsarev, and A. V. Tepikin. Calcium clamp in single nerve cells. *Cell Calcium*, 14:419–425, 1993.

[88] F. Helmchen, K. Imoto, and B. Sakmann. Ca^{2+} buffering and action potential-evoked Ca^{2+} signaling in dendrites of pyramidal neurons. *Biophys J*, 70:1069–1081, 1996.

[89] B. L. Sabatini and W. G. Regehr. Optical measurement of presynaptic calcium currents. *Biophys J*, 74:1549–1563, 1998.

[90] J. Wagner and J. Keizer. Effects of rapid buffers on Ca^{2+} diffusion and Ca^{2+} oscillations. *Biophys J*, 67:447–456, 1994.

[91] E. Neher. Usefulness and limitations of linear approximations to the understanding of Ca^{2+} signals. *Cell Calcium*, 24:345–357, 1998.

[92] A. L. Hodgkin and A. F. Huxley. A quantitative description of membrane current and its application to conduction and excitation in nerve. *Bull Math Biol*, 52:25–71, 1952.

[93] F. Helmchen, J. G. Borst, and B. Sakmann. Calcium dynamics associated with a single action potential in a CNS presynaptic terminal. *Biophys J*, 72:1458–1471, 1997.

[94] R. E. Fisher, R. Gray, and D. Johnston. Properties and distribution of single voltage-gated calcium channels in adult hippocampal neurons. *J Neurophysiol*, 64:91–104, 1990.

[95] M. Gollasch, J. Hescheler, J. M. Quayle, J. B. Patlak, and M. T. Nelson. Single calcium channel currents of arterial smooth muscle at physiological calcium concentrations. *Am J Physiol*, 263:C948–C952, 1992.

[96] T. P. Stauffer, H. Hilfiker, E. Carafoli, and E. E. Strehler. Quantitative analysis of alternative splicing options of human plasma membrane calcium pump genes. *J Biol Chem*, 268:25993–26003, 1993.

[97] A. Enyedi, A. G. Filoteo, G. Gardos, and J. T. Penniston. Calmodulin-binding domains from isozymes of the plasma membrane Ca^{2+} pump have different regulatory properties. *J Biol Chem*, 266:8952–8956, 1991.

[98] A. G. Filoteo, A. Enyedi, A. K. Verma, N. L. Elwess, and J. T. Penniston. Plasma membrane Ca^{2+} pump isoform 3f is weakly stimulated by calmodulin. *J Biol Chem*, 275:4323–4328, 2000.

[99] A. Enyedi, A. K. Verma, A. G. Filoteo, and J. T. Penniston. A highly active 120-kda truncated mutant of the plasma membrane Ca^{2+} pump. *J Biol Chem*, 268:10621–10626, 1993.

[100] M. Kappl and K. Hartung. Rapid charge translocation by the cardiac $Na^{+} - Ca^{2+}$ exchanger after a Ca^{2+} concentration jump. *Biophys J*, 71:2473–2485, 1996.

[101] C. B. Klee, T. H. Crouch, and P. G. Richman. Calmodulin. *Annu Rev Biochem*, 49:489–515, 1980.

[102] N. Volfovsky, H. Parnas, M. Segal, and E. Korkotian. Geometry of dendritic spines affects calcium dynamics in hippocampal neurons: theory and experiments. *J Neurophysiol*, 82:450–462, 1999.

[103] M. L. Albritton, T. Meyer, and L. Stryer. Range of messenger action of calcium ion and inositol 1,4,5-triphosphate. *Science*, 258:1812–1815, 1992.

[104] M. G. Tansey, K. Luby-Phelps, K. E. Kamm, and J. T. Stull. Ca^{2+}-dependent phosphorylation of myosin light chain kinase decreases the Ca^{2+} sensitivity of light chain phosphorylation within smooth muscle cells. *J Biol Chem*, 269:9912–9920, 1994.

[105] K. Luby-Phelps, M. Hori, J. M. Phelps, and D. Won. Ca^{2+}-regulated dynamic compartmentalization of calmodulin in living smooth muscle cells. *J Biol Chem*, 270:21532–21538, 1995.

[106] J. A. Connor, J. Petrozzino, L. D. Pozzo-Miller, and S. Otani. Calcium signals in long-term potentiation and long-term depression. *Can. J Physiol Pharmacol.*, 77:722–734, 1999.

[107] M. P. Charlton, S. J. Smith, and R. S. Zucker. Role of presynaptic calcium ions and channels in synaptic facilitation and depression at the squid giant synapse. *J Physiol*, 323:173–193, 1982.

[108] J. T. Rick and N. W. Milgram. Frequency dependence of long-term potentiation and depression in the dentate gyrus of the freely moving rat. *Hippocampus*, 6:118–124, 1996.

[109] S. N. Yang, Y. G. Tang, and R. S. Zucker. Selective induction of LTP and LTD by postsynaptic Ca^{2+} elevation. *J Neurophysiol*, 81:781–787, 1999.

[110] S. Wang, J. M. Wojtowicz, and H. L. Atwood. Synaptic recruitment during long-term potentiation at synapses of the medial perforant pathway in the dentate gyrus of the rat brain. *Synapse*, 22:78–86, 1996.

[111] C. Rosenmund, A. Sigler, I. Augustin, K. Reim, N. Brose, and J. S. Rhee. Differential control of vesicle priming and short-term plasticity by Munc13 isoforms. *Neuron*, 33:411–424, 2002.

[112] Y. Tang, T. Schlumpberger, T. Kim, M. Lueker, and R. S. Zucker. Effects of mobile buffers on facilitation: experimental and computational studies. *Biophys J*, 78:2735–2751, 2000.

[113] R. S. Zucker and N. Stockbridge. Presynaptic calcium diffusion and the time courses of transmitter release and synaptic facilitation at the squid giant synapse. *J Neurosci*, 3:1263–1269, 1983.

[114] R. C. Malenka, J. A. Kauer, D. J. Perkel, M. D. Mauk, P. T. Kelly, R. A. Nicoll, and M. N. Waxham. An essential role for postsynaptic calmodulin and protein kinase activity in long-term potentiation. *Nature*, 340:554–557, 1989.

[115] V. Matveev, A. Sherman, and R. S. Zucker. New and corrected simulations of synaptic facilitation. *Biophys J*, 83:1368–1373, 2002.

[116] J. E. Heuser and T. S. Reese. Structural changes after transmitter release at the frog neuromuscular junction. *J Cell Biol*, 88:564–580, 1981.

[117] R. L. Cooper, J. L. Winslow, C. K. Govind, and H. L. Atwood. Synaptic structural complexity as a factor enhancing probability of calcium-mediated transmitter release. *J Neurophysiol*, 75:2451–2466, 1996.

[118] M. Naraghi and E. Neher. Linearized buffered Ca^{2+} diffusion in microdomains and its implications for calculation of [Ca^{2+}] at the mouth of a calcium channel. *J Neurosci*, 17:6961–6973, 1997.

[119] D. A. DiGregorio, A. Peskoff, and J. L. Vergara. Measurement of action potential-induced presynaptic calcium domains at a cultured neuromuscular junction. *J Neurosci*, 19:7846–7859, 1999.

[120] M. R. Bennett, L. Farnell, and W. G. Gibson. The probability of quantal secretion near a single calcium channel of an active zone. *Biophys J*, 78:2201–2221, 2000.

[121] J. W. Shuai and P. Jung. Optimal ion channel clustering for intracellular calcium signaling. *Proc Natl Acad Sci U S A*, 100:506–510, 2003.

[122] R. S. Zucker and A. L. Fogelson. Relationship between transmitter release and presynaptic calcium influx when calcium enters through discrete channels. *Proc Natl Acad Sci U S A*, 83:3032–3036, 1986.

[123] C. J. Meinrenken, J. G. Borst, and B. Sakmann. Calcium secretion coupling at Calyx of Held governed by nonuniform channel-vesicle topography. *J Neurosci*, 22:1648–1667, 2002.

[124] D. Khananshvili. Structure, mechanism, and regulation of the cardiac sarcolemma Na/Ca exchanger. *Advances in Molecular and Cell Biology*, 23:311–358, 1998.

[125] J. S. Dittman, A. C. Kreitzer, and W. G. Regehr. Interplay between facilitation, depression, and residual calcium at three presynaptic terminals. *J Neurosci*, 20:1374–1385, 2000.

[126] M. Meyer-Hermann, F. Erler, Frido, and G. Soff. *Presynaptic calcium dynamics of neurons in answer to various stimulation protocols. In A. Deutsch, M. Falcke, J. Howard, W. Zimmermann (eds.), Function and regulation of cellular systems: experiments and models.* Birkhäuser, Basel, 2004.

[127] A. Rozov, N. Burnashev, B. Sakmann, and E. Neher. Transmitter release modulation by intracellular Ca^{2+} buffers in facilitating and depressing nerve terminals of pyramidal cells in layer 2/3 of the rat neocortex indicates a target cell-specific difference in presynaptic calcium dynamics. *J Physiol*, 531:807–826, 2001.

[128] C. Hansel, A. Artola, and W. Singer. Different threshold levels of postsynaptic Ca^{2+} have to be reached to induce LTP and LTD in neocortical pyramidal cells. *J Physiol Paris*, 90:317–319, 1996.

[129] C. Hansel, A. Artola, and W. Singer. Relation between dendritic Ca^{2+} levels and the polarity of synaptic long-term modifications in rat visual cortex neurons. *Eur J Neurosci*, 9:2309–2322, 1997.

[130] S. Williams and D. Johnston. Long-term potentiation of hippocampal mossy fiber synapses is blocked by postsynaptic injection of calcium chelators. *Neuron*, 3:583–588, 1989.

[131] M. C. Nowycky and M. J. Pinter. Time courses of calcium and calcium-bound buffers following calcium influx in a model cell. *Biophys J*, 64:77–91, 1993.

[132] D. W. Tank, W. G. Regehr, and K. R. Delaney. A quantitative analysis of presynaptic calcium dynamics that contribute to short-term enhancement. *J Neurosci*, 15:7940–7952, 1995.

[133] F. Erler, M. Meyer-Hermann, and G. Soff. A quantitative model for presynaptic free calcium dynamics during the induction of long-term effects. *Neurocomputing, in press*, 2004.

Erklärung

Hiermit versichere ich, dass ich die vorliegende Arbeit ohne unzulässige Hilfe Dritter und ohne Benutzung anderer als der angegebenen Hilfsmittel angefertigt habe; die aus fremden Quellen direkt oder indirekt übernommenen Gedanken sind als solche kentlich gemacht. Die Arbeit wurde bisher weder im Inland noch im Ausland in gleicher oder ähnlicher Form einer anderen Prüfungsbehörde vorgelegt. Die vorliegende Dissertation wurde an der Technischen Universität Dresden unter der wissenschaftlichen Betreuung von Prof. Dr. Gerhard Soff angefertigt.